The Important Contribution of Secondary Formation and Biomass Burning to Oxidized Organic Nitrogen (OON) in a Polluted Urban Area: Insights from In Situ FIGAERO-CIMS Measurements

Yiyu Cai[1,2,3,4,5&], Chenshuo Ye[6&], Wei Chen[1,2,3,4,5], Weiwei Hu[1,2,3,4], Wei Song[1,2,3,4], Yuwen Peng[7,8], Shan Huang[7,8], Jipeng Qi[7,8], Sihang Wang[7,8], Chaomin Wang[7,8], Caihong Wu[7,8], Zelong Wang[7,8], Baolin Wang[9], Xiaofeng Huang[10], Lingyan He[10], Sasho Gligorovski[1,2,3,4], Bin Yuan[7,8], Min Shao[7,8], Xinming Wang[1,2,3,4]

[1]State Key Laboratory of Organic Geochemistry, Guangzhou Institute of Geochemistry, Chinese Academy of Sciences, Guangzhou 510640. China
[2]CAS Center for Excellence in Deep Earth Science, Guangzhou, 510640, China
[3]Guangdong-Hong Kong-Macao, Joint Laboratory for Environmental Pollution and Control, Guangzhou Institute of Geochemistry, Chinese Academy of Science, Guangzhou 510640, China
[4]Guangdong Provincial Key Laboratory of Environmental Protection and Resources Utilization, Chinese Academy of Science, Guangzhou 510640, China
[5]University of Chinese Academy of Sciences, Beijing 100049, China
[6]Guangdong Provincial Academy of Environmental Science, Guangzhou, 510640, China
[7]Institute for Environmental and Climate Research, Jinan University, Guangzhou 511443, China
[8]Guangdong-Hongkong-Macau Joint Laboratory of Collaborative Innovation for Environmental Quality, Guangzhou 511443, China
[9]School of Environmental Science and Engineering, Qilu University of Technology, Jinan 250353, China
[10]Key Laboratory for Urban Habitat Environmental Science and Technology, School of Environment and Energy, Peking University Shenzhen Graduate School, Shenzhen, 518055, China
&Yiyu Cai and Chenshuo Ye contributed equally to this work.

Correspondence to: Weiwei Hu (weiweihu@gig.ac.cn); Bin Yuan (byuan@jnu.edu.cn).

Abstract. To investigate the sources and formation mechanism of oxidized organic nitrogen (OON), field measurements of OON were conducted using an iodide-adduct chemical ionization mass spectrometer equipped with a Filter Inlet for Gases and AEROsols (FIGAERO-CIMS) during fall of 2018 in the megacity of Guangzhou, China. Using levoglucosan as tracer of biomass burning emissions, the results show that biomass burning (49 ± 25%) and secondary formation (51 ~~%)~~± 25%) accounted for comparable fractions to the total particle-phase OON (pOON), while 24 ± 23% and 76 ± 23% to the gas-phase OON (gOON), respectively, signifying the important contribution of biomass burning to pOON and secondary formation to gOON in this urban area. Calculations of production rates of gOON indicated that hydroxyl radical (42%) and nitrate radical (NO_3) (49%) oxidation pathways potentially dominated the secondary formation of gOON. High concentration of NO_3 radical during the afternoon was observed, demonstrating that the daytime NO_3 oxidation might be more important than the previous recognition. Monoterpenes, found to be major precursors of secondary gOON, were mainly from anthropogenic emissions in this urban area. The ratio of secondary pOON to O_x ($[O_x] = [O_3] + [NO_2]$) increased as a function of relative humidity and aerosol surface area, indicating that heterogeneous reaction might be an important formation pathway for secondary pOON. Finally, the highly oxidized gOON and pOON with 6 to 11 oxygen atoms were observed, highlighting the complex secondary reaction processes of OON in the ambient air. Overall, our results improve the understanding of the sources and dynamic variation of OON in the urban atmosphere.

1 Introduction

Oxidized organic nitrogen (OON, including organic nitrates (ONs) and nitroaromatics), acting as an important reservoir of atmospheric nitrogen oxides (NO_x = NO + NO_2) (Fisher et al., 2016; Romer Present et al., 2020; Romer et al., 2016; Ditto et al., 2022), substantially influence the NO_x cycling, formation of ozone (O_3) (Farmer et al., 2011; Perring et al., 2013), and secondary organic aerosol (SOA) (Lee et al., 2016; Rollins et al., 2012), thus affect air quality, climate, and ecosystem nutrient cycling (Kiendler-Scharr et al., 2016; Pye et al., 2015). A comprehensive and in-depth understanding of dynamic variations of *in situ* OON (including in gas phase (gOON) and particle phase (pOON)) and their sources is crucial for accurately assessing their environmental impacts.

With the rapid development of measurement techniques, high-time resolution measurement of OONs has become more available. Currently, online measurement of OONs can be conducted by the following routes: (I) by thermodenuder dissociation to NO_2 and then detection by laser-induced fluorescence (TD-LIF) (Day et al., 2002; Rollins et al., 2010) or cavity-related spectroscopy (Keehan et al., 2020; Sadanaga et al., 2016); (II) by using aerosol mass spectrometer (AMS) (Decarlo et al., 2006) based on NO_2^+/NO^+ apportionment (Farmer et al., 2010; Fry et al., 2013; Hao et al., 2014; Day et al., 2022; Xu et al., 2015) and/or thermodenuder (Xu et al., 2021b); and (III) by using chemical ionization mass spectrometer (CIMS) with different ionization sources, typically with iodide-adduct chemistry (Huang et al., 2019; Lee et al., 2014; Lee et al., 2016) or extractive electrospray ionization (Bell et al., 2021; Lopez-Hilfiker et al., 2019; Pospisilova et al., 2020). Although the first two methods can quantify nitrate functional group (–ONO_2 or -NO_2) in bulk; CIMS, by taking advantage of soft ionization, can provide information on molecular compositions and better comprehend particle-phase ONs (pON) and nitroaromatics at the molecular level (Lee et al., 2014; Pospisilova et al., 2020; Wang et al., 2020b; Salvador et al., 2021). In general, nitroaromatics have also been included in the quantification of ONs by CIMS under negative ionization mode, due to the difficulty encountered in distinguishing the nitro functional group (–NO_2) from –ONO_2 and –NO_2 groups based solely on chemical formulas of ions (Huang et al., 2019). So far, gOON and pOON (containing 4–12 oxygen atoms) formed from multiple oxidation process of volatile organic compounds (VOCs) have been quantified by a high-resolution time-of-flight CIMS installed with a Filter Inlet for Gases and AEROsols (FIGAERO-CIMS) in the forests (Lee et al., 2018; Lee et al., 2016) and at ~~a~~ rural ~~site~~sites (Huang et al., 2019; Chen et al., 2020). However, limited measurement results were reported in the polluted urban areas (Le Breton et al., 2019).

Both primary emission and secondary formation can contribute to mass concentrations of ambient OON. Biomass burning and/or fossil fuel combustion have been suggested to be important primary emission sources of gOON (Liu et al., 2017; Palm et al., 2020; Peng et al., 2021) and pOON (Gaston et al., 2016; Mohr et al., 2013; Wang et al., 2019; Zhang et al., 2016). Furthermore, secondary formation of OON in biomass burning plumes has also been observed. For example, Juncosa Calahorrano et al. (2021)

observed the existence of gOON in aged plumes of wildfires. Kodros et al. (2020) showed that pOON could not only be directly emitted from laboratory-generated biomass burning emissions but also formed quickly through nitrate radical (NO_3) oxidation within biomass burning plumes. Based on aircraft measurements, Palm et al. (2020) found that the VOCs and vapors evaporated from primary biomass burning could be quickly subjected to radical-driven oxidation, thus contributing to the formation of SOA including nitroaromatics. For the secondary formation pathway in ambient air, gOON is formed mainly through the oxidation of VOCs by hydroxyl radical (OH), NO_3, and ozone in the presence of NO_x (Ng et al., 2017; Perring et al., 2013). Functionalization of gOON in ambient air reduces their volatility, leading to condensation of gOON on particles to form secondary pOON (Capouet and Müller, 2006).

Previous studies indicated that the oxidation of biogenic VOCs by NO_3 dominated gOON formation at a forest-urban site in Germany (56% of average gOON production rate) (Sobanski et al., 2017), as well as at a boreal forest site in Finland (70% of total gOON production rate) (Liebmann et al., 2019) and the southeast US (84% of monoterpene organic nitrate mass) (Ayres et al., 2015; Pye et al., 2015; Xu et al., 2015). For urban areas, the contributions of the above-mentioned three secondary formation pathways to total gOON remain poorly understood (Yu et al., 2019). Initiation of oxidation by OH under high NO_x condition is traditionally regarded as the main formation pathway for urban OONs during the day (Perring et al., 2013). However, Hamilton et al. (2021) recently found that a large fraction of isoprene-derived OONs was formed through unexpected NO_3 oxidation pathway in the afternoon in the Beijing urban area. Thus, a better understanding of the OON sources and formation mechanism in urban areas is still needed.

In this study, quantitative measurements of gOON and pOON were carried out using a high-resolution time-of-flight FIGAERO-CIMS and an AMS in a Chinese megacity. The contributions of biomass burning and secondary formation to ambient total gOON and pOON measured by CIMS were quantified, and the secondary oxidation pathways were systematically explored based on the production rates of gOON. Finally, the molecular compositions of ambient OON measured by CIMS were comprehensively investigated.

2 Experimental Methods

2.1 Sampling site.

Measurements were conducted on the campus of Guangzhou Institute of Geochemistry, Chinese Academy of Sciences (23.14°N, 113.36°E) in the urban area of megacity Guangzhou, during the coordinated campaign “Particles, Radicals, and Intermediates from oxidation of primary Emissions over the Great Bay Area” (PRIDE-GBA) (Wu et al., 2020). The observation site is located 25 m above the ground on the ninth floor of the highest building on the campus. The campus was surrounded with

industrialized and urbanized downtown areas in a typically subtropical climate, thus strongly influenced by both anthropogenic and biogenic emissions, as shown in Fig. S1. The average ambient temperature and relative humidity (RH) during the campaign were 23.7 ± 2.9 °C and 71.9 ± 17.4%, respectively. The site was mostly affected by northerly winds with an average speed of 4.5 ± 2.18 m s^{-1}.

2.2 Measurement and analysis.

2.2.1 Operation of FIGAERO-CIMS

During the campaign, a CIMS installed with a long time-of-flight detector ($10000 < m/\Delta m < 11000$) with an iodide source (Aerodyne Research Inc, USA) was deployed (Lee et al., 2014; Wang et al., 2020d). The FIGAERO inlet was installed with the CIMS to measure speciated gOON and pOON (Lopez-Hilfiker et al., 2014; Bannan et al., 2019; Schobesberger et al., 2018; Thornton et al., 2020). The detailed performance and calibration information of the CIMS can be found in a recent paper about this campaign (Ye et al., 2021). A brief description is introduced here. The sampling flow rate is 3.8 L min^{-1} for gas sampling line and 5 L min^{-1} for particle line. A $PM_{2.5}$ cyclone inlet and a nafion dryer (Perma Pure, model PD-07018T-12MSS) were set ahead of the particle sampling inlet of the FIGAERO to keep the filter for aerosol sampling not getting wet due to the high ambient RH (72 ± 17%) in this campaign. Recent studies show that aerosol in equilibrium with semi-/intermediate-volatility organic compounds (S/IVOCs) will be perturbed by the removal of the gases by the nafion (Liu et al. 2019). However, in this study, the retention time for particles through the nafion dryer was ~0.12 s, which might lead to a very small change of S/IVOCs signal on such a timescale (< a few percents) based on the partitioning delay model (Pagonis et al., 2017). In addition, an accurate correction for S/IVOCs loss in nafion dryer is also not available in current (Liu et al. 2019). Thus, no S/IVOCs correction on aerosol phase was performed in this study.

In general, to measure the gOON and pOON, the FIGEARO was operated alternately at two main stages during the measurement: (i) For the first 24 min in one hour cycle, ambient air was continuously sampled into two inlets, i.e., gas and particle inlets. The gas inlet was connected to an ion-molecule reaction region (IMR) of the CIMS. An X-ray source was used in this campaign, which has lower ionization efficiency compared to the polonium-210 radioactive source used in the previous studies (Faxon et al., 2018; Lee et al., 2021; Palm et al., 2019). Therefore, a higher pressure (370–390 mbar) in the IMR than in previous studies (e.g., 93–200 mbar) (Faxon et al., 2018; Lee et al., 2021; Palm et al., 2019) was used to achieve similar strength of reagent ions in the CIMS system. The sampled VOCs were first ionized in the IMR ($VOC{\bullet}I^-$), in which the primary ions were generated by flowing 2 mL/min 1000 ppm methyl iodide in 2.4 L/min N_2 through the X-ray source, and then moved into the mass spectrometer for measurement at a resolution of 1 s. Moreover, the ambient air was also introduced in the particle sampling inlet where a sliding Teflon tray held a polytetrafluoroethylene membrane filter (Zefluor®, Pall Inc., USA) for aerosol collection for 24 min. (ii) Next, after 24 min when the gas-phase measurement was completed, a linear actuator was used to move the Teflon tray on which the filter

was placed in front of the IMR, while the gas phase inlet was blocked. Then, ultrahigh-purity N_2 gas at a flow rate of 2 L min^{-1} was passed through a stainless steel "heating tube" to thermally desorb the collected particles on the filter into gas phase, and then into the IMR and mass spectrometer for measurement. The temperature of N_2 flow was ramped from room temperature to 175 ℃ in 12 min and then kept at 175 ℃ for another 20 min. The temperature of the IMR was kept almost constant by setting the temperature constant (80 ℃) of the heater strip in the IMR. Meanwhile, the room temperature, which was maintained by an air-conditioner, was relatively stable (23.7 ± 2.9 °C). The gas sampling line inside the room was covered by heat insulation associated with a heating cable to hold the temperature of sampling gas steady. These protocols reduce the effect of the temperature dependence of IMR, as indicated by Robinson et al. (2022) that I^- CIMS sensitivity may be influenced by the temperature of IMR.

The background signal of the gas-phase measurement was determined by pure N_2 signal at the last 3 min within the 24-min sampling time (Palm et al., 2019). The background signal of the particle measurement was determined by the measured signals from every sixth 1-h running cycle, in which particle-free air was obtained with ambient air passing through a High-Efficiency Particulate Air (HEPA) filter set ahead of the FIGAERO filter (Ye et al., 2021). The TofWare software (version 3.0.3) was used to perform high-resolution peak fitting of the CIMS mass spectra.

2.2.2 Oxidized Organic nitrogen quantification based on CIMS measurement

Based on the CIMS measurement, speciated OON (nitrogen-containing oxygenated hydrocarbons, 339 closed-shell compounds with oxygen versus carbon atom ratio no less than 3, $C_{\geq1}H_{\geq1}O_{\geq3}N_{1-2}$) in both gas and particle phases were quantified. These OON compounds can be fitted well in the HR analysis after the background signals have been removed. In this study, nitroaromatics were also a subset of OON due to (I) their similar chemical and optical properties as the bulk OON compounds (He et al., 2021; Lin et al., 2017) and (II) interferences between ONs and nitroaromatics in the CIMS measurement due to desorption and fragmentation (Ye et al., 2021). The composition of OON was mainly contributed by the CHON (one nitrogen atom containing species), and the $CHON_2$ (two nitrogen atom containing species) only contributed 6.8% of the gOON and 8.3% of the pOON.

For quantification, 39 species in total including levoglucosan ($C_6H_{10}O_5$), 4-nitrophenol ($C_6H_5NO_3$), 2,4-dinitrophenol ($C_6H_4N_2O_5$), and 4-nitrocatechol ($C_6H_4NO_4$) were calibrated with standard compounds, where the effect of humidity on the sensitivities was also accounted for (Ye et al., 2021). ~~For other uncalibrated species, a voltage scanning procedure was carried out every few days throughout the campaign to determine their sensitivities (including ON species) (Lee et al., 2016; Lopez-Hilfiker et al., 2016). Relative transmission efficiency as a Gaussian curve of m/z was also fitted and considered for the final ON quantification.~~ Their calibration factors were shown in the excel file of the supplement zip package of Ye et al. (2021). For other uncalibrated species, a voltage scanning procedure was carried out every few days throughout the campaign to determine their sensitivities

(including ON species) (Bi et al., 2021a, b; Lopez-Hilfiker et al., 2016). Lopez-Hilfiker et al. (2016) and Iyer et al. (2016) have verified the connections among the binding energy of the iodide-adduct bond, the voltage dissociating iodide adducts and the sensitivity of corresponding species. The relationship between the voltage difference (*dV*) and signal fraction remaining of an iodide-molecule adduct is established by scanning the *dV* between the skimmer of the first quadrupole and the entrance to the second quadrupole ion guide of the mass spectrometer. This relationship curve of an individual iodide adduct can be fitted by a sigmoid function and yields two parameters: S_0, the relative signal at the weakest *dV* compared to the signal under operational *dV*; dV_{50}, the voltage at which half of the maximum signal is removed (i.e., half the adducts that could be formed are de-clustered). A sigmoidal fit was then applied to the results of all the iodide adducts. An empirical relationship between relative sensitivity ($1/S_0$) and dV_{50} of each ion (includes levoglucosan) based on average values of the entire campaign was obtained. By linking the relative sensitivity of levoglucosan with its absolute sensitivity based on the authentic standard the absolute sensitivity of all the uncalibrated OON species was determined, after taking into account the relative transmission efficient of all the ions. The detailed data of these response factors can be found in the supporting information of Ye et al. (2021). Three OON species which are 4-nitrophenol ($C_6H_5NO_3$), 2,4-dinitrophenol ($C_6H_4N_2O_5$), and 4-nitrocatechol ($C_6H_5NO_4$) were calibrated in both authentic standards and voltage scanning methods. By comparing their sensitivity (Fig. S3), the uncertainty of the voltage scanning method can be roughly estimated. Detailed description of the calibration curves and the application of the calibration curve to estimate the sensitivity can be refferred to the supporting information text of Ye et al. (2021). In general, the voltage scanning method underestimates (32−56%) the sensitivity of OON in this study compared to the values using the standard compounds as real. This uncertainty was comparable with 30% uncertainty of all analytes in Bi et al. (2021b) and 60% uncertainty of total carbon in Isaacman-Vanwertz et al. (2018) measured by the Iodide-CIMS. Finally, an avergae underestimation of 47% on sensitivity was taken as the uncertainty of the whole OON mass loading in this study.

In summary, nitroaromatics, i.e., nitrophenol ($C_6H_5NO_3$), methyl nitrophenol ($C_7H_7NO_3$), dinitrophenol ($C_6H_4N_2O_5$), nitrocatechol ($C_6H_5NO_4$), methyl nitrocatechol ($C_7H_7NO_4$), and nitrosalicylic acid ($C_7H_5NO_5$), which were assumed to be identified with the ions containing the same molecule compositions detected by the CIMS (Wang et al., 2018; Wang and Li, 2021; Chen et al., 2021b), accounted for 18% and 5% of total gOON and pOON mass concentrations, respectively. ~~Thus, ONs were the dominated components in OON compound observed in this campaign. Note that there might also be other nitrogen-containing species rather than nitro-aromatics that contributed to these ions.~~Some nitroaromatic signal may be detected as elemental formulas other than those listed above, and some of the signal at the elemental formulas identified here as nitroaromatics may have contribution from ON species. While the uncertainty exists, it is likely that ONs dominated the OON observed during this campaign. For the total OON, the Iodide-CIMS may underestimate or poorly detect some types of OON, e.g., simple alkyl or keto nitrates (Lee et al., 2016).

Moreover, the thermal fragmentation reactions that result from heating on the FIGAERO filter may also lead to underestimation of OON due to the loss of the nitrogen-containing groups, such as peroxy nitrates, which have the propensity to thermally dissociate into NO_2 and other non-nitrogen-containing species (Lee et al., 2016).

~~The levoglucosan ($C_6H_{10}O_5$) in the particle phase measured using the CIMS was used as a tracer for biomass burning emission herein~~In the ambient air, the $C_6H_{10}O_5$ measured in the particle phase using the CIMS was probably composed by levoglucosan and its isomers (mannosan and galactosan) (Ye et al., 2021). The isomer measurement of $C_6H_{10}O_5$ in this campaign have revealed that the levoglucosan contributed 90 ± 2% mass loading of the three isomers of $C_6H_{10}O_5$ (Jiang et al., 2023), thus $C_6H_{10}O_5$ signal in this study can be used as a tracer for biomass burning emission ~~(Bhattarai et al., 2019). The averaged photochemical age was 0.2 days during the night to maximum 0.5 days in the daytime~~(Bhattarai et al., 2019). The good correlation (R=0.78) between $C_6H_{10}O_5$ and another biomass burning tracer potassium (K^+) (Wang et al., 2017c; Andreae, 1983), also supports this statement (Fig. S11a). Multiple studies show that levoglucosan might be degraded due to photochemistry (Lai et al., 2014; Bai et al., 2013; Hennigan et al., 2010). We calculated the ambient photochemical age based on the ratios of two hydrocarbons (m+p-xylene and ethylbenzene) that react at different rates with OH radicals (Yuan et al., 2013; Wu et al., 2020; De Gouw et al., 2005). A daily average OH concentration of 1.5×10^6 molecule cm^{-3} was assumed here (Mao et al., 2009; Wang et al., 2020d; Chen et al., 2021a). The estimated results show that the average diurnal photochemical age varied from 0.2 days during the night to maximum 0.5 days in the daytime in this campaign (Chen et al., 2021a), which was lower than the lifetime of levoglucosan (>1 day –26 days) determined in laboratory and field studies (Hennigan et al., 2010; Hoffmann et al., 2010; Lai et al., 2014; Bai et al., 2013; Bhattarai et al., 2019). It suggests that the levoglucosan observed in this study shall be stable for being the tracer of biomass burning emissions.

2.2.3 Other instruments

Besides the CIMS, a high-resolution time-of-flight aerosol mass spectrometer (HR-ToF-AMS, Aerodyne Research Inc., hereinafter referred to as "AMS") was used to provide online quantitative measurement of submicron non-refractory aerosols (PM_1) at a time resolution of 4 min (Canagaratna et al., 2007; Decarlo et al., 2006). In addition to the total organic aerosol (OA), the mass concentration of $–ONO_2$ group from pON ($pOrgNO_{3,\ AMS}$) was also estimated by NO_2^+/ NO^+ ratio method (Farmer et al., 2010; Fry et al., 2013; Day et al., 2022; Xu et al., 2015), positive matrix factorization (PMF) method (Hao et al., 2014), and thermodenuder (TD) method ~~(Xu et al., 2021) based on the AMS data. The comparative analysis among the CIMS and these three methods by the AMS aided in evaluating the measurement accuracy of OON in this study. Detailed description and intercomparison of these three methods can be found in the supporting information (Text S1), where some insights into the pros and cons of the AMS based methods are also presented.~~(Xu et al., 2021b) based on the AMS data. The NO_2^+/ NO^+ ratio method was based on the different ratios of NO_2^+ to NO^+ fragmented from $pOrgNO_{3,\ AMS}$ and inorganic nitrate. The PMF method was performed by including the NO^+ and

NO_2^+ ions into the PMF analysis combined with spectral matrix of organic ions. The TD method was conducted based on the difference of volatility between $pOrgNO_{3,\ AMS}$ and inorganic nitrates in particles. Detailed description and intercomparison of these three methods can be found in the supporting information (Text S1), where some insights into the pros and cons of the AMS-based methods are also presented. The comparative analysis among the CIMS and these three methods by the AMS aided in evaluating the measurement accuracy of OON in this study. Herein, pON estimated by NO_2^+/ NO^+ ratio method was selected as representative data for the following discussion due to the better performance achieved by this method. More detailed information on calibrations and operations of the AMS during this campaign can be found elsewhere (Chen et al., 2021a).

VOCs were measured by online gas chromatography-mass spectrometry and using a flame ionization detector (GC-MS/FID) (Wuhan Tianhong Instrument Co., Ltd.) at a time resolution of 1 h and by proton transfer reaction time-of-flight mass spectrometry (PTR-ToF-MS, IONICON Analytik) at a time resolution of 10 s (Wu et al., 2020; Yuan et al., 2017). A 56-component VOC gas standard was used for daily calibration of the GC-MS/FID (Wang et al., 2020c). For the PTR-ToF-MS, a 16-component VOC gas standard was used for daily calibration under both dry (RH < 1%) and ambient humidity during the whole campaign, and an additional 23-component VOC gas standard was used during the last period of the campaign (Wang et al., 2020a; Wu et al., 2020). The uncertainties for the VOC measurements by both instruments were below 20%. Trace gases, i.e., O_3 (TL43i), NO/NO_2 (TL42i), and CO (TL48i), were measured using Thermo Fisher Scientific instruments at a time resolution of 1 min (Wang et al., 2020d). Meteorological parameters were measured on a Vantage Pro2 weather station (Davis Instruments) at a time resolution of 10 s.

2.3 Calculation of the production rates of gas-phase oxidized organic nitrogen.

The production rates of gOON from VOCs oxidized by OH, NO_3, and O_3 were calculated using the reactant concentrations and reaction rate coefficients combined with formation branching ratios and yields (Liebmann et al., 2019), of which the detailed calculation process can be found in Text S2. In this calculation, the production rates mainly from organic nitrates were shown. The parameters for secondary nitroaromatics are not available, thus, was not included here. The concentrations of VOCs and O_3 were obtained from direct measurements, while those of OH radicals were derived from a box model simulation with the Master Chemical Mechanism v3.3.1 (MCM v3.3.1) (Wang et al., 2020c; Wolfe et al., 2016). The NO_3 radical was calculated based on the measured N_2O_5 by the CIMS (Ye et al., 2021) based on temperature equilibrium between these two species (Brown and Stutz, 2012; Chen et al., 2022). The remaining parameters were obtained from the previous studies (Liebmann et al., 2019; Perring et al., 2013). The different VOC species and corresponding parameters are listed in Table 1. An overall uncertainty of 56% was estimated by the Monte Carlo method through 10,000 calculations in this method. The detailed uncertainties of different parameters can be found in Text S3.

Table 1. The VOC species and their average mass concentrations with standard deviations; The reaction rate coefficients, branch ratios for OH and O_3 pathway and yields for NO_3 pathway used for the calculations of gOON production rates.

OH-initiated pathway VOC species	Average concentration (ppb)	k_{OH} at 298K (cm^3 $molecules^{-1}$ s^{-1})	α^{RO_2}
Isoprene	0.15 ± 0.17	1.00×10^{-10}	0.070
d-Limonene [a]	0.07 ± 0.07	1.70×10^{-10}	0.230
α-pinene [a]	0.07 ± 0.07	5.30×10^{-11}	0.180
Propane	6.23 ± 4.92	1.09×10^{-12}	0.036
iso-Butane	1.56 ± 1.27	2.12×10^{-12}	0.096
n-Butane	2.80 ± 2.35	2.36×10^{-12}	0.077
Cyclopentane	0.09 ± 0.05	4.97×10^{-12}	0.045
iso-Pentane	1.17 ± 1.01	3.60×10^{-12}	0.070
n-Pentane	0.65 ± 0.65	3.80×10^{-11}	0.105
2,2-Dimethylbutane	0.03 ± 0.02	2.23×10^{-12}	0.152
2,3-Dimethylbutane	0.05 ± 0.05	2.23×10^{-12}	0.152
2-Methylpentane	0.26 ± 0.27	5.20×10^{-12}	0.097
3-Methylpentane	0.25 ± 0.25	5.20×10^{-12}	0.109
n-Hexane	0.50 ± 0.75	5.20×10^{-12}	0.141
2,4-Dimethylpentane	0.03 ± 0.03	3.34×10^{-12}	0.140
Methylcyclopentane	0.09 ± 0.09	5.60×10^{-12}	0.140
Cyclohexane	0.05 ± 0.05	6.97×10^{-12}	0.160
n-Heptane	0.09 ± 0.15	6.76×10^{-12}	0.178
Methylcyclohexane	0.07 ± 0.09	9.64×10^{-12}	0.170
n-Octane	0.04 ± 0.05	8.11×10^{-12}	0.226
Nonane	0.03 ± 0.03	9.70×10^{-12}	0.393
n-Decane	0.02 ± 0.02	1.10×10^{-11}	0.417
Benzene	0.43 ± 0.16	1.22×10^{-12}	0.034
Toluene	1.75 ± 1.86	5.96×10^{-12}	0.029
Ethylbenzene	0.28 ± 0.30	7.00×10^{-12}	0.072
m-p-Xylene	0.79 ± 0.82	2.30×10^{-11}	0.074
o-Xylene	0.29 ± 0.31	1.36×10^{-11}	0.081
Isopropylbenzene	0.01 ± 0.01	6.30×10^{-12}	0.110
m-Ethyltoluene	0.03 ± 0.03	1.86×10^{-11}	0.094
p-Ethyltoluene	0.02 ± 0.02	1.18×10^{-11}	0.137
1,3,5-Trimethylbenzene	0.02 ± 0.02	5.76×10^{-11}	0.031
o-Ethyltoluene	0.02 ± 0.02	1.19×10^{-11}	0.106
1,2,4-Trimethylbenzene	0.06 ± 0.06	3.25×10^{-11}	0.105
1,2,3-Trimethylbenzene	0.02 ± 0.01	3.25×10^{-11}	0.119
Propene	0.37 ± 0.37	2.63×10^{-11}	0.015
trans-2-Butene	0.03 ± 0.03	6.40×10^{-11}	0.034
1-Butene	0.07 ± 0.05	3.14×10^{-11}	0.025
cis-2-Butene	0.02 ± 0.02	5.64×10^{-11}	0.034
1-Pentene	0.03 ± 0.02	3.14×10^{-11}	0.059
trans-2-Pentene	0.01 ± 0.02	6.70×10^{-11}	0.064
cis-2-Pentene	0.01 ± 0.01	6.50×10^{-11}	0.064
1-Hexene	0.02 ± 0.01	3.70×10^{-11}	0.055
NO_3-initiated pathway VOC species	Average concentration (ppb)	k_{NO_3} at 298K (cm^3 $molecules^{-1}$ s^{-1})	α_i
Isoprene	0.15 ± 0.17	6.95×10^{-13}	0.700
d-Limonene	0.07 ± 0.07	1.22×10^{-11}	0.670
α-pinene	0.07 ± 0.07	6.21×10^{-12}	0.150
Phenol	0.04 ± 0.03	3.92×10^{-12}	0.251
Cresol	0.03 ± 0.03	1.37×10^{-11}	0.128
Styrene	0.17 ± 0.26	1.50×10^{-12}	0.251 [b]
O_3-initiated pathway VOC species	Average	k_{O_3} at 298K	α^{O3}

	concentration (ppb)	(cm^3 $molecules^{-1}$ s^{-1})	
Isoprene	0.15 ± 0.17	1.28×10^{-17}	1.000
d-Limonene	0.07 ± 0.07	2.20×10^{-16}	0.750
α-pinene	0.07 ± 0.07	9.40×10^{-17}	0.800

Note that all the reaction rate coefficients and the formation branching ratios or yields are from MCM v3.3.1 and previous studies (Perring et al., 2013; Liebmann et al., 2019; Atkinson and Arey, 2003). [a] We assumed total monoterpenes measured from PTR-MS are composed of *d*-limonene and *α*-pinene with a ratio of 1:1 based on the anthropogenic origins of monoterpene, as discussed in text S2. [b] The parameters were assumed to be equal to that of phenol.

3 Results and Discussion

3.1 Quantification and chemical composition of oxidized organic nitrogen

Fig. 1a shows a subset of the time series of pOON measured using the CIMS (i.e., $pOON_{CIMS}$) and $pOrgNO_{3,\,AMS}$ ($-ONO_2$ + NO_2 group) measured with the AMS. Total OA measured with the AMS is also shown in Fig. 1a. During the entire campaign, a moderate correlation (Pearson correlation coefficient, R = 0.42, Fig. S6) was observed between $pOON_{CIMS}$ and $pOrgNO_{3,\,AMS}$ ~~(Fig. 1b),~~, which is probably due to the high uncertainty of $pOrgNO_{3,\,AMS}$ estimation from the AMS when organic nitrate fraction in total nitrate signal is low (<10%, the details can be found in Text S1), as well as is probably due to the fact that only $–ONO_2/NO_2$ groups not entire ON molecule was measured with AMS. The description of the correlation coefficient (R) within this study is defined based on the interpretation by Dancey and Reidy (2007), as shown in detail in Text S1. When the mass concentration of total nitrates from the AMS is below 5 μg m^{-3} (corresponding to $pOrgNO_{3,\,AMS}$ signal fraction in total nitrate signal >60%), an improved correlation between $pOON_{CIMS}$ and $pOrgNO_{3,\,AMS}$ is found (R = 0.86, Fig. 1b ~~and Fig. S5~~), validating the robustness of $pOON_{CIMS}$ measured here. A similar moderate correlation between $pOrgNO_{3,\,AMS}$ and $pOON_{CIMS}$ was also observed at a rural site in the southwest Germany (R = 0.52) (Huang et al., 2019), and a much better agreement (R = 0.82) was obtained in the southeast US when the $pOrgNO_{3,\,AMS}$ fraction in total nitrate is above 70% (Lee et al., 2016; Xu et al., 2015).

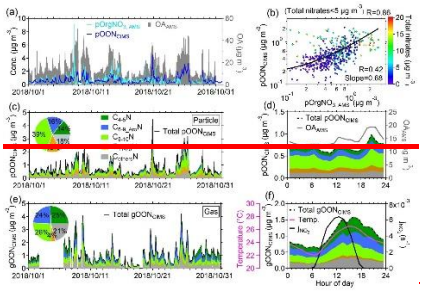

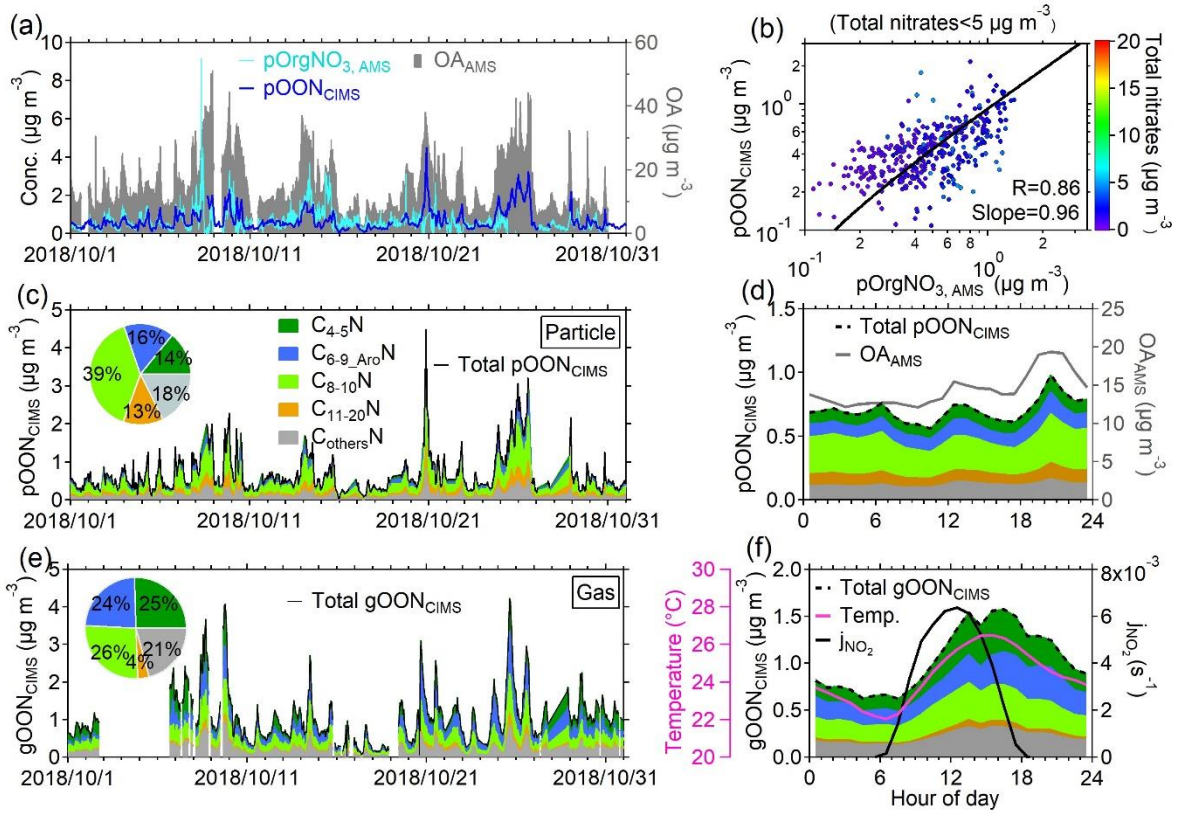

Figure 1. Time series and variations of OON during the PRIDE-GBA campaign. (a) Time series of $pOON_{CIMS}$ and $pOrgNO_{3,AMS}$. Time series of total OA detected by the AMS is shown on the right axis. (b) Scatterplot of $pOON_{CIMS}$ versus $pOrgNO_{3,AMS}$ during the campaign. The term "total nitrates <5 μg m^{-3}" indicates the data used in this scatterplot is under the condition that the mass concentration of total nitrates (including organic nitrate and inorganic nitrate) measured by the AMS is lower than 5 μg m^{-3}. The points are color-coded using the total nitrate signals measured by the AMS. The scatterplot from all AMS and CIMS measurement can be found in Fig. S6. The logarithm was applied to both of the axes. ~~The corresponding joint histogram plot can be found in Fig. S5.~~ Time series of (c) $pOON_{CIMS}$ and (e) $gOON_{CIMS}$, as well as the time series of their C_xN groups from the CIMS measurement. The insets show their average mass contributions to total $gOON_{CIMS}$ and $pOON_{CIMS}$ during the campaign, respectively. The average diurnal variations of (d) $pOON_{CIMS}$ and its C_xN groups, as well as OA; (f) Average diurnal variations of total $gOON_{CIMS}$ and its C_xN groups, photolysis rate of NO_2 (j_{NO2}), and temperature during the entire campaign. All the diurnal variations calculated throughout the manuscript are based on the average values. All the linear fitting are based on the orthogonal distance regression (ODR) algorithm in this study. All the acronyms can be found in appendix A.

The average concentrations of the $gOON_{CIMS}$ and $pOON_{CIMS}$ measured using the CIMS were 1.00 ± 0.67 and 0.66 ± 0.53 μg m^{-3}, respectively. Moreover, an average concentration of 0.60 ± 0.46 μg m^{-3} for $pOrgNO_{3,AMS}$ during the campaign was obtained. Notably, different size cuts between the AMS (PM_1) and the CIMS ($PM_{2.5}$) should only play a minor role in the quantification of pOON, as the measured total aerosol mass concentrations of $PM_{2.5}$ and PM_1 during the campaign are very similar (a regression slope of 0.96) (Chen et al., 2021a). The average mass-weighted chemical compositions for $gOON_{CIMS}$ and $pOON_{CIMS}$ observed in this campaign were determined to be $C_{6.6}H_{9.4}N_{1.1}O_{5.3}$ and $C_{8.5}H_{12.2}N_{1.1}O_{6.5}$, respectively, corresponding to molecular weight (MW) of

189 ± 7.8 and 234 ± 7.9 g mol^{-1}. The molecular weight of $pOON_{CIMS}$ in this study (234 ± 7.9 g mol^{-1}) is comparable to the reported values in forest (256 g mol^{-1}) and rural (220 and 296 g mol^{-1}) sites (Lee et al., 2018; Huang et al., 2019; Chen et al., 2020). If such average MW of $pOON_{CIMS}$ was applied, the $pOON_{AMS}$ (in addition to $-ONO_2$/-NO_2 groups, the organics part was also accounted for) would be 2.3 μg m^{-3} based on multiplying a factor of 3.8 to $pOrgNO_{3,\ AMS}$, which is well within the range of 0.06–2.94 μg m^{-3} of $pOON_{AMS}$ as reported in the previous studies around the world, as shown in Fig. ~~S6~~S7. On the other side, if only $-ONO_2$/-NO_2 groups are considered to calculate pON_{CIMS} to be $pOrgNO_{3,\ CIMS}$, the calculated $pOrgNO_{3,\ CIMS}$ can explain 28 ± 18% of $pOrgNO_{3,\ AMS}$, which is consistent with the fraction (23%) of total functionalized OA detected using the CIMS versus total OA measured using the AMS (Ye et al., 2021). The detailed analysis process on comparison uncertainty between AMS and CIMS can be found in Text S3 of the supporting information.

For this study, an average mass fraction of 15 ± 12% of pON_{AMS} in total OA (14.7 ± 8.20 μg m^{-3} on average) ~~based on~~measured by the AMS ~~data~~ was observed (calculation method referred to Takeuchi and Ng (2019)). In spite of the absolute mass concentrations of pON varied largely in different studied urban environments, the pON/OA ratios are very similar (15 ± 3% on average, Fig. ~~S6~~S7), suggesting a potential similar pON formation process/fate in the urban areas (Day et al., 2010; Rollins et al., 2012; Xu et al., 2015).

To further illustrate the contributions of different components of speciated gOON and pOON measured by the CIMS, five C_xN groups, namely (1) $C_{4–5}N$, (2) $C_{6–9\ Aro}N$, (3) $C_{8–10}N$, (4) $C_{11–20}N$, and (5) $C_{others}N$ (Figs. 1c and 1e) were categorized only based on the number of carbon atoms in the molecules. The $C_{6–9\_Aro}N$ group was recognized based on the number of 6–9 carbon atoms and positive aromaticity index (0–1) (Text S4) (Koch and Dittmar, 2016; Wang et al., 2019; Koch and Dittmar, 2006). $C_{11–20}N$ group contains species with large carbon backbones from 10 to 20 and/or oligomers, $C_{others}N$ includes the remaining nitrogen-containing short-chain ions which are not possible to fit into the previous four categories, such as the ions with carbon atoms less than 4 (e.g., $C_3H_7NO_4$ and $C_3H_7NO_5$) and the ions with 6–9 carbon atoms excluded in $C_{6–9\ Aro}N$ group (e.g., $C_6H_9NO_3$ and $C_7H_{11}NO_5$). In general, it is observed that the contributions of $C_{4–5}N$ (25%) and $C_{6–9\ Aro}N$ (24%) to total gOON are higher than those to total pOON (14% and 16%, respectively), while $C_{8–10}N$ (39%) and $C_{11–20}N$ (13%) contributed more to total pOON than to total gOON (26% and 4%, respectively). These results are consistent with the lower volatility for $C_{8–10}N$ and $C_{11–20}N$ than those for $C_{4–5}N$ and $C_{6–9\ Aro}N$ due to the longer backbones of compounds in the former groups (Kroll and Seinfeld, 2008; Odum et al., 1996). In general, the time series of all groups for the gOON shows similar variability as the pOON (correlation coefficient R > 0.6), except for $C_{4–5}N$ groups that show a positive correlation of R = 0.31 (Fig. ~~S7~~S8). The slightly poor correlation of $C_{4–5}N$ groups between gas and aerosol phase was probably caused by ~~their high susceptibility influenced by temperature.~~less partitioning of substantial formed isoprene-oxidized gOON in the daytime to the pOON compared to other long-chain compounds. The regression slope between gOON and pOON of

each category (3.61 to 1.80) decreases with the increase of the carbon number, as shown in Fig. ~~S7~~S8, which is reasonable considering their gas/particle partitioning balances (Odum et al., 1996).

The overall average diurnal variations of gOON and pOON and their C_xN groups are shown in Figs. 1d and 1f. Despite the boundary layer expansion in the daytime (Fig. ~~S8a~~S9a), the gOON peaks in the afternoon and drops slowly with tail toward the night. The enhancement of the gOON increases with the ~~photolysis rate~~j_{NO2} (Fig. 1f), indicating that daytime secondary formation is an important source of gOON (Sobanski et al., 2017). The primary biomass burning (e.g., levoglucosan as a tracer) and vehicle emissions (e.g., NO/NO_x as tracers), which are also potential sources for gOON, usually show enhancement during nighttime (levoglucosan and isomers in Fig. ~~S10f~~S11f and NO/NO_x in Fig. ~~S8b~~S9b) and morning rush hour time (NO/NO_x only), respectively, in their diurnal variations, indicating that both primary sources are unlikely to contribute to the gOON enhancement during daytime. In contrast to the gOON, the pOON exhibits two peaks during the afternoon and nighttime (Fig. ~~1f~~1d), indicating the possibility of different sources and formation mechanisms for the pOON compared to the gOON, e.g., biomass burning contribution during nighttime (Rollins et al., 2012). A more detailed analysis about the sources of the gOON and pOON is presented in the next section.

In general, the average diurnal concentration of each gOON (pOON) group shows a similar trend (Figs. ~~S8d~~S9d and ~~S8g~~S9g). The fraction of $C_{4-5}N$ group in gOON enhances slightly during daytime (Fig. ~~S8e~~S9e), which might be due to strong photochemical formation of isoprene-nitrates (Fisher et al., 2016; Reeves et al., 2020; Mayhew et al., 2022; Hamilton et al., 2021). The $C_{8-10}N$ fraction in total pOON slightly enhances during nighttime (Fig. ~~S8h~~S9h), which was probably due to the primary emissions and the formation of monoterpene-nitrates by NO_3 oxidation chemistry (Peng et al., 2021; Fisher et al., 2016).

3.2 Source apportionment of oxidized organic nitrogen.

To elucidate the sources of OON measured using the CIMS, the correlations between OON and a wide range of trace species representing different sources were explored to filter the best tracer for source apportionment. The scatterplots of gOON and pOON (hereinafter represent the $gOON_{CIMS}$ and $pOON_{CIMS}$) with selected species, including particle-phase $C_6H_{10}O_5$ (levoglucosan ~~($C_6H_{10}O_5$~~and its isomers) measured using the CIMS; *m/z* 60 measured using the AMS, benzene, NO_x, and CO are shown in Fig. 2 and Fig. ~~S9~~S10. It was observed herein that the scatterplots of gOON (and pOON) versus ~~levoglucosan, a~~$C_6H_{10}O_5$, the tracer for biomass burning emissions (Li et al., 2021b; Simoneit, 2002; Simoneit et al., 1999), exhibit two different regression slopes during daytime and nighttime (Figs. 2a and 2c). However, different regression slopes were not observed in the scatterplots of OON versus other tracers, e.g., CO, benzene. It suggests the biomass burning which usually peaks during the night might be an important source for OON. The time series of OON, in particular pOON, indeed peak consistently with ~~levoglucosan~~$C_6H_{10}O_5$ during high concentration episodes (Figs. ~~S11a~~S12a and ~~S12a~~S13a), indicating biomass burning emissions contributed substantially to

OON during this campaign. For other biomass burning tracer, e.g., *m/z* 60, did not show separated regression slope with OON, which is probably due to elevated background of *m/z* 60 contributed by non-biomass burning emissions (Cubison et al., 2011; Mohr et al., 2009). Another two potential biomass burning tracers, i.e., $C_7H_8O_2$ (methoxyphenol and its isomers) and $C_8H_8O_4$ (vanillic acid and its isomers), the former of which exhibits relatively low concentration and the latter shows larger background than $C_6H_{10}O_5$ (levoglucosan and its isomer) (Fig. ~~S10~~S11), are both not the ideal biomass burning tracers in this study.

In contrast to that ~~levoglucosan~~$C_6H_{10}O_5$ and OON peak consistent with each other, the time series of OON did not peak during the episodes with strong influences of vehicle emissions (as indicative of high ~~NO~~ and NO_x ~~concentration~~concentrations >50 ppb) (Harrison et al., 2003; Wormhoudt et al., 2015), as shown in Figs. ~~S13a and~~ S14a and S15a. In addition, the anti-correlations between OON and NO/NO_x during some of these episodes were even found, indicating that vehicle emission is not a significant source of primary OON. Furthermore, it was found that the diurnal variation of pOON peaks one-hour earlier than NO_x in the morning time, thus, supports their different origins (Fig. ~~S14g~~S15g). The coincidence of the peaking time between pOON and NO_x during nighttime is probably more influenced by biomass burning. Another piece of evidence is that multiple laboratory studies found negligible emission of gOON from emission tests of vehicle exhaust based on Iodide-CIMS direct measurement (Le Breton et al., 2019; Li et al., 2021a). Thus, the biomass burning emissions and secondary formation should be the main sources of OON observed in this campaign.

To quantify the contributions of biomass burning (OON_{bb}) and secondary formation (OON_{sec}) to OON in both gas and particle phases, the following Eqs. (1) and (2) were proposed to allocate the OON sources:

$$OON_{bb} = ([OON_{measured}]/[levo.])_{bb} \times [levo.] \quad (1)$$

$$OON_{sec} = OON_{measured} - OON_{bb} \quad (2)$$

Where [levo.] is the concentration of particulate ~~levoglucosan~~$C_6H_{10}O_5$ measured using the CIMS, $([OON_{measured}]/[levo.])_{bb}$ is the averaged ambient concentration ratio determined from slopes between ambient OON and particulate ~~levoglucosan~~$C_6H_{10}O_5$ during selected episodes with strong influences of biomass burning (Figs. ~~S11~~S12 and ~~S12~~S13). This approach relies on a concept similar to the widely-used "elemental carbon tracer method" for source apportionment of primary and secondary organic carbon (Turpin and Huntzicker, 1995). A similar method was used by Salvador et al. (2021) to quantify the sources of nitro-aromatic compounds. The episodes were selected based on the following three criteria: (1) the peak concentration of ~~levoglucosan~~$C_6H_{10}O_5$ should be above 0.2 μg m^{-3} for selecting periods strongly influenced by biomass burning plumes; (2) the regression coefficient R between gOON (pOON) and ~~levoglucosan~~$C_6H_{10}O_5$ during each episode should be >0.7; and (3) the number of the fitting points

during each episode should be above 4, due to the hourly data of particle-phase ~~levoglucosan~~$C_6H_{10}O_5$ were used. The averaged ambient concentration ratios were determined to be 3.95 ± 1.67 μg m^{-3}/μg m^{-3} for gOON and 5.05 ± 1.01 μg m^{-3}/μg m^{-3} for pOON, as presented in Table S1. The variability of $[OON_{measured}]/[levo.]$ ratios from multiple biomass burning episodes for pOON is 20%. The slightly larger ratio uncertainty for gOON (42%) is mainly due to active gas-phase reaction and low contributions of biomass burning emissions to total gOON, as discussed below.

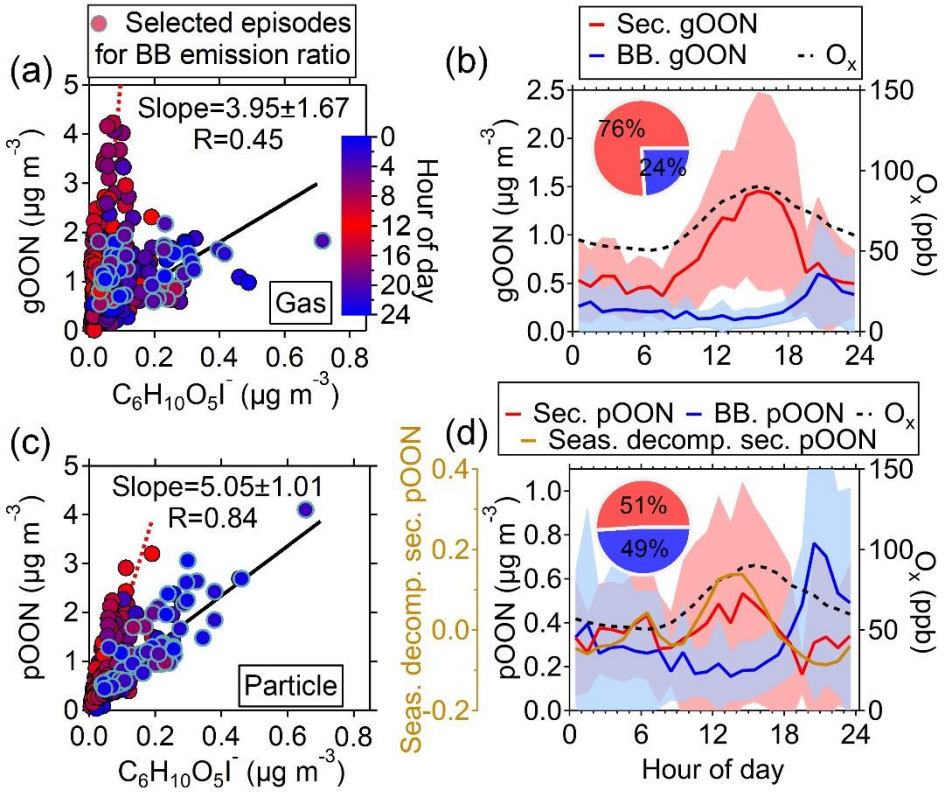

Figure 2. Scatterplots of (a) gOON and (~~d~~c) pOON versus ~~levoglucosan~~$C_6H_{10}O_5$ measured by CIMS with the data points color-coded using hour of day. The blue circles indicate the data points from multiple strongly influenced episodes by biomass burning emission, of which the ratios between gOON or pOON and ~~levoglucosan~~$C_6H_{10}O_5$ were used to determine the average ratio (black regression line). The red dotted line means the line regression during the daytime. The diurnal variations of (b) gOON and (~~e~~d) pOON from biomass burning (BB.) and secondary formation (sec.). The shaded areas mean the standard deviations. The seasonal decomposed secondary pOON (corresponding method is referred to Text S4) and O_x are also shown. The inset pies are the contributions from biomass burning and secondary formation to total gOON and pOON, respectively.

The ratios, i.e., $([OON_{measured}]/[levo.])_{bb}$, were obtained based on ambient measurement; therefore, the ratios might be influenced by secondary formation within biomass burning plumes, the OON_{bb} herein is referred to as the total primary and rapidly formed secondary OON from biomass burning emissions. OON_{sec} is defined as secondary OON from non-biomass burning sources, e.g., biogenic and non-biomass burning anthropogenic sources and possible OON slowly formed from biomass burning sources (i.e.,

next day), which shall be minor. By using this approach, the estimated diurnal variation and time series of OON_{bb} and OON_{sec} are shown in Figs. 2 and 3. Compared with the measured total OON, the OON_{sec} exhibits better agreement with the total gOON production rate in terms of both time series and correlation coefficients (R increases from 0.61 to 0.65 for gOON, and 0.19 to 0.45 for pOON, Fig. ~~S15)~~S16). In particular, better agreement was found during 24–26 October 2018 when the contribution of biomass burning to OON was high. The precursors, e.g., alkanes, alkenes, aromatics (phenol and cresol), and terpenes (isoprene and monoterpenes), considered in the calculation were also contributed by biomass burning (Liu et al., 2017; Gilman et al., 2015), especially during the strong biomass burning emission period. The particle-phase OON_{sec} also showed consistent variation (R=0.70) to semi-volatile oxygenated OA (SV-OOA), which was treated as freshly formed SOA during the day (Fig. S17) (Chen et al., 2021a), supporting the secondary origins of $pOON_{sec}$. These results validated the source apportionment of OON applied herein.

On average, biomass burning emissions accounted for 49 ± ~~10~~25% of total pOON measured by the CIMS, while the contribution was much lower (24 ± ~~11~~23%) for gOON (Figs. 2b and 2d), indicating that biomass burning is one of the major sources for pOON measured by the CIMS, and gOON is predominately from secondary formation (76 ± 23%) (Huang et al., 2019; Lee et al., 2016). The uncertainty of these ratios representing the error of this source apportionment method, the detailed calculation process of which can be found in Text S3 of the supporting information. The high contribution of biomass burning to total pOON is also consistent with the results of relevant previous studies (Mohr et al., 2013; Wang and Li, 2021; Wang et al., 2017c; Wang et al., 2019), in which substantial OON compounds were observed in biomass burning plumes. In this study, the nighttime enhancement of ~~levoglucosan~~$C_6H_{10}O_5$ indicates that the influence of biomass burning at this site was mainly contributed by the plumes of the agricultural residue combustion transported from the vicinity of Guangzhou city, as shown in the MODIS wildfire point plot in Fig. ~~S16~~S18 (Wang et al., 2017b; Yuan et al., 2010). Moreover, the ambient ratio of ~~levoglucosan~~$C_6H_{10}O_5$ to water-soluble potassium (K^+) (0.20 ± 0.04) observed in this study also supports that the biomass burning at this site was contributed by the combustion of crop residuals (0.1–0.2) rather than wood combustion (5.8–24.0) (Cheng et al., 2013). Fig. S19 presents the Van Krevelen diagram of all OON compounds in this study. The appearance of OON compounds observed herein is linked with both fresh and aged biomass burning emissions (Wang et al., 2019). In general, most of the biomass burning OON were found in particle phases, indicating that the OON formed in biomass burning plumes have generally lower volatility than OON formed via O_3, NO_3 oxidation, or OON oxidized from non-biomass burning related precursors.

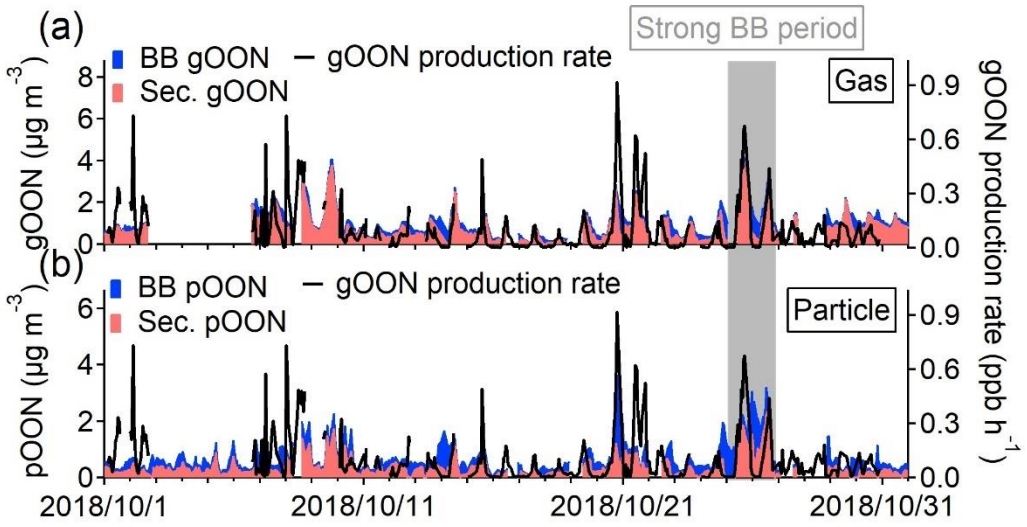

Figure 3. Stacked time series of secondary and biomass burning (a) gOON, (b) pOON. The gOON production rate is presented on the right axis in both of the figures. The grey period represents a strong biomass burning emission period during 24–26 October 2018, which was selected based on the high mass concentrations of ~~levoglucosan~~$C_6H_{10}O_5$ and other biomass burning tracers in their time series in Fig. ~~S10~~S11.

Based on the diurnal pattern, secondary gOON peaks during the afternoon (1.49 ± 0.49 μg m^{-3}), which is consistent with the peaking time of O_x ($[O_x] = [O_3] + [NO_2]$), and then reduces rapidly to 0.43–0.83 μg m^{-3} at night (Fig. 2b). The similar averaged diurnal variations of gOON and O_x indicate that the daytime chemistry corresponds to the major formation pathway of gOON. Secondary pOON also shows a slight peak (0.39 ± 0.07 μg m^{-3}) corresponding to O_x during daytime, however, exhibits much larger uncertainty than the secondary gOON. To elucidate this large uncertainty, a seasonal decomposition method~~, which can down weight the impact of daily peak intensity variation, was applied (detailed process can be found in Text S4).~~ (Hilas et al., 2006), which was performed by locally weighted linear regression to decompose the time series into three components, i.e., trend component, seasonal component and remainder, was applied (detailed process can be found in Text S4). By replacing seasonal variation with hour variation, the method can down weight the impact of daily peak intensity variation. Clear diurnal variation of secondary pOON after seasonal decomposition is displayed in Fig. 2d, which supports the daytime peak of secondary pOON. During nighttime, the concentration of pOON (0.32 ± 0.07 μg m^{-3}) remains at a high level with a peak at 6 o'clock (Fig. 2d), indicating that there is a different formation pathway or formation yield for secondary pOON compared to secondary gOON at night. It is speculated that the enhanced secondary pOON formation at night is probably associated with higher yield of pOON from NO_3 chemistry, as well as heterogeneous reactions of NO_3 and N_2O_5 at particle surface, which is discussed in detail in the following section. Following Eqs. (1) and (2), the averaged concentration ratios for each category of particle-phase C_xN (pC_xN) were also calculated separately, thus the contributions of biomass burning and secondary formation for each pC_xN group were estimated (Fig. ~~S18~~S20). The contribution

from biomass burning to each pC_xN group only shows small difference, ranging from 52% for the $C_{6-9\ Aro}N$ group to 40% for the $C_{4-5}N$ group, indicating biomass burning is an important source for OON at wide carbon numbers.

3.3 Secondary formation pathways of oxidized organic nitrogen.

To further elucidate the secondary formation mechanism of gOON, the diurnal patterns of gOON production rates from the three pathways following the procedure mentioned in section 2.3 are ~~shown in Fig. 4a and Fig. S19.~~calculated and shown in Fig. 4a and Fig. S21. Although the production rate did not consider the loss of OON, the calculation of production rate still serves as a useful tool to assess the formation pathway and precursor contribution to OON (Liebmann et al., 2019; Sobanski et al., 2017; Hamilton et al., 2021). As expected, the gOON production rates from OH- and O_3-initiated oxidation peaking (0.14 ppb h^{-1} and 0.01 ppb h^{-1}, respectively) at noon (11:00–13:00) are due to the high concentrations of these two oxidants during this period (3.9×10^6 and 1.4×10^8 molecule cm^{-3}, respectively) (Wang et al., 2020c). Interestingly, the gOON production rate from NO_3-initiated oxidation peaks at around 0.10 ± 0.18 ppb h^{-1} from late afternoon to evening (16:00–19:00, Fig. 4a). This is mainly due to the high NO_3 concentration (2.08 ± 1.32 ppt, Fig. ~~S3d~~S4d) when the low NO (1.37 ± 0.34 ppb) and moderate O_3 (53 ± 34 ppb) and NO_2 (31 ± 13 ppb) (Fig. ~~S8b~~S9b) concentrations appear during that period of the day. The precursors, i.e., cresol, phenol, isoprene, and monoterpenes, do not show rising concentrations during the period (16:00–19:00) except for some aromatics (Figs. ~~S8c, S8f~~S9c, S9f, and ~~S8i~~S9i), indicating that not the precursor VOCs but the high NO_3 concentration is the main contributor for this enhancement of NO_3-initiated gOON production rate during the day. The inconsistent peaks for the secondary gOON production rate and secondary gOON mass loading may be due to the (i) counteraction of photochemical formation and degradation, and or (ii) effect of survivor bias from measured VOCs (Wang et al., 2022b; Perring et al., 2013).

In general, OH- and NO_3-initiated oxidation pathways dominated the secondary gOON formation in this study and accounted for 42% and 49% of total gOON production rate, respectively, while the remaining was attributed to the O_3-initiated oxidation pathway (9%). Fig. ~~S19~~S21 shows that the contribution to total gOON production rate from 8:00 to 14:00 mainly came from OH chemistry (73%), then quickly changed to NO_3 chemistry during the late afternoon (mean 55%) and onward (mean 86% at night). These results emphasize the importance of NO_3 chemistry for the gOON production rate during later daytime and the entire night in this urban area. The importance of NO_3 chemistry toward ON formation was also found in other locations. For example, high contributions of NO_3 chemistry to secondary gOON production rate in Finnish boreal forest (41% during the day and almost 100% at night) (Liebmann et al., 2019) and isoprene-derived gOON production rate in Beijing urban area (32% in the afternoon and 86% at nighttime) (Hamilton et al., 2021) were observed. The low contribution of O_3 pathway (9%) at this site is also consistent with the estimated fraction (12%) at a forest area (Liebmann et al., 2019).

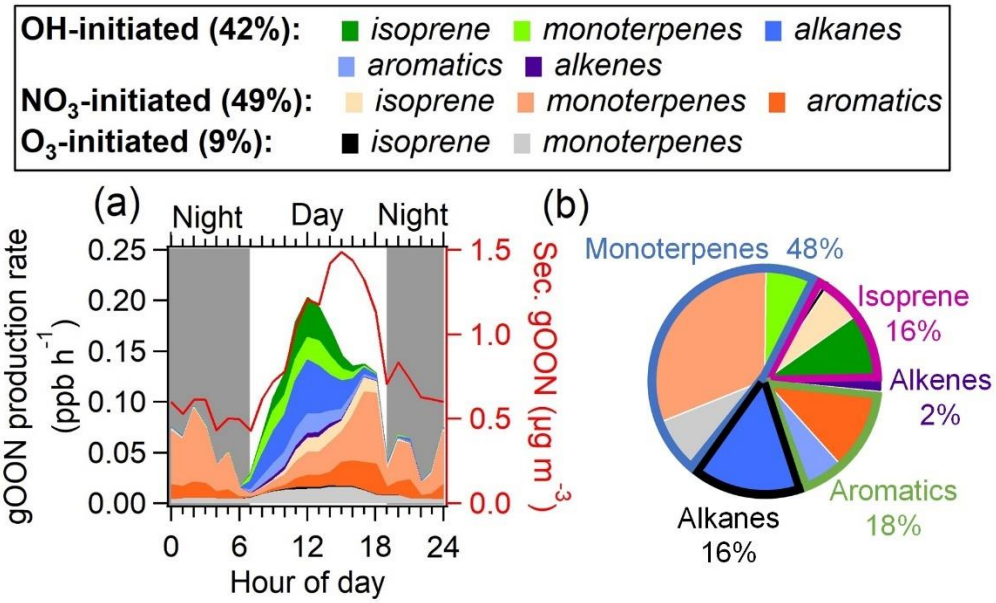

Figure 4. (a) Average diurnal variations of categorized gOON production rates and the concentration of secondary gOON for the whole campaign. (b) Contributions of various VOC precursors to total gOON production rate.

Fig. 4b displays the contributions to the gOON production rate from different VOC precursors, among which monoterpenes account for 48% of total gOON production rate. The remaining contribution is attributed to biogenic VOC, i.e., isoprene (16%), and other anthropogenic VOCs including aromatics (18%), alkanes (16%), and alkenes (2%). These results indicate that monoterpenes are the largest contributor to the secondary formation of multifunctional gOON in this urban region. Relatively high concentrations of monoterpenes were observed during the campaign (mean: 0.14 ± 0.14 ppb; range: 0.003–1.5 ppb). Strong correlations of the daily-averaged values from nighttime monoterpenes with two tracers of volatile chemical product (VCP) sources (C8 aromatics, R = 0.85 and ethanol, R = 0.78), and moderate correlation with CO (R = 0.62) as well as biomass burning tracer ~~levoglucosan~~$C_6H_{10}O_5$ (R = 0.50) (Fig. 5) were also found. These strong and moderate correlations with monoterpene are in contrast with the poor correlations of these anthropogenic tracers with biogenic-derived isoprene during daytime (R = –0.09 to 0.20, Fig. ~~S20~~S22). The ambient ratio of monoterpenes to CO (1.82 ppb ppm^{-1}) determined in Fig. 5c is significantly higher than their emission ratios from vehicle exhausts (0.001–0.35 ppb ppm^{-1}) (Wang et al., 2022a). Combining these results, it is concluded that the monoterpenes observed during this campaign should be mainly of anthropogenic origin (Hellén et al., 2012), with VCPs as the potentially most important source. Recent studies in the US also demonstrated that monoterpenes are strongly emitted by the VCP sources in highly populated areas (Coggon et al., 2021; Gkatzelis et al., 2021). In addition, a field study conducted in the tower located in the Guangzhou urban area found the ambient monoterpenes at an altitude of 450 m were predominantly come from VCP sources (Li et al., 2022), which is consistent with the findings here. In summary, considering monoterpenes of anthropogenic origin, anthropogenic VOCs accounted for 80% of total gOON production rate. Note that certain contributions of biogenic-derived monoterpenes might offset the anthropogenic-origin OON; however, other anthropogenic VOCs, such as long-chain or cyclic alkanes/alkenes (Wang et

al., 2020a; Zhao et al., 2016), which are important precursors for OONs in urban areas (Lee et al., 2015; Lim and Ziemann, 2009; Matsunaga and Ziemann, 2010), were not considered herein due to the omission of data. Thus, anthropogenic contribution to the gOON estimated via secondary gOON production rates might still be biased low.

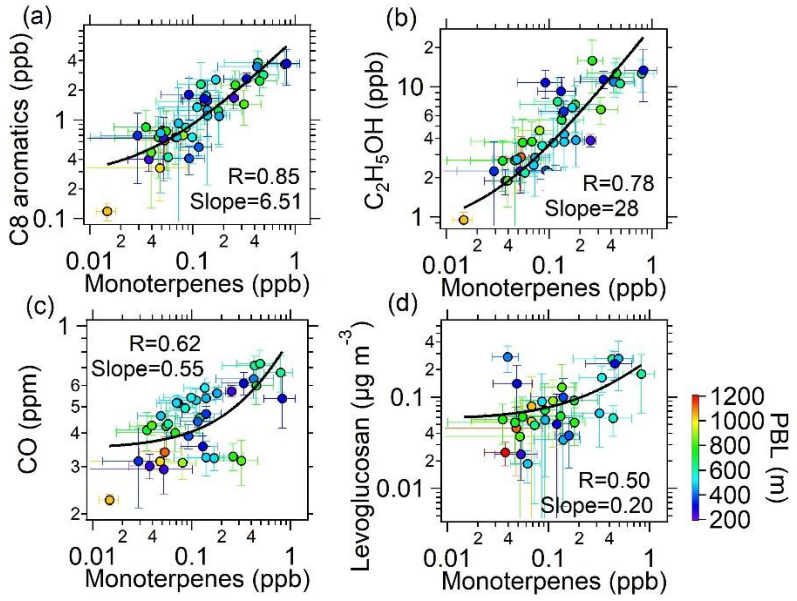

Figure 5. Scatter plots between the averaged concentrations of (a) C8 aromatics, (b) ethanol, (c) CO, and (d) ~~levoglucosan~~$C_6H_{10}O_5$ versus monoterpenes at night (19:00−6:00 next day) during the entire campaign. The color represents the planetary boundary layer height (PBL). The error bars were the standard deviations of average values during nighttime. The logarithm was applied to both of the axes.

Fig. 6a shows a strong correlation between secondary gOON and O_x (R = 0.83, slope = 0.02 μg m^{-3}/ppb), which is within expectation as the major channel of gOON formation between peroxy radicals (RO_2) and NO can lead to the formation of ~~O_3 by continual radical propagation and photolysis of NO_2 (Perring et al., 2013).~~OONs and O_3 by continual radical propagation and photolysis of NO_2 (Perring et al., 2013; Xu et al., 2021a). Fig. 6b demonstrates that secondary pOON shows moderate correlation (R = 0.39) with O_x and secondary pOON/O_x ratio increases as a function of RH (from ~0.002 to ~0.03 μg m^{-3}/ppb), aerosol liquid water content (ALWC) (Fig. ~~S21b~~S23b) and wet aerosol surface area (Fig. ~~S21c~~S23c). The elevated RH and ALWC may lead to an increase in the aerosol surface area to facilitate more highly functionalized and water-soluble gOON partitioning into particle phase and/or to promote NO_2, NO_3, and/or N_2O_5 uptake onto aerosol phase (George et al., 2015; George and Abbatt, 2010). Moreover, aerosols become more liquified at higher RH, thus leading to the increase in molecular diffusion in aerosols to promote heterogeneous reactions (George et al., 2015) of NO_3 with unsaturated species (Xiao and Bertram, 2011; Zhao et al., 2011), NO_2 with aromatic species, and N_2O_5 with alcohols to form pOON (Gross et al., 2009; Lee et al., 2015). Indeed, lower gas/particle partitioning coefficient (saturation mass concentration, *C**) of OON at RH >70% than low RH (<70%) was found (Fig. ~~S22a~~S24a), which supports the favored pOON formation from heterogeneous reactions. A study in an anthropogenic-emission-dominated region

also showed the heterogeneous reactions through N_2O_5 uptake can explain around half of the formation of particle-phase alkyl nitrates (Lee et al., 2015), thus signifying the important contribution from heterogeneous reactions to pOON. The secondary pOON/O_x ratio shows a much worse correlation with temperature (Fig. ~~S21d~~S23d), indicating that lower temperature-induced higher partition to particles contributes little to higher pOON during nighttime.

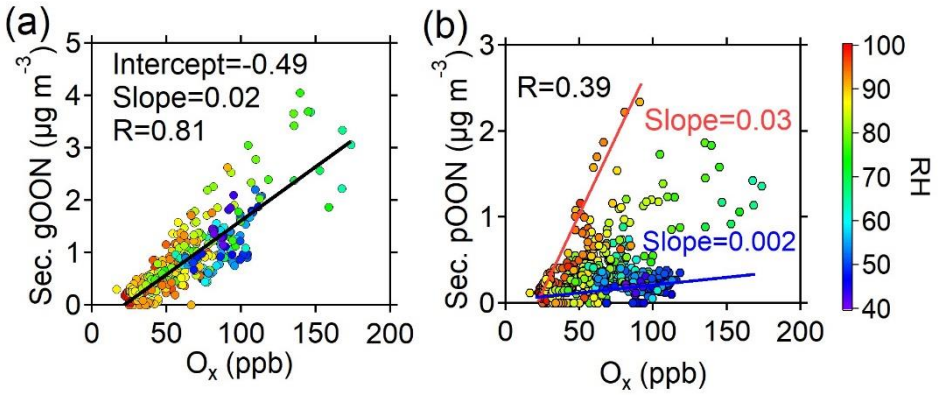

Figure 6. Scatterplots of (a) secondary gOON and (b) secondary pOON versus O_x color-coded using RH during the campaign. The red and blue lines are plotted for guiding eyes.

Furthermore, the lifetime of ~~gON in this study was calculated based on the correlation between secondary gOON and the secondary gON production rate (Liebmann et al., 2019) as shown in Fig. S22b. The roughly estimated lifetime of gON~~gOON in this study can be approximately estimated by a steady-state approach (gOON mixing ratio versus total production rate) as shown in Liebmann et al. (2019). A scatterplot of the secondary gOON versus the secondary gOON production rate at 1 hour time resolution is shown in Fig. S24b. The roughly estimated lifetime of secondary gOON is around 0.54–0.78 h during daytime and nighttime, respectively, which is shorter than the lifetime of alkyl nitrates (~2 ± 3 h) found in the boreal forest (Liebmann et al., 2019). This might be associated with the stronger photolysis, oxidative degradation, and different chemical composition of gOON in urban area compared to boreal forest (Perring et al., 2013). The incomplete measurement of gOON by the CIMS was one of the potential reasons as well. For the lifetime of pOON, a modeling study including explicit formation mechanism as conducted by Lee et al. (2016) is required for systematic explorations in the future.

3.4 Molecular chemical compositions of oxidized organic nitrogen.

In this section, the molecular components of the gOON and pOON measured by the CIMS categorized with different oxygen and carbon atom numbers are briefly discussed. Fig. 7 shows the overview of the distribution of molecular OON during the entire campaign, as well as secondary-dominated period for gOON and biomass burning-dominated period for pOON. In general, the gOON abundance is dominated by C_5-C_8 and C_{10} compounds (65–70%), while the pON shows peaks around C_8 and C_{10} compounds. The highly oxidized molecules (containing at least 6 oxygen atoms) contributed 44% and 71% to gOON and pOON,

respectively. By comparing the ion distribution of total gOON in the whole campaign versus in the period dominated by secondary sources (Fig. 7a), we found that the mass concentration fraction of C_4 compounds in total gOON is much enhanced, while C_6 and C_{10} compounds are significantly decreased. The enhanced C_4 compounds (e.g., $C_4H_7NO_5$ as the most abundant ion in gOON, Fig. ~~S17~~S19) are probably contributed by the isoprene oxidation during the day (Wennberg et al., 2018; Brownwood et al., 2021). The decreases of C_6 and C_{10} compounds in gOON during secondary-dominated period indicate a large fraction of these compounds might come from biomass burning sources. For example, $C_6H_5NO_3$ (nitrophenol and its isomers) in C_6 is the second most (7.4%) abundant compound in gOON. Multiple ambient studies had shown that biomass burning emission can contribute substantially to $C_6H_5NO_3$ (Mohr et al., 2013; Wang et al., 2018), e.g., 58% in Beijing (Song et al., 2021), consistent with the finding shown here.

The almost identical distributions of pOON during the whole campaign and biomass burning-dominated period mainly result from approximate contributions from biomass burning (49% and ~70%, respectively). The C_{10} compounds contribute both high (~22%) in pOON during the whole campaign and biomass burning-dominated period (biomass burning contribution of pOON > 60%, Fig. ~~S23b~~S25b), confirming the important contribution of biomass burning to this type of compounds (Fig. 7b). In pOON, the abundance of $C_{10}H_xNO_y$ ($y \geq 6$) in pOON (19%) is higher than that in gOON (9%), which is reasonable due to their low volatility with multiple functional groups (Odum et al., 1996). ~~The good correlations of the time series between $C_{10}H_xNO_y$ ($y \geq 6$) ions and the biomass burning tracer levoglucosan ($0.52 < R < 0.79$) suggested these ions indeed mainly come from emission or oxidation processes within biomass burning plumes.~~ The extremely oxidized C_{10} compounds (containing at least 8 oxygen atoms) might come from multiple oxidation steps and autoxidation mechanism (Iyer et al., 2021; Zhao et al., 2018; Pye et al., 2019; Shen et al., 2021; Mayorga et al., 2022), demonstrating that the complex secondary formation processes indeed happened within the biomass burning plumes. There are high mass peaks at the positions corresponding to C_{16} and C_{20} species in pOON (Fig. 7b), which are oligomers. These ions might come from direct emission and/or oxidation process in biomass burning plumes, e.g., dimerization of C_8 and C_{10} species (Wu et al., 2021; Lee et al., 2018).

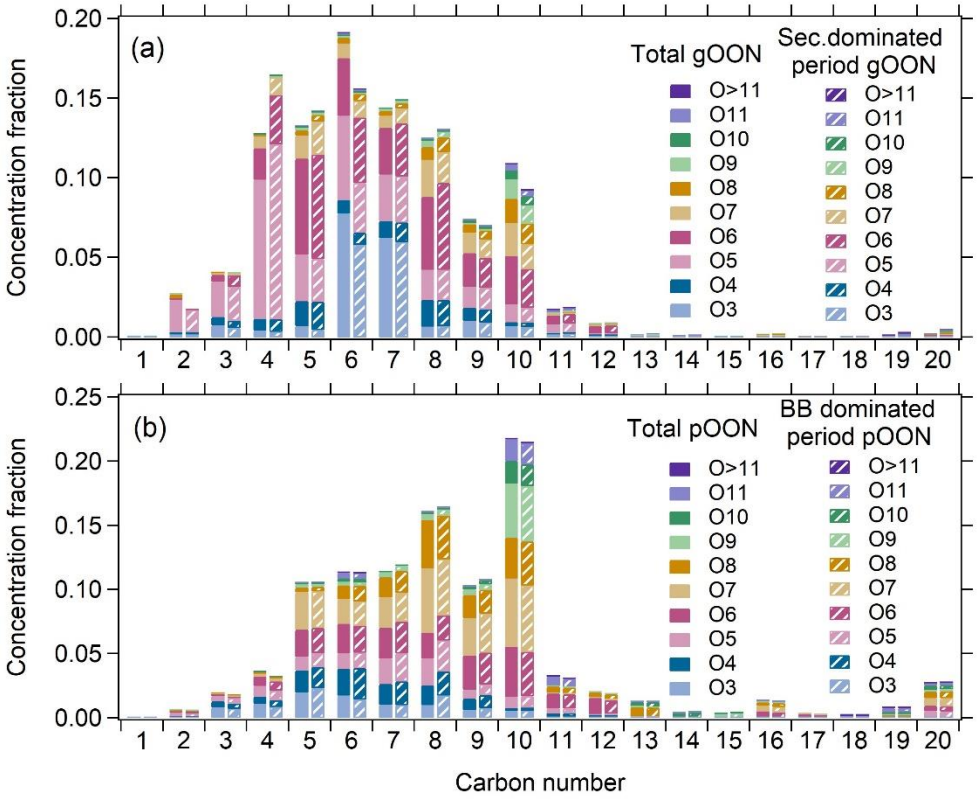

Figure 7. Concentration fractions of (a) gOON categorized based on carbon numbers and oxygen numbers during the whole campaign and the secondary (sec.) formation-dominated period (13:00−15:00) (Fig. ~~S23a~~S25a). Similar plot is displayed for (b) pOON during the whole campaign and the biomass burning (BB) dominated period (19:00−21:00) (Fig. ~~S23b~~S25b).

4 Conclusions

The mass concentrations, sources, and formation mechanism of gas- and particle-phase OON were systematically investigated in a megacity in southern China. The good comparison of pOON measured by AMS and FIGAERO-I-CIMS indicates that the CIMS can measure a fraction of 28 ± 18% of total pOON in this study. Compared to AMS, the missed pOON mass measured by CIMS is probably due to the lack of detection of less-polar OON (keto/alkyl ON) and/or non-nitrogen-containing pOON resulting from the loss of $-NO_2$ group by thermal desorption in CIMS measurement.

Using $C_6H_{10}O_5$ (~90% of levoglucosan) as the biomass burning tracer for source apportionment, almost half of the pOON measured by the CIMS is attributed to biomass burning in this study, underscoring the important contribution of biomass burning to pOON in this urban area. Biomass burning is a very common source across the world. The proposed estimation method in this study might help to clarify the exact biomass burning contribution to OON and their potential atmospheric implication. Note that the sources of the undetected pOON from CIMS are still unknown, which shall be further investigated. The gOON measured by CIMS was mainly produced by secondary formation processes (76%), initiated by OH (42%) and NO_3 (49%) chemistry. The significant contribution of NO_3 chemistry to gOON and potentially to other secondary products, e.g., SOA, was not only observed

in Guangzhou but also in the megacity of Beijing (Hamilton et al., 2021), highlighting the important daytime NO_3 chemistry in urban areas. This indicates that the importance of daytime NO_3 chemistry might not be unique and should be considered in other locations that are impacted by strong anthropogenic emissions. By ranking the precursors of OONs in the ambient atmosphere, monoterpenes are determined to be the most important VOC precursors for secondary gOON formation. Multiple evidences suggest that the monoterpene observed in this study is anthropogenic-origins from VCP source. The monoterpene isomer measurement, which has seldomly been carried out in current Chinese urban areas, is highly recommended for future studies to evaluate the impact of biogenic and anthropogenic emissions (e.g., VCPs) on ozone and other secondary products in the ambient atmosphere.

Furthermore, in this study, it is also found that heterogeneous reactions might contribute substantially to the secondary formation of pOON in urban areas; however, the detailed mechanism and its quantified contribution to pOON in ambient air are still unclear, which warrants further investigation. A thorough comparison between modelled and measured pOON might shed light on this question. Highly functionalized gOON and pOON, as well as oligomers can be formed through multigenerational oxidation and autoxidation during biomass burning plumes, highlighting the complexity of sources and chemical processes in the urban environment. The results of this study provide valuable data and insights to understand the chemistry of reactive organic nitrogen in urban areas.

Data Availability

The data sets (Cai, 2022) used to evaluate the conclusions in the study are available at https://data.mendeley.com/datasets/s8s6wk32fy/1. Figures were made with Igor Pro version 6.37 and Igor Pro version 8.04, available under the Igor Pro license at https://www.wavemetrics.com. The more detailed data can be provided by contacting the corresponding authors.

Competing Interests

The authors declare no conflicts of interest relevant to this study.

Author contributions

YC and CY contributed equally to this work. YC and WH: writing, visualization, and validation; YC, CY, WC, WH, YP, BW, XH, LH, SG, and BY: data curation, methodology; CY, WC, WH, WS, YP, SH, JQ, SW, CW, CW, ZW, BY: experiment, investigation, and formal analysis; WH, BY, MS, and XW: conceptualization, supervision, project administration and funding acquisition.

Acknowledgements

This work was supported by the National Key Research and Development Program of China (2022YFC3701000, 2021YFA1601800), the National Natural Science Foundation of China (grant No 42230701, 41905111), Guangdong Pearl River Talents Program (2019QN01L948), Guangdong Foundation for Program of Science and Technology Research (Grant No. 2019B121205006), Guangdong Foundation for Program of Science and Technology Research (Grant No. 2020B1212060053), State Key Laboratory of Organic Geochemistry, GIGCAS (SKLOG2020−5, SKLOG2020−6). We would like to appreciate Joel A. Thornton and Brett B. Palm for their helpful comments.

Appendices A: Summary of the acronym

Table A1. The summary of the acronym and corresponding full name in this study.

Acronym	Full name	Acronym	Full name
ALWC	aerosol liquid water content	ONs	organic nitrates
$C_{11-20}N$	oxidized organic nitrogen molecules with 11−20 carbon atoms	OON	oxidized organic nitrogen
$C_{4-5}N$	oxidized organic nitrogen molecules with 4−5 carbon atoms	OON_{bb}	oxidized organic nitrogen from biomass burning
$C_{6-9\ Aro}N$	oxidized organic nitrogen molecules with 6−9 carbon atoms and benzene ring	OON_{sec}	oxidized organic nitrogen from secondary formation
$C_{8-10}N$	oxidized organic nitrogen molecules with 8−10 carbon atoms	O_x	odd oxygen, sum of O_3 and NO_2
CHON	oxidized organic nitrogen with only one nitrogen atom	pC_xN	particle-phase C_xN
$CHON_2$	oxidized organic nitrogen with two nitrogen atoms	PMF	positive matrix factorization
CIMS	chemical ionization mass spectrometer	pON	particle-phase organic nitrates
$C_{others}N$	oxidized organic nitrogen molecules not in other four group	pOON	particle-phase oxidized organic nitrogen
C_xN	oxidized organic nitrogen molecules with x carbon atoms	$pOON_{AMS}$	particle-phase oxidized organic nitrogen derived from aerosol mass spectrometer measurement.
dV	voltage difference	$pOON_{CIMS}$	particle-phase oxidized organic nitrogen measured by chemical ionization mass spectrometer
dV_{50}	the voltage at which half the signal is removed (i.e., half of iodide adducts dissociate)	$pOrgNO_{3,\ AMS}$	nitrate functional group from particle-phase oxidized organic nitrogen measured by aerosol mass spectrometer
FIGAERO-I-CIMS	an iodide-adduct chemical ionization mass spectrometer equipped with a Filter Inlet for Gases and AEROsols	$pOrgNO_{3,CIMS}$	nitrate functional group in particle-phase oxidized organic nitrogen based on the data by chemical ionization mass spectrometer
GC-MS/FID	gas chromatography coupled with mass spectrometry and flame ionization detector	PRIDE-GBA	Particles, Radicals, and Intermediates from oxidation of primary Emissions over the Great Bay Area
gON	gas-phase organic nitrates	PTR-ToF-MS	proton transfer reaction time-of-flight mass spectrometry
gOON	gas-phase oxidized organic nitrogen	RH	relative humidity

$gOON_{CIMS}$	gas-phase oxidized organic nitrogen measured by the chemical ionization mass spectrometer	S_0	the relative signal at weakest *dV* compared to the signal under operational *dV*
HR-ToF-AMS	high-resolution time-of-flight aerosol mass spectrometer	TD	thermodenuder
IMR	ion-molecule reaction region	TD-LIF	thermal dissociation laser induced fluorescence
MW	molecular weight	VCP	volatile chemical product
NO_x	Sum of NO and NO_2	VOCs	volatile organic compounds

595

Reference

Andreae, M. O.: Soot Carbon and Excess Fine Potassium: Long-Range Transport of Combustion-Derived Aerosols, Science, 220, 1148-1151, https://doi.org/10.1126/science.220.4602.1148, 1983.

Atkinson, R. and Arey, J.: Atmospheric Degradation of Volatile Organic Compounds, Chem. Rev., 103, 4605-4638, https://doi.org/10.1021/cr0206420, 2003.

Ayres, B. R., Allen, H. M., Draper, D. C., Brown, S. S., Wild, R. J., Jimenez, J. L., Day, D. A., Campuzano-Jost, P., Hu, W., de Gouw, J., Koss, A., Cohen, R. C., Duffey, K. C., Romer, P., Baumann, K., Edgerton, E., Takahama, S., Thornton, J. A., Lee, B. H., Lopez-Hilfiker, F. D., Mohr, C., Wennberg, P. O., Nguyen, T. B., Teng, A., Goldstein, A. H., Olson, K., and Fry, J. L.: Organic nitrate aerosol formation via NO3+ biogenic volatile organic compounds in the southeastern United States, Atmos. Chem. Phys., 15, 13377-13392, https://doi.org/10.5194/acp-15-13377-2015, 2015.

Bai, J., Sun, X., Zhang, C., Xu, Y., and Qi, C.: The OH-initiated atmospheric reaction mechanism and kinetics for levoglucosan emitted in biomass burning, Chemosphere, 93, 2004-2010, https://doi.org/10.1016/j.chemosphere.2013.07.021, 2013.

Bannan, T. J., Le Breton, M., Priestley, M., Worrall, S. D., Bacak, A., Marsden, N. A., Mehra, A., Hammes, J., Hallquist, M., Alfarra, M. R., Krieger, U. K., Reid, J. P., Jayne, J., Robinson, W., McFiggans, G., Coe, H., Percival, C. J., and Topping, D.: A method for extracting calibrated volatility information from the FIGAERO-HR-ToF-CIMS and its experimental application, Atmos. Meas. Tech., 12, 1429-1439, https://doi.org/10.5194/amt-12-1429-2019, 2019.

Bell, D. M., Wu, C., Bertrand, A., Graham, E., Schoonbaert, J., Giannoukos, S., Baltensperger, U., Prevot, A. S. H., Riipinen, I., El Haddad, I., and Mohr, C.: Particle-phase processing of α-pinene NO3 secondary organic aerosol in the dark, Atmos. Chem. Phys. Discuss., 2021, 1-28, https://doi.org/10.5194/acp-2021-379, 2021.

Bhattarai, H., Saikawa, E., Wan, X., Zhu, H., Ram, K., Gao, S., Kang, S., Zhang, Q., Zhang, Y., Wu, G., Wang, X., Kawamura, K., Fu, P., and Cong, Z.: Levoglucosan as a tracer of biomass burning: Recent progress and perspectives, Atmospheric Research, 220, 20-33, https://doi.org/10.1016/j.atmosres.2019.01.004, 2019.

Bi, C., Krechmer, J. E., Frazier, G. O., Xu, W., Lambe, A. T., Claflin, M. S., Lerner, B. M., Jayne, J. T., Worsnop, D. R., Canagaratna, M. R., and Isaacman-VanWertz, G.: Coupling a gas chromatograph simultaneously to a flame ionization detector and chemical ionization mass spectrometer for isomer-resolved measurements of particle-phase organic compounds, Atmos. Meas. Tech., 14, 3895-3907, https://doi.org/10.5194/amt-14-3895-2021, 2021a.

Bi, C., Krechmer, J. E., Frazier, G. O., Xu, W., Lambe, A. T., Claflin, M. S., Lerner, B. M., Jayne, J. T., Worsnop, D. R., Canagaratna, M. R., and Isaacman-VanWertz, G.: Quantification of isomer-resolved iodide chemical ionization mass spectrometry sensitivity and uncertainty using a voltage-scanning approach, Atmos. Meas. Tech., 14, 6835-6850, https://doi.org/10.5194/amt-14-6835-2021, 2021b.

Boyd, C. M., Sanchez, J., Xu, L., Eugene, A. J., Nah, T., Tuet, W. Y., Guzman, M. I., and Ng, N. L.: Secondary organic aerosol formation from the β-pinene+NO3 system: effect of humidity and peroxy radical fate, Atmos. Chem. Phys., 15, 7497-7522, https://doi.org/10.5194/acp-15-7497-2015, 2015.

Brown, S. S. and Stutz, J.: Nighttime radical observations and chemistry, Chem Soc Rev, 41, 6405-6447, https://doi.org/10.1039/c2cs35181a, 2012.

Brownwood, B., Turdziladze, A., Hohaus, T., Wu, R., Mentel, T. F., Carlsson, P. T. M., Tsiligiannis, E., Hallquist, M., Andres, S., Hantschke, L., Reimer, D., Rohrer, F., Tillmann, R., Winter, B., Liebmann, J., Brown, S. S., Kiendler-Scharr, A., Novelli, A., Fuchs, H., and Fry, J. L.: Gas-Particle Partitioning and SOA Yields of Organonitrate Products from NO3-Initiated Oxidation of Isoprene under Varied Chemical Regimes, ACS Earth Space Chem., 5, 785-800, https://doi.org/10.1021/acsearthspacechem.0c00311, 2021.

Cai, Y.: PRIDEGBA_Dataset [Dataset], Mendeley Data, V1, https://doi.org/10.17632/s8s6wk32fy.1, 2022.

Canagaratna, M. R., Jayne, J. T., Jimenez, J. L., Allan, J. D., Alfarra, M. R., Zhang, Q., Onasch, T. B., Drewnick, F., Coe, H., Middlebrook, A., Delia, A., Williams, L. R., Trimborn, A. M., Northway, M. J., DeCarlo, P. F., Kolb, C. E., Davidovits, P., and Worsnop, D. R.: Chemical and microphysical characterization of ambient aerosols with the aerodyne aerosol mass spectrometer, Mass Spectrom. Rev., 26, 185-222, https://doi.org/10.1002/mas.20115, 2007.

Capouet, M. and Müller, J. F.: A group contribution method for estimating the vapour pressures of α-pinene oxidation products, Atmos. Chem. Phys., 6, 1455-1467, https://doi.org/10.5194/acp-6-1455-2006, 2006.

Chen, W., Ye, Y. Q., Hu, W. W., Zhou, H. S., Pan, T. L., Wang, Y. K., Song, W., Song, Q. C., Ye, C. S., Wang, C. M., Wang, B. L., Huang, S., Yuan, B., Zhu, M., Lian, X. F., Zhang, G. H., Bi, X. H., Jiang, F., Liu, J. W., Canonaco, F., Prevot, A. S. H., Shao, M., and Wang, X. M.: Real-Time Characterization of Aerosol Compositions, Sources, and Aging Processes in Guangzhou During PRIDE-GBA 2018 Campaign, J. Geophys. Res.: Atmos., 126, e2021JD035114. , https://doi.org/10.1029/2021JD035114, 2021a.

Chen, X., Wang, H., and Lu, K.: Interpretation of NO3–N2O5 observation via steady state in high-aerosol air mass: the impact of equilibrium coefficient in ambient conditions, Atmos. Chem. Phys., 22, 3525-3533, https://doi.org/10.5194/acp-22-3525-2022, 2022.

Chen, Y., Takeuchi, M., Nah, T., Xu, L., Canagaratna, M. R., Stark, H., Baumann, K., Canonaco, F., Prévôt, A. S. H., Huey, L. G., Weber, R. J., and Ng, N. L.: Chemical characterization of secondary organic aerosol at a rural site in the southeastern US: insights from simultaneous high-resolution time-of-flight aerosol mass spectrometer (HR-ToF-AMS) and FIGAERO chemical ionization mass spectrometer (CIMS) measurements, Atmos. Chem. Phys., 20, 8421-8440, https://doi.org/10.5194/acp-20-8421-2020, 2020.

Chen, Y., Zheng, P., Wang, Z., Pu, W., Tan, Y., Yu, C., Xia, M., Wang, W., Guo, J., Huang, D., Yan, C., Nie, W., Ling, Z., Chen, Q., Lee, S., and Wang, T.: Secondary Formation and Impacts of Gaseous Nitro-Phenolic Compounds in the Continental Outflow Observed at a Background Site in South China, Environ. Sci. Technol., https://doi.org/10.1021/acs.est.1c04596, 2021b.

Cheng, Y., Engling, G., He, K. B., Duan, F. K., Ma, Y. L., Du, Z. Y., Liu, J. M., Zheng, M., and Weber, R. J.: Biomass burning contribution to Beijing aerosol, Atmos. Chem. Phys., 13, 7765-7781, https://doi.org/10.5194/acp-13-7765-2013, 2013.

Coggon, M. M., Gkatzelis, G. I., McDonald, B. C., Gilman, J. B., Schwantes, R. H., Abuhassan, N., Aikin, K. C., Arend, M. F., Berkoff, T. A., Brown, S. S., Campos, T. L., Dickerson, R. R., Gronoff, G., Hurley, J. F., Isaacman-VanWertz, G., Koss, A. R., Li, M., McKeen, S. A., Moshary, F., Peischl, J., Pospisilova, V., Ren, X., Wilson, A., Wu, Y., Trainer, M., and Warneke, C.: Volatile chemical product emissions enhance ozone and modulate urban chemistry, Proc. Natl. Acad. Sci. U. S. A., 118, e2026653118, https://doi.org/10.1073/pnas.2026653118, 2021.

Cubison, M. J., Ortega, A. M., Hayes, P. L., Farmer, D. K., Day, D., Lechner, M. J., Brune, W. H., Apel, E., Diskin, G. S., Fisher, J. A., Fuelberg, H. E., Hecobian, A., Knapp, D. J., Mikoviny, T., Riemer, D., Sachse, G. W., Sessions, W., Weber, R. J., Weinheimer, A. J., Wisthaler, A., and Jimenez, J. L.: Effects of aging on organic aerosol from open biomass burning smoke in aircraft and laboratory studies, Atmos. Chem. Phys., 11, 12049-12064, https://doi.org/10.5194/acp-11-12049-2011, 2011.

Dai, Q., Schulze, B. C., Bi, X., Bui, A. A. T., Guo, F., Wallace, H. W., Sanchez, N. P., Flynn, J. H., Lefer, B. L., Feng, Y., and Griffin, R. J.: Seasonal differences in formation processes of oxidized organic aerosol near Houston, TX, Atmos. Chem. Phys., 19, 9641-9661, 10.5194/acp-19-9641-2019, 2019.

Dancey, C. and Reidy, J.: Statistics without Maths for Psychology, London: Prentice Hall Paerson.2007.

Day, D. A., Liu, S., Russell, L. M., and Ziemann, P. J.: Organonitrate group concentrations in submicron particles with high nitrate and organic fractions in coastal southern California, Atmos. Environ., 44, 1970-1979, https://doi.org/10.1016/j.atmosenv.2010.02.045, 2010.

Day, D. A., Wooldridge, P. J., Dillon, M. B., Thornton, J. A., and Cohen, R. C.: A thermal dissociation laser-induced fluorescence instrument for in situ detection of NO2, peroxy nitrates, alkyl nitrates, and HNO3, Journal of Geophysical Research-Atmospheres, 107, ACH 4-1-ACH 4-14, https://doi.org/10.1029/2001jd000779, 2002.

Day, D. A., Campuzano-Jost, P., Nault, B. A., Palm, B. B., Hu, W., Guo, H., Wooldridge, P. J., Cohen, R. C., Docherty, K. S., Huffman, J. A., de Sá, S. S., Martin, S. T., and Jimenez, J. L.: A systematic re-evaluation of methods for quantification of

bulk particle-phase organic nitrates using real-time aerosol mass spectrometry, Atmos. Meas. Tech., 15, 459-483, https://doi.org/10.5194/amt-15-459-2022, 2022.

de Gouw, J. A., Warneke, C., Stohl, A., Holloway, J., Trainer, M., and Fehsenfeld, F. C.: Emissions and Photochemistry of Oxygenated VOCs in the Outflow from Urban Centers in the Northeastern U.S, 2005/12/1, A31E-05,

DeCarlo, P. F., Kimmel, J. R., Trimborn, A., Northway, M. J., Jayne, J. T., Aiken, A. C., Gonin, M., Fuhrer, K., Horvath, T., Docherty, K. S., Worsnop, D. R., and Jimenez, J. L.: Field-Deployable, High-Resolution, Time-of-Flight Aerosol Mass Spectrometer, Anal. Chem., 78, 8281-8289, https://doi.org/10.1021/ac061249n, 2006.

Ditto, J. C., Machesky, J., and Gentner, D. R.: Analysis of reduced and oxidized nitrogen-containing organic compounds at a coastal site in summer and winter, Atmos. Chem. Phys., 22, 3045-3065, https://doi.org/10.5194/acp-22-3045-2022, 2022.

Farmer, D. K., Matsunaga, A., Docherty, K. S., Surratt, J. D., Seinfeld, J. H., Ziemann, P. J., and Jimenez, J. L.: Response of an aerosol mass spectrometer to organonitrates and organosulfates and implications for atmospheric chemistry, Proc. Natl. Acad. Sci. U. S. A., 107, 6670-6675, https://doi.org/10.1073/pnas.0912340107, 2010.

Farmer, D. K., Perring, A. E., Wooldridge, P. J., Blake, D. R., Baker, A., Meinardi, S., Huey, L. G., Tanner, D., Vargas, O., and Cohen, R. C.: Impact of organic nitrates on urban ozone production, Atmos. Chem. Phys., 11, 4085-4094, https://doi.org/10.5194/acp-11-4085-2011, 2011.

Faxon, C., Hammes, J., Le Breton, M., Pathak, R. K., and Hallquist, M.: Characterization of organic nitrate constituents of secondary organic aerosol (SOA) from nitrate-radical-initiated oxidation of limonene using high-resolution chemical ionization mass spectrometry, Atmos. Chem. Phys., 18, 5467-5481, https://doi.org/10.5194/acp-18-5467-2018, 2018.

Fisher, J. A., Jacob, D. J., Travis, K. R., Kim, P. S., Marais, E. A., Miller, C. C., Yu, K., Zhu, L., Yantosca, R. M., Sulprizio, M. P., Mao, J., Wennberg, P. O., Crounse, J. D., Teng, A. P., Nguyen, T. B., St Clair, J. M., Cohen, R. C., Romer, P., Nault, B. A., Wooldridge, P. J., Jimenez, J. L., Campuzano-Jost, P., Day, D. A., Hu, W., Shepson, P. B., Xiong, F., Blake, D. R., Goldstein, A. H., Misztal, P. K., Hanisco, T. F., Wolfe, G. M., Ryerson, T. B., Wisthaler, A., and Mikoviny, T.: Organic nitrate chemistry and its implications for nitrogen budgets in an isoprene- and monoterpene-rich atmosphere: constraints from aircraft (SEAC(4)RS) and ground-based (SOAS) observations in the Southeast US, Atmos. Chem. Phys., 16, 5969-5991, https://doi.org/10.5194/acp-16-5969-2016, 2016.

Fry, J. L., Draper, D. C., Zarzana, K. J., Campuzano-Jost, P., Day, D. A., Jimenez, J. L., Brown, S. S., Cohen, R. C., Kaser, L., Hansel, A., Cappellin, L., Karl, T., Roux, A. H., Turnipseed, A., Cantrell, C., Lefer, B. L., and Grossberg, N.: Observations of gas- and aerosol-phase organic nitrates at BEACHON-RoMBAS 2011, Atmos. Chem. Phys., 13, 8585-8605, https://doi.org/10.5194/acp-13-8585-2013, 2013.

Fry, J. L., Brown, S. S., Middlebrook, A. M., Edwards, P. M., Campuzano-Jost, P., Day, D. A., Jimenez, J. L., Allen, H. M., Ryerson, T. B., Pollack, I., Graus, M., Warneke, C., de Gouw, J. A., Brock, C. A., Gilman, J., Lerner, B. M., Dubé, W. P., Liao, J., and Welti, A.: Secondary organic aerosol (SOA) yields from NO3 radical + isoprene based on nighttime aircraft power plant plume transects, Atmos. Chem. Phys., 18, 11663-11682, https://doi.org/10.5194/acp-18-11663-2018, 2018.

Gaston, C. J., Lopez-Hilfiker, F. D., Whybrew, L. E., Hadley, O., McNair, F., Gao, H., Jaffe, D. A., and Thornton, J. A.: Online molecular characterization of fine particulate matter in Port Angeles, WA: Evidence for a major impact from residential wood smoke, Atmos. Environ., 138, 99-107, https://doi.org/10.1016/j.atmosenv.2016.05.013, 2016.

George, C., Ammann, M., D'Anna, B., Donaldson, D. J., and Nizkorodov, S. A.: Heterogeneous photochemistry in the atmosphere, Chem. Rev., 115, 4218-4258, https://doi.org/10.1021/cr500648z, 2015.

George, I. J. and Abbatt, J. P.: Heterogeneous oxidation of atmospheric aerosol particles by gas-phase radicals, Nature Chemistry, 2, 713-722, https://doi.org/10.1038/nchem.806, 2010.

Gilman, J. B., Lerner, B. M., Kuster, W. C., Goldan, P. D., Warneke, C., Veres, P. R., Roberts, J. M., de Gouw, J. A., Burling, I. R., and Yokelson, R. J.: Biomass burning emissions and potential air quality impacts of volatile organic compounds and other trace gases from fuels common in the US, Atmos. Chem. Phys., 15, 13915-13938, https://doi.org/10.5194/acp-15-13915-2015, 2015.

Gkatzelis, G. I., Coggon, M. M., McDonald, B. C., Peischl, J., Aikin, K. C., Gilman, J. B., Trainer, M., and Warneke, C.: Identifying Volatile Chemical Product Tracer Compounds in U.S. Cities, Environ. Sci. Technol., 55, 188-199, https://doi.org/10.1021/acs.est.0c05467, 2021.

Gross, S., Iannone, R., Xiao, S., and Bertram, A. K.: Reactive uptake studies of NO3 and N2O5 on alkenoic acid, alkanoate, and polyalcohol substrates to probe nighttime aerosol chemistry, Phys. Chem. Chem. Phys., 11, 7792-7803, https://doi.org/10.1039/B904741G, 2009.

Hamilton, J. F., Bryant, D. J., Edwards, P. M., Ouyang, B., Bannan, T. J., Mehra, A., Mayhew, A. W., Hopkins, J. R., Dunmore, R. E., Squires, F. A., Lee, J. D., Newland, M. J., Worrall, S. D., Bacak, A., Coe, H., Percival, C., Whalley, L. K., Heard, D. E., Slater, E. J., Jones, R. L., Cui, T., Surratt, J. D., Reeves, C. E., Mills, G. P., Grimmond, S., Sun, Y., Xu, W., Shi, Z., and Rickard, A. R.: Key Role of NO3 Radicals in the Production of Isoprene Nitrates and Nitrooxyorganosulfates in Beijing, Environ. Sci. Technol., 55, 842-853, https://doi.org/10.1021/acs.est.0c05689, 2021.

Hao, L. Q., Kortelainen, A., Romakkaniemi, S., Portin, H., Jaatinen, A., Leskinen, A., Komppula, M., Miettinen, P., Sueper, D., Pajunoja, A., Smith, J. N., Lehtinen, K. E. J., Worsnop, D. R., Laaksonen, A., and Virtanen, A.: Atmospheric submicron aerosol composition and particulate organic nitrate formation in a boreal forestland–urban mixed region, Atmos. Chem. Phys., 14, 13483-13495, https://doi.org/10.5194/acp-14-13483-2014, 2014.

Harrison, R. M., Tilling, R., Callén Romero, M. a. S., Harrad, S., and Jarvis, K.: A study of trace metals and polycyclic aromatic hydrocarbons in the roadside environment, Atmos. Environ., 37, 2391-2402, https://doi.org/10.1016/S1352-2310(03)00122-5, 2003.

Hayes, P. L., Ortega, A. M., Cubison, M. J., Froyd, K. D., Zhao, Y., Cliff, S. S., Hu, W. W., Toohey, D. W., Flynn, J. H., Lefer, B. L., Grossberg, N., Alvarez, S., Rappenglück, B., Taylor, J. W., Allan, J. D., Holloway, J. S., Gilman, J. B., Kuster, W. C., de Gouw, J. A., Massoli, P., Zhang, X., Liu, J., Weber, R. J., Corrigan, A. L., Russell, L. M., Isaacman, G., Worton, D. R., Kreisberg, N. M., Goldstein, A. H., Thalman, R., Waxman, E. M., Volkamer, R., Lin, Y. H., Surratt, J. D., Kleindienst, T. E., Offenberg, J. H., Dusanter, S., Griffith, S., Stevens, P. S., Brioude, J., Angevine, W. M., and Jimenez, J. L.: Organic aerosol composition and sources in Pasadena, California, during the 2010 CalNex campaign, J. Geophys. Res.: Atmos., 118, 9233-9257, 10.1002/jgrd.50530, 2013.

He, Q., Tomaz, S., Li, C., Zhu, M., Meidan, D., Riva, M., Laskin, A., Brown, S. S., George, C., Wang, X., and Rudich, Y.: Optical Properties of Secondary Organic Aerosol Produced by Nitrate Radical Oxidation of Biogenic Volatile Organic Compounds, Environ. Sci. Technol., 55, 2878-2889, https://doi.org/10.1021/acs.est.0c06838, 2021.

Hellén, H., Tykkä, T., and Hakola, H.: Importance of monoterpenes and isoprene in urban air in northern Europe, Atmos. Environ., 59, 59-66, https://doi.org/10.1016/j.atmosenv.2012.04.049, 2012.

Hennigan, C. J., Sullivan, A. P., Collett, J. L., and Robinson, A. L.: Levoglucosan stability in biomass burning particles exposed to hydroxyl radicals, Geophys. Res. Lett., 37, n/a-n/a, https://doi.org/10.1029/2010gl043088, 2010.

Hilas, C. S., Goudos, S. K., and Sahalos, J. N.: Seasonal decomposition and forecasting of telecommunication data: A comparative case study, Technological Forecasting and Social Change, 73, 495-509, https://doi.org/10.1016/j.techfore.2005.07.002, 2006.

Hoffmann, D., Tilgner, A., Iinuma, Y., and Herrmann, H.: Atmospheric Stability of Levoglucosan: A Detailed Laboratory and Modeling Study, Environ. Sci. Technol., 44, 694-699, https://doi.org/10.1021/es902476f, 2010.

Hu, W., Hu, M., Hu, W., Jimenez, J. L., Yuan, B., Chen, W., Wang, M., Wu, Y., Chen, C., Wang, Z., Peng, J., Zeng, L., and Shao, M.: Chemical composition, sources, and aging process of submicron aerosols in Beijing: Contrast between summer and winter, J. Geophys. Res.: Atmos., 121, 1955-1977, 10.1002/2015jd024020, 2016.

Huang, W., Saathoff, H., Shen, X., Ramisetty, R., Leisner, T., and Mohr, C.: Chemical Characterization of Highly Functionalized Organonitrates Contributing to Night-Time Organic Aerosol Mass Loadings and Particle Growth, Environ. Sci. Technol., 53, 1165-1174, https://doi.org/10.1021/acs.est.8b05826, 2019.

Huffman, J. A., Ziemann, P. J., Jayne, J. T., Worsnop, D. R., and Jimenez, J. L.: Development and Characterization of a Fast-Stepping/Scanning Thermodenuder for Chemically-Resolved Aerosol Volatility Measurements, Aerosol Sci. Technol., 42, 395-407, https://doi.org/10.1080/02786820802104981, 2008.

Isaacman-VanWertz, G., Massoli, P., O'Brien, R., Lim, C., Franklin, J. P., Moss, J. A., Hunter, J. F., Nowak, J. B., Canagaratna, M. R., Misztal, P. K., Arata, C., Roscioli, J. R., Herndon, S. T., Onasch, T. B., Lambe, A. T., Jayne, J. T., Su, L., Knopf, D. A., Goldstein, A. H., Worsnop, D. R., and Kroll, J. H.: Chemical evolution of atmospheric organic carbon over multiple generations of oxidation, Nature Chemistry, 10, 462-468, https://doi.org/10.1038/s41557-018-0002-2, 2018.

Iyer, S., Lopez-Hilfiker, F., Lee, B. H., Thornton, J. A., and Kurtén, T.: Modeling the Detection of Organic and Inorganic Compounds Using Iodide-Based Chemical Ionization, The Journal of Physical Chemistry A, 120, 576-587, https://doi.org/10.1021/acs.jpca.5b09837, 2016.

Iyer, S., Rissanen, M. P., Valiev, R., Barua, S., Krechmer, J. E., Thornton, J., Ehn, M., and Kurtén, T.: Molecular mechanism for rapid autoxidation in α-pinene ozonolysis, Nat. Commun., 12, 878., https://doi.org/10.1038/s41467-021-21172-w, 2021.

Jiang, F., Liu, J., Cheng, Z., Ding, P., Zhu, S., Yuan, X., Chen, W., Zhang, Z., Zong, Z., Tian, C., Hu, W., Zheng, J., Szidat, S., Li, J., and Zhang, G.: Quantitative evaluation for the sources and aging processes of organic aerosols in urban

Guangzhou: Insights from a comprehensive method of dual-carbon isotopes and macro tracers, Sci Total Environ, 164182, https://doi.org/10.1016/j.scitotenv.2023.164182, 2023.

Juncosa Calahorrano, J. F., Lindaas, J., O'Dell, K., Palm, B. B., Peng, Q., Flocke, F., Pollack, I. B., Garofalo, L. A., Farmer, D. K., Pierce, J. R., Collett Jr, J. L., Weinheimer, A., Campos, T., Hornbrook, R. S., Hall, S. R., Ullmann, K., Pothier, M. A., Apel, E. C., Permar, W., Hu, L., Hills, A. J., Montzka, D., Tyndall, G., Thornton, J. A., and Fischer, E. V.: Daytime Oxidized Reactive Nitrogen Partitioning in Western U.S. Wildfire Smoke Plumes, J. Geophys. Res.: Atmos., 126, e2020JD033484, https://doi.org/10.1029/2020JD033484, 2021.

Keehan, N. I., Brownwood, B., Marsavin, A., Day, D. A., and Fry, J. L.: A thermal-dissociation–cavity ring-down spectrometer (TD-CRDS) for the detection of organic nitrates in gas and particle phases, Atmos. Meas. Tech., 13, 6255-6269, https://doi.org/10.5194/amt-13-6255-2020, 2020.

Kiendler-Scharr, A., Mensah, A. A., Friese, E., Topping, D., Nemitz, E., Prevot, A. S. H., Äijälä, M., Allan, J., Canonaco, F., Canagaratna, M., Carbone, S., Crippa, M., Dall Osto, M., Day, D. A., De Carlo, P., Di Marco, C. F., Elbern, H., Eriksson, A., Freney, E., Hao, L., Herrmann, H., Hildebrandt, L., Hillamo, R., Jimenez, J. L., Laaksonen, A., McFiggans, G., Mohr, C., O'Dowd, C., Otjes, R., Ovadnevaite, J., Pandis, S. N., Poulain, L., Schlag, P., Sellegri, K., Swietlicki, E., Tiitta, P., Vermeulen, A., Wahner, A., Worsnop, D., and Wu, H. C.: Ubiquity of organic nitrates from nighttime chemistry in the European submicron aerosol, Geophys. Res. Lett., 43, 7735-7744, https://doi.org/10.1002/2016gl069239, 2016.

Koch, B. P. and Dittmar, T.: From mass to structure: an aromaticity index for high-resolution mass data of natural organic matter, Rapid Commun. Mass Spectrom., 20, 926-932, https://doi.org/10.1002/rcm.2386, 2006.

Koch, B. P. and Dittmar, T.: From mass to structure: an aromaticity index for high-resolution mass data of natural organic matter, Rapid Commun. Mass Spectrom., 30, 250-250, https://doi.org/10.1002/rcm.7433, 2016.

Kodros, J. K., Papanastasiou, D. K., Paglione, M., Masiol, M., Squizzato, S., Florou, K., Skyllakou, K., Kaltsonoudis, C., Nenes, A., and Pandis, S. N.: Rapid dark aging of biomass burning as an overlooked source of oxidized organic aerosol, Proc. Natl. Acad. Sci. U. S. A., 117, 33028-33033, https://doi.org/10.1073/pnas.2010365117, 2020.

Krecl, P., Johansson, C., Targino, A. C., Ström, J., and Burman, L.: Trends in black carbon and size-resolved particle number concentrations and vehicle emission factors under real-world conditions, Atmos. Environ., 165, 155-168, https://doi.org/10.1016/j.atmosenv.2017.06.036, 2017.

Kroll, J. H. and Seinfeld, J. H.: Chemistry of secondary organic aerosol: Formation and evolution of low-volatility organics in the atmosphere, Atmos. Environ., 42, 3593-3624, https://doi.org/10.1016/j.atmosenv.2008.01.003, 2008.

Lai, C., Liu, Y., Ma, J., Ma, Q., and He, H.: Degradation kinetics of levoglucosan initiated by hydroxyl radical under different environmental conditions, Atmos. Environ., 91, 32-39, https://doi.org/10.1016/j.atmosenv.2014.03.054, 2014.

Lanz, V. A., Prévôt, A. S. H., Alfarra, M. R., Weimer, S., Mohr, C., DeCarlo, P. F., Gianini, M. F. D., Hueglin, C., Schneider, J., Favez, O., D'Anna, B., George, C., and Baltensperger, U.: Characterization of aerosol chemical composition with aerosol mass spectrometry in Central Europe: an overview, Atmos. Chem. Phys., 10, 10453-10471, https://doi.org/10.5194/acp-10-10453-2010, 2010.

Le Breton, M., Psichoudaki, M., Hallquist, M., Watne, Å. K., Lutz, A., and Hallquist, Å. M.: Application of a FIGAERO ToF CIMS for on-line characterization of real-world fresh and aged particle emissions from buses, Aerosol Sci. Technol., 53, 244-259, https://doi.org/10.1080/02786826.2019.1566592, 2019.

Lee, A. K. Y., Adam, M. G., Liggio, J., Li, S.-M., Li, K., Willis, M. D., Abbatt, J. P. D., Tokarek, T. W., Odame-Ankrah, C. A., Osthoff, H. D., Strawbridge, K., and Brook, J. R.: A large contribution of anthropogenic organo-nitrates to secondary organic aerosol in the Alberta oil sands, Atmos. Chem. Phys., 19, 12209-12219, https://doi.org/10.5194/acp-19-12209-2019, 2019.

Lee, B. H., Lopez-Hilfiker, F. D., Mohr, C., Kurten, T., Worsnop, D. R., and Thornton, J. A.: An iodide-adduct high-resolution time-of-flight chemical-ionization mass spectrometer: application to atmospheric inorganic and organic compounds, Environ. Sci. Technol., 48, 6309-6317, https://doi.org/10.1021/es500362a, 2014.

Lee, B. H., Lopez-Hilfiker, F. D., D'Ambro, E. L., Zhou, P., Boy, M., Petäjä, T., Hao, L., Virtanen, A., and Thornton, J. A.: Semi-volatile and highly oxygenated gaseous and particulate organic compounds observed above a boreal forest canopy, Atmos. Chem. Phys., 18, 11547-11562, https://doi.org/10.5194/acp-18-11547-2018, 2018.

Lee, B. H., Mohr, C., Lopez-Hilfiker, F. D., Lutz, A., Hallquist, M., Lee, L., Romer, P., Cohen, R. C., Iyer, S., Kurten, T., Hu, W., Day, D. A., Campuzano-Jost, P., Jimenez, J. L., Xu, L., Ng, N. L., Guo, H., Weber, R. J., Wild, R. J., Brown, S. S., Koss, A., de Gouw, J., Olson, K., Goldstein, A. H., Seco, R., Kim, S., McAvey, K., Shepson, P. B., Starn, T., Baumann, K., Edgerton, E. S., Liu, J., Shilling, J. E., Miller, D. O., Brune, W., Schobesberger, S., D'Ambro, E. L., and Thornton, J. A.: Highly functionalized organic nitrates in the southeast United States: Contribution to secondary organic aerosol and reactive nitrogen budgets, Proc. Natl. Acad. Sci. U. S. A., 113, 1516-1521, https://doi.org/10.1073/pnas.1508108113, 2016.

Lee, C. P., Surdu, M., Bell, D. M., Lamkaddam, H., Wang, M., Ataei, F., Hofbauer, V., Lopez, B., Donahue, N. M., Dommen, J., Prevot, A. S. H., Slowik, J. G., Wang, D., Baltensperger, U., and El Haddad, I.: Effects of aerosol size and coating thickness on the molecular detection using extractive electrospray ionization, Atmos. Meas. Tech., 14, 5913-5923, https://doi.org/10.5194/amt-14-5913-2021, 2021.

Lee, L., Wooldridge, P. J., deGouw, J., Brown, S. S., Bates, T. S., Quinn, P. K., and Cohen, R. C.: Particulate organic nitrates observed in an oil and natural gas production region during wintertime, Atmos. Chem. Phys., 15, 9313-9325, https://doi.org/10.5194/acp-15-9313-2015, 2015.

Li, T., Wang, Z., Yuan, B., Ye, C., Lin, Y., Wang, S., Sha, Q. e., Yuan, Z., Zheng, J., and Shao, M.: Emissions of carboxylic acids, hydrogen cyanide (HCN) and isocyanic acid (HNCO) from vehicle exhaust, Atmos. Environ., 247, 118218., https://doi.org/10.1016/j.atmosenv.2021.118218, 2021a.

Li, X. B., Yuan, B., Wang, S., Wang, C., Lan, J., Liu, Z., Song, Y., He, X., Huangfu, Y., Pei, C., Cheng, P., Yang, S., Qi, J., Wu, C., Huang, S., You, Y., Chang, M., Zheng, H., Yang, W., Wang, X., and Shao, M.: Variations and sources of volatile organic compounds (VOCs) in urban region: insights from measurements on a tall tower, Atmos. Chem. Phys., 22, 10567-10587, https://doi.org/10.5194/acp-22-10567-2022, 2022.

Li, Y., Fu, T. M., Yu, J. Z., Feng, X., Zhang, L., Chen, J., Boreddy, S. K. R., Kawamura, K., Fu, P., Yang, X., Zhu, L., and Zeng, Z.: Impacts of Chemical Degradation on the Global Budget of Atmospheric Levoglucosan and Its Use As a Biomass Burning Tracer, Environ. Sci. Technol., 55, 5525-5536, https://doi.org/10.1021/acs.est.0c07313, 2021b.

Liebmann, J., Sobanski, N., Schuladen, J., Karu, E., Hellén, H., Hakola, H., Zha, Q., Ehn, M., Riva, M., Heikkinen, L., Williams, J., Fischer, H., Lelieveld, J., and Crowley, J. N.: Alkyl nitrates in the boreal forest: formation via the NO3-, OH- and O3 induced oxidation of biogenic volatile organic compounds and ambient lifetimes, Atmos. Chem. Phys., 19, 10391-10403, https://doi.org/10.5194/acp-19-10391-2019, 2019.

Lim, Y. B. and Ziemann, P. J.: Chemistry of Secondary Organic Aerosol Formation from OH Radical-Initiated Reactions of Linear, Branched, and Cyclic Alkanes in the Presence of NOx, Aerosol Sci. Technol., 43, 604-619, https://doi.org/10.1080/02786820902802567, 2009.

Lin, P., Bluvshtein, N., Rudich, Y., Nizkorodov, S. A., Laskin, J., and Laskin, A.: Molecular Chemistry of Atmospheric Brown Carbon Inferred from a Nationwide Biomass Burning Event, Environ. Sci. Technol., 51, 11561-11570, https://doi.org/10.1021/acs.est.7b02276, 2017.

Liu, X., Huey, L. G., Yokelson, R. J., Selimovic, V., Simpson, I. J., Müller, M., Jimenez, J. L., Campuzano-Jost, P., Beyersdorf, A. J., Blake, D. R., Butterfield, Z., Choi, Y., Crounse, J. D., Day, D. A., Diskin, G. S., Dubey, M. K., Fortner, E., Hanisco, T. F., Hu, W., King, L. E., Kleinman, L., Meinardi, S., Mikoviny, T., Onasch, T. B., Palm, B. B., Peischl, J., Pollack, I. B., Ryerson, T. B., Sachse, G. W., Sedlacek, A. J., Shilling, J. E., Springston, S., St. Clair, J. M., Tanner, D. J., Teng, A. P., Wennberg, P. O., Wisthaler, A., and Wolfe, G. M.: Airborne measurements of western U.S. wildfire emissions: Comparison with prescribed burning and air quality implications, J. Geophys. Res.: Atmos., 122, 6108-6129, https://doi.org/10.1002/2016jd026315, 2017.

Lopez-Hilfiker, F., Mohr, C., Ehn, M., Rubach, F., Kleist, E., Wildt, J., Mentel, T., Lutz, A., Hallquist, M., Worsnop, D., and Thornton, J.: A novel method for online analysis of gas and particle composition: description and evaluation of a Filter Inlet for Gases and AEROsols (FIGAERO), Atmos. Meas. Tech., 7, 983–1001, https://doi.org/10.5194/amt-7-983-2014, 2014.

Lopez-Hilfiker, F. D., Iyer, S., Mohr, C., Lee, B. H., D'Ambro, E. L., Kurtén, T., and Thornton, J. A.: Constraining the sensitivity of iodide adduct chemical ionization mass spectrometry to multifunctional organic molecules using the collision limit and thermodynamic stability of iodide ion adducts, Atmos. Meas. Tech., 9, 1505-1512, https://doi.org/10.5194/amt-9-1505-2016, 2016.

Lopez-Hilfiker, F. D., Pospisilova, V., Huang, W., Kalberer, M., Mohr, C., Stefenelli, G., Thornton, J. A., Baltensperger, U., Prevot, A. S. H., and Slowik, J. G.: An extractive electrospray ionization time-of-flight mass spectrometer (EESI-TOF) for online measurement of atmospheric aerosol particles, Atmos. Meas. Tech., 12, 4867-4886, https://doi.org/10.5194/amt-12-4867-2019, 2019.

Mao, J., Ren, X., Brune, W. H., Olson, J. R., Crawford, J. H., Fried, A., Huey, L. G., Cohen, R. C., Heikes, B., Singh, H. B., Blake, D. R., Sachse, G. W., Diskin, G. S., Hall, S. R., and Shetter, R. E.: Airborne measurement of OH reactivity during INTEX-B, Atmos. Chem. Phys., 9, 163-173, https://doi.org/10.5194/acp-9-163-2009, 2009.

Matsunaga, A. and Ziemann, P. J.: Yields of beta-hydroxynitrates, dihydroxynitrates, and trihydroxynitrates formed from OH radical-initiated reactions of 2-methyl-1-alkenes, Proc. Natl. Acad. Sci. U. S. A., 107, 6664-6669, https://doi.org/10.1073/pnas.0910585107, 2010.

Mayhew, A. W., Lee, B. H., Thornton, J. A., Bannan, T. J., Brean, J., Hopkins, J. R., Lee, J. D., Nelson, B. S., Percival, C., Rickard, A. R., Shaw, M. D., Edwards, P. M., and Hamilton, J. F.: Evaluation of isoprene nitrate chemistry in detailed chemical mechanisms, Atmos. Chem. Phys., 22, 14783-14798, https://doi.org/10.5194/acp-22-14783-2022, 2022.

Mayorga, R., Xia, Y., Zhao, Z., Long, B., and Zhang, H.: Peroxy Radical Autoxidation and Sequential Oxidation in Organic Nitrate Formation during Limonene Nighttime Oxidation, Environ. Sci. Technol., https://doi.org/10.1021/acs.est.2c04030, 2022.

McKay, M. D., Beckman, R. J., and Conover, W. J.: A Comparison of Three Methods for Selecting Values of Input Variables in the Analysis of Output From a Computer Code, Technometrics, 42, 55-61, https://doi.org/10.1080/00401706.2000.10485979, 2000.

Mohr, C., Huffman, J. A., Cubison, M. J., Aiken, A. C., Docherty, K. S., Kimmel, J. R., Ulbrich, I. M., Hannigan, M., and Jimenez, J. L.: Characterization of Primary Organic Aerosol Emissions from Meat Cooking, Trash Burning, and Motor Vehicles with High-Resolution Aerosol Mass Spectrometry and Comparison with Ambient and Chamber Observations, Environ. Sci. Technol., 43, 2443-2449, https://doi.org/10.1021/es8011518, 2009.

Mohr, C., Lopez-Hilfiker, F. D., Zotter, P., Prévôt, A. S. H., Xu, L., Ng, N. L., Herndon, S. C., Williams, L. R., Franklin, J. P., Zahniser, M. S., Worsnop, D. R., Knighton, W. B., Aiken, A. C., Gorkowski, K. J., Dubey, M. K., Allan, J. D., and Thornton, J. A.: Contribution of Nitrated Phenols to Wood Burning Brown Carbon Light Absorption in Detling, United Kingdom during Winter Time, Environ. Sci. Technol., 47, 6316-6324, https://doi.org/10.1021/es400683v, 2013.

Nault, B. A., Jo, D. S., McDonald, B. C., Campuzano-Jost, P., Day, D. A., Hu, W., Schroder, J. C., Allan, J., Blake, D. R., Canagaratna, M. R., Coe, H., Coggon, M. M., DeCarlo, P. F., Diskin, G. S., Dunmore, R., Flocke, F., Fried, A., Gilman, J. B., Gkatzelis, G., Hamilton, J. F., Hanisco, T. F., Hayes, P. L., Henze, D. K., Hodzic, A., Hopkins, J., Hu, M., Huey, L. G., Jobson, B. T., Kuster, W. C., Lewis, A., Li, M., Liao, J., Nawaz, M. O., Pollack, I. B., Peischl, J., Rappenglück, B., Reeves, C. E., Richter, D., Roberts, J. M., Ryerson, T. B., Shao, M., Sommers, J. M., Walega, J., Warneke, C., Weibring, P., Wolfe, G. M., Young, D. E., Yuan, B., Zhang, Q., de Gouw, J. A., and Jimenez, J. L.: Secondary organic aerosols from anthropogenic volatile organic compounds contribute substantially to air pollution mortality, Atmos. Chem. Phys., 21, 11201-11224, 10.5194/acp-21-11201-2021, 2021.

Ng, N. L., Brown, S. S., Archibald, A. T., Atlas, E., Cohen, R. C., Crowley, J. N., Day, D. A., Donahue, N. M., Fry, J. L., Fuchs, H., Griffin, R. J., Guzman, M. I., Herrmann, H., Hodzic, A., Iinuma, Y., Jimenez, J. L., Kiendler-Scharr, A., Lee, B. H., Luecken, D. J., Mao, J., McLaren, R., Mutzel, A., Osthoff, H. D., Ouyang, B., Picquet-Varrault, B., Platt, U., Pye, H. O. T., Rudich, Y., Schwantes, R. H., Shiraiwa, M., Stutz, J., Thornton, J. A., Tilgner, A., Williams, B. J., and Zaveri, R. A.: Nitrate radicals and biogenic volatile organic compounds: oxidation, mechanisms, and organic aerosol, Atmos. Chem. Phys., 17, 2103-2162, https://doi.org/10.5194/acp-17-2103-2017, 2017.

Odum, J. R., Hoffmann, T., Bowman, F., Collins, D., Flagan, R. C., and Seinfeld, J. H.: Gas/Particle Partitioning and Secondary Organic Aerosol Yields, Environ. Sci. Technol., 30, 2580-2585, https://doi.org/10.1021/es950943+, 1996.

Pagonis, D., Krechmer, J. E., de Gouw, J., Jimenez, J. L., and Ziemann, P. J.: Effects of gas–wall partitioning in Teflon tubing and instrumentation on time-resolved measurements of gas-phase organic compounds, Atmos. Meas. Tech., 10, 4687-4696, https://doi.org/10.5194/amt-10-4687-2017, 2017.

Palm, B. B., Liu, X., Jimenez, J. L., and Thornton, J. A.: Performance of a new coaxial ion–molecule reaction region for low-pressure chemical ionization mass spectrometry with reduced instrument wall interactions, Atmos. Meas. Tech., 12, 5829-5844, https://doi.org/10.5194/amt-12-5829-2019, 2019.

Palm, B. B., Peng, Q., Fredrickson, C. D., Lee, B. H., Garofalo, L. A., Pothier, M. A., Kreidenweis, S. M., Farmer, D. K., Pokhrel, R. P., Shen, Y., Murphy, S. M., Permar, W., Hu, L., Campos, T. L., Hall, S. R., Ullmann, K., Zhang, X., Flocke, F., Fischer, E. V., and Thornton, J. A.: Quantification of organic aerosol and brown carbon evolution in fresh wildfire plumes, Proc. Natl. Acad. Sci. U. S. A., 117, 29469-29477, https://doi.org/10.1073/pnas.2012218117, 2020.

Peng, Q., Palm, B. B., Fredrickson, C. D., Lee, B. H., Hall, S. R., Ullmann, K., Campos, T., Weinheimer, A. J., Apel, E. C., Flocke, F., Permar, W., Hu, L., Garofalo, L. A., Pothier, M. A., Farmer, D. K., Ku, I. T., Sullivan, A. P., Collett, J. L., Fischer, E., and Thornton, J. A.: Observations and Modeling of NOx Photochemistry and Fate in Fresh Wildfire Plumes, ACS Earth Space Chem., https://doi.org/10.1021/acsearthspacechem.1c00086, 2021.

Perring, A. E., Pusede, S. E., and Cohen, R. C.: An observational perspective on the atmospheric impacts of alkyl and multifunctional nitrates on ozone and secondary organic aerosol, Chem. Rev., 113, 5848-5870, https://doi.org/10.1021/cr300520x, 2013.

Pospisilova, V., Lopez-Hilfiker., F. D., Bell., D. M., Haddad., I. E., Mohr., C., Huang., W., Heikkinen., L., Xiao., M., Dommen., J., Prevot., A. S. H., Baltensperger., U., and Slowik., J. G.: On the fate of oxygenated organic molecules in atmospheric aerosol particles, Sci. Adv., 6, eaax8922, https://doi.org/10.1126/sciadv.aax8922, 2020.

Pye, H. O., Luecken, D. J., Xu, L., Boyd, C. M., Ng, N. L., Baker, K. R., Ayres, B. R., Bash, J. O., Baumann, K., Carter, W. P., Edgerton, E., Fry, J. L., Hutzell, W. T., Schwede, D. B., and Shepson, P. B.: Modeling the Current and Future Roles of Particulate Organic Nitrates in the Southeastern United States, Environ. Sci. Technol., 49, 14195-14203, https://doi.org/10.1021/acs.est.5b03738, 2015.

Pye, H. O. T., D'Ambro, E. L., Lee, B. H., Schobesberger, S., Takeuchi, M., Zhao, Y., Lopez-Hilfiker, F., Liu, J., Shilling, J. E., Xing, J., Mathur, R., Middlebrook, A. M., Liao, J., Welti, A., Graus, M., Warneke, C., de Gouw, J. A., Holloway, J. S., Ryerson, T. B., Pollack, I. B., and Thornton, J. A.: Anthropogenic enhancements to production of highly oxygenated molecules from autoxidation, Proc. Natl. Acad. Sci. U. S. A., 116, 6641-6646, https://doi.org/10.1073/pnas.1810774116, 2019.

Reeves, C. E., Mills, G. P., Whalley, L. K., Acton, W. J. F., Bloss, W. J., Crilley, L. R., Grimmond, S., Heard, D. E., Hewitt, C. N., Hopkins, J. R., Kotthaus, S., Kramer, L. J., Jones, R. L., Lee, J. D., Liu, Y., Ouyang, B., Slater, E., Squires, F., Wang, X., Woodward-Massey, R., and Ye, C.: Observations of speciated isoprene nitrates in Beijing: implications for isoprene chemistry, Atmos. Chem. Phys. Discuss., Preprint, https://doi.org/10.5194/acp-2019-964, 2020.

Robinson, M. A., Neuman, J. A., Huey, L. G., Roberts, J. M., Brown, S. S., and Veres, P. R.: Temperature-dependent sensitivity of iodide chemical ionization mass spectrometers, Atmos. Meas. Tech., 15, 4295-4305, https://doi.org/10.5194/amt-15-4295-2022, 2022.

Rollins, A. W., Smith, J. D., Wilson, K. R., and Cohen, R. C.: Real Time In Situ Detection of Organic Nitrates in Atmospheric Aerosols, Environ. Sci. Technol., 44, 5540-5545, https://doi.org/10.1021/es100926x, 2010.

Rollins, A. W., Browne, E. C., Min, K. E., Pusede, S. E., Wooldridge, P. J., Gentner, D. R., Goldstein, A. H., Liu, S., Day, D. A., Russell, L. M., and Cohen, R. C.: Evidence for NO(x) control over nighttime SOA formation, Science, 337, 1210-1212, https://doi.org/10.1126/science.1221520, 2012.

Romer Present, P. S., Zare, A., and Cohen, R. C.: The changing role of organic nitrates in the removal and transport of NOx, Atmos. Chem. Phys., 20, 267-279, https://doi.org/10.5194/acp-20-267-2020, 2020.

Romer, P. S., Duffey, K. C., Wooldridge, P. J., Allen, H. M., Ayres, B. R., Brown, S. S., Brune, W. H., Crounse, J. D., de Gouw, J., Draper, D. C., Feiner, P. A., Fry, J. L., Goldstein, A. H., Koss, A., Misztal, P. K., Nguyen, T. B., Olson, K., Teng, A. P., Wennberg, P. O., Wild, R. J., Zhang, L., and Cohen, R. C.: The lifetime of nitrogen oxides in an isoprene-dominated forest, Atmos. Chem. Phys., 16, 7623-7637, https://doi.org/10.5194/acp-16-7623-2016, 2016.

Sadanaga, Y., Takaji, R., Ishiyama, A., Nakajima, K., Matsuki, A., and Bandow, H.: Thermal dissociation cavity attenuated phase shift spectroscopy for continuous measurement of total peroxy and organic nitrates in the clean atmosphere, Review of Scientific Instruments, 87, 074102., https://doi.org/10.1063/1.4958167, 2016.

Salvador, C. M., Chou, C. C. K., Cheung, H. C., Ho, T. T., Tsai, C. Y., Tsao, T. M., Tsai, M. J., and Su, T. C.: Measurements of submicron organonitrate particles: Implications for the impacts of NOx pollution in a subtropical forest, Atmospheric Research, 245, https://doi.org/10.1016/j.atmosres.2020.105080, 2020.

Salvador, C. M. G., Tang, R., Priestley, M., Li, L., Tsiligiannis, E., Le Breton, M., Zhu, W., Zeng, L., Wang, H., Yu, Y., Hu, M., Guo, S., and Hallquist, M.: Ambient nitro-aromatic compounds – biomass burning versus secondary formation in rural China, Atmos. Chem. Phys., 21, 1389-1406, https://doi.org/10.5194/acp-21-1389-2021, 2021.

Sato, K., Takami, A., Isozaki, T., Hikida, T., Shimono, A., and Imamura, T.: Mass spectrometric study of secondary organic aerosol formed from the photo-oxidation of aromatic hydrocarbons, Atmos. Environ., 44, 1080-1087, https://doi.org/10.1016/j.atmosenv.2009.12.013, 2010.

Schobesberger, S., D'Ambro, E. L., Lopez-Hilfiker, F. D., Mohr, C., and Thornton, J. A.: A model framework to retrieve thermodynamic and kinetic properties of organic aerosol from composition-resolved thermal desorption measurements, Atmos. Chem. Phys., 18, 14757-14785, https://doi.org/10.5194/acp-18-14757-2018, 2018.

Shen, H., Zhao, D., Pullinen, I., Kang, S., Vereecken, L., Fuchs, H., Acir, I. H., Tillmann, R., Rohrer, F., Wildt, J., Kiendler-Scharr, A., Wahner, A., and Mentel, T. F.: Highly Oxygenated Organic Nitrates Formed from NO3 Radical-Initiated Oxidation of beta-Pinene, Environ. Sci. Technol., https://doi.org/10.1021/acs.est.1c03978, 2021.

Simoneit, B. R. T.: Biomass burning — a review of organic tracers for smoke from incomplete combustion, Appl. Geochem, 17, 129-162, https://doi.org/10.1016/S0883-2927(01)00061-0, 2002.

Simoneit, B. R. T., Schauer, J. J., Nolte, C. G., Oros, D. R., Elias, V. O., Fraser, M. P., Rogge, W. F., and Cass, G. R.: Levoglucosan, a tracer for cellulose in biomass burning and atmospheric particles, Atmos. Environ., 33, 173-182, https://doi.org/10.1016/S1352-2310(98)00145-9, 1999.

Singla, V., Mukherjee, S., Pandithurai, G., Dani, K. K., and Safai, P. D.: Evidence of Organonitrate Formation at a High Altitude Site, Mahabaleshwar, during the Pre-monsoon Season, Aerosol and Air Quality Research, 19, 1241-1251, https://doi.org/10.4209/aaqr.2018.03.0110, 2019.

Sobanski, N., Thieser, J., Schuladen, J., Sauvage, C., Song, W., Williams, J., Lelieveld, J., and Crowley, J. N.: Day and night-time formation of organic nitrates at a forested mountain site in south-west Germany, Atmos. Chem. Phys., 17, 4115-4130, https://doi.org/10.5194/acp-17-4115-2017, 2017.

Sommers, J. M., Stroud, C. A., Adam, M. G., O'Brien, J., Brook, J. R., Hayden, K., Lee, A. K. Y., Li, K., Liggio, J., Mihele, C., Mittermeier, R. L., Stevens, R. G., Wolde, M., Zuend, A., and Hayes, P. L.: Evaluating SOA formation from different sources of semi- and intermediate-volatility organic compounds from the Athabasca oil sands, Environmental Science: Atmospheres, 2, 469-490, https://doi.org/10.1039/D1EA00053E, 2022.

Song, K., Guo, S., Wang, H., Yu, Y., Wang, H., Tang, R., Xia, S., Gong, Y., Wan, Z., Lv, D., Tan, R., Zhu, W., Shen, R., Li, X., Yu, X., Chen, S., Zeng, L., and Huang, X.: Measurement Report: Online Measurement of Gas-Phase Nitrated Phenols Utilizing CI-LToF-MS: Primary Sources and Secondary Formation, Atmos. Chem. Phys., 21, 7917–7932, https://doi.org/10.5194/acp-2020-1294, 2021.

Sun, Y. L., Zhang, Q., Schwab, J. J., Yang, T., Ng, N. L., and Demerjian, K. L.: Factor analysis of combined organic and inorganic aerosol mass spectra from high resolution aerosol mass spectrometer measurements, Atmos. Chem. Phys., 12, 8537-8551, https://doi.org/10.5194/acp-12-8537-2012, 2012.

Takeuchi, M. and Ng, N. L.: Chemical composition and hydrolysis of organic nitrate aerosol formed from hydroxyl and nitrate radical oxidation of α-pinene and β-pinene, Atmos. Chem. Phys., 19, 12749-12766, https://doi.org/10.5194/acp-19-12749-2019, 2019.

Thornton, J. A., Mohr, C., Schobesberger, S., D'Ambro, E. L., Lee, B. H., and Lopez-Hilfiker, F. D.: Evaluating Organic Aerosol Sources and Evolution with a Combined Molecular Composition and Volatility Framework Using the Filter Inlet for Gases and Aerosols (FIGAERO), Acc Chem Res, 53, 1415-1426, https://doi.org/10.1021/acs.accounts.0c00259, 2020.

Turpin, B. J. and Huntzicker, J. J.: Identification of secondary organic aerosol episodes and quantitation of primary and secondary organic aerosol concentrations during SCAQS, Atmos. Environ., 29, 3527-3544, https://doi.org/10.1016/1352-2310(94)00276-Q, 1995.

Urban, R. C., Lima-Souza, M., Caetano-Silva, L., Queiroz, M. E. C., Nogueira, R. F. P., Allen, A. G., Cardoso, A. A., Held, G., and Campos, M. L. A. M.: Use of levoglucosan, potassium, and water-soluble organic carbon to characterize the origins of biomass-burning aerosols, Atmos. Environ., 61, 562-569, https://doi.org/10.1016/j.atmosenv.2012.07.082, 2012.

Wang, C., Yuan, B., Wu, C., Wang, S., Qi, J., Wang, B., Wang, Z., Hu, W., Chen, W., Ye, C., Wang, W., Sun, Y., Wang, C., Huang, S., Song, W., Wang, X., Yang, S., Zhang, S., Xu, W., Ma, N., Zhang, Z., Jiang, B., Su, H., Cheng, Y., Wang, X., and Shao, M.: Measurements of higher alkanes using NO+ chemical ionization in PTR-ToF-MS: important contributions of higher alkanes to secondary organic aerosols in China, Atmos. Chem. Phys., 20, 14123-14138, https://doi.org/10.5194/acp-20-14123-2020, 2020a.

Wang, H., Lu, K., Chen, X., Zhu, Q., Chen, Q., Guo, S., Jiang, M., Li, X., Shang, D., Tan, Z., Wu, Y., Wu, Z., Zou, Q., Zheng, Y., Zeng, L., Zhu, T., Hu, M., and Zhang, Y.: High N2O5 Concentrations Observed in Urban Beijing: Implications of a Large Nitrate Formation Pathway, Environmental Science & Technology Letters, 4, 416-420, https://doi.org/10.1021/acs.estlett.7b00341, 2017a.

Wang, L., Wu, D., and Zhang, Z.: Characterization of typical biomass burning tracers among atmospheric particles in urban Guangzhou, J. Grad. Univ. Chin. Acad. Sci., 34, 567-572, https://doi.org/10.7523/j.issn.2095-6134.2017.05.006, 2017b.

Wang, L., Wang, X., Gu, R., Wang, H., Yao, L., Wen, L., Zhu, F., Wang, W., Xue, L., Yang, L., Lu, K., Chen, J., Wang, T., Zhang, Y., and Wang, W.: Observations of fine particulate nitrated phenols in four sites in northern China: concentrations, source apportionment, and secondary formation, Atmos. Chem. Phys., 18, 4349-4359, https://doi.org/10.5194/acp-18-4349-2018, 2018.

Wang, M., Chen, D., Xiao, M., Ye, Q., Stolzenburg, D., Hofbauer, V., Ye, P., Vogel, A. L., Mauldin, R. L., 3rd, Amorim, A., Baccarini, A., Baumgartner, B., Brilke, S., Dada, L., Dias, A., Duplissy, J., Finkenzeller, H., Garmash, O., He, X. C., Hoyle, C. R., Kim, C., Kvashnin, A., Lehtipalo, K., Fischer, L., Molteni, U., Petaja, T., Pospisilova, V., Quelever, L. L. J., Rissanen, M., Simon, M., Tauber, C., Tome, A., Wagner, A. C., Weitz, L., Volkamer, R., Winkler, P. M., Kirkby, J., Worsnop, D. R., Kulmala, M., Baltensperger, U., Dommen, J., El-Haddad, I., and Donahue, N. M.: Photo-oxidation of Aromatic Hydrocarbons Produces Low-Volatility Organic Compounds, Environ. Sci. Technol., 54, 7911-7921, https://doi.org/10.1021/acs.est.0c02100, 2020b.

Wang, S. and Li, H.: NO3·-Initiated Gas-Phase Formation of Nitrated Phenolic Compounds in Polluted Atmosphere, Environ. Sci. Technol., 55, 2899-2907, https://doi.org/10.1021/acs.est.0c08041, 2021.

Wang, S., Peng, Y., Peng, Q., Wu, C., Wang, C., Wang, B., Wang, Z., Kuang, Y., Song, W., Wang, X., Hu, W., Chen, W., Shen, J., Chen, D., Shao, M., and Yuan, B.: Different chemical removal pathways of volatile organic compounds (VOCs): Comparison of urban and regional sites, Acta Sci. Circumstantiae, 40, 2311-2322, https://doi.org/10.13671/j.hjkxxb.2020.0153, 2020c.

Wang, S. H., Yuan, B., Wu, C. H., Wang, C. M., Li, T. G., He, X. J., Huangfu, Y. B., Qi, J. P., Li, X. B., Sha, Q. E., Zhu, M. N., Lou, S. R., Wang, H. L., Karl, T., Graus, M., Yuan, Z. B., and Shao, M.: Oxygenated volatile organic compounds (VOCs) as significant but varied contributors to VOC emissions from vehicles, Atmos. Chem. Phys., 22, 9703-9720, https://doi.org/10.5194/acp-22-9703-2022, 2022a.

Wang, Y., Hu, M., Lin, P., Guo, Q., Wu, Z., Li, M., Zeng, L., Song, Y., Zeng, L., Wu, Y., Guo, S., Huang, X., and He, L.: Molecular Characterization of Nitrogen-Containing Organic Compounds in Humic-like Substances Emitted from Straw Residue Burning, Environ. Sci. Technol., 51, 5951-5961, https://doi.org/10.1021/acs.est.7b00248, 2017c.

Wang, Y., Hu, M., Lin, P., Tan, T., Li, M., Xu, N., Zheng, J., Du, Z., Qin, Y., Wu, Y., Lu, S., Song, Y., Wu, Z., Guo, S., Zeng, L., Huang, X., and He, L.: Enhancement in Particulate Organic Nitrogen and Light Absorption of Humic-Like Substances over Tibetan Plateau Due to Long-Range Transported Biomass Burning Emissions, Environ. Sci. Technol., 53, 14222-14232, https://doi.org/10.1021/acs.est.9b06152, 2019.

Wang, Z., Shi, Z., Wang, F., Liang, W., Shi, G., Wang, W., Chen, D., Liang, D., Feng, Y., and Russell, A. G.: Implications for ozone control by understanding the survivor bias in observed ozone-volatile organic compounds system, npj Climate and Atmospheric Science, 5, https://doi.org/10.1038/s41612-022-00261-7, 2022b.

Wang, Z., Yuan, B., Ye, C., Roberts, J., Wisthaler, A., Lin, Y., Li, T., Wu, C., Peng, Y., Wang, C., Wang, S., Yang, S., Wang, B., Qi, J., Wang, C., Song, W., Hu, W., Wang, X., Xu, W., Ma, N., Kuang, Y., Tao, J., Zhang, Z., Su, H., Cheng, Y., Wang, X., and Shao, M.: High Concentrations of Atmospheric Isocyanic Acid (HNCO) Produced from Secondary Sources in China, Environ. Sci. Technol., 54, 11818-11826, https://doi.org/10.1021/acs.est.0c02843, 2020d.

Wennberg, P. O., Bates, K. H., Crounse, J. D., Dodson, L. G., McVay, R. C., Mertens, L. A., Nguyen, T. B., Praske, E., Schwantes, R. H., Smarte, M. D., St Clair, J. M., Teng, A. P., Zhang, X., and Seinfeld, J. H.: Gas-Phase Reactions of Isoprene and Its Major Oxidation Products, Chem. Rev., 118, 3337-3390, https://doi.org/10.1021/acs.chemrev.7b00439, 2018.

Wolfe, G. M., Marvin, M. R., Roberts, S. J., Travis, K. R., and Liao, J.: The Framework for 0-D Atmospheric Modeling (F0AM) v3.1, Geosci. Model Dev., 9, 3309-3319, https://doi.org/10.5194/gmd-9-3309-2016, 2016.

Wood, E. C., Canagaratna, M. R., Herndon, S. C., Onasch, T. B., Kolb, C. E., Worsnop, D. R., Kroll, J. H., Knighton, W. B., Seila, R., Zavala, M., Molina, L. T., DeCarlo, P. F., Jimenez, J. L., Weinheimer, A. J., Knapp, D. J., Jobson, B. T., Stutz, J., Kuster, W. C., and Williams, E. J.: Investigation of the correlation between odd oxygen and secondary organic aerosol in Mexico City and Houston, Atmos. Chem. Phys., 10, 8947-8968, 10.5194/acp-10-8947-2010, 2010.

Wormhoudt, J., Wood, E. C., Knighton, W. B., Kolb, C. E., Herndon, S. C., and Olaguer, E. P.: Vehicle emissions of radical precursors and related species observed in the 2009 SHARP campaign, J. Air Waste Manage. Assoc., 65, 699-706, https://doi.org/10.1080/10962247.2015.1008654, 2015.

Wu, C., Bell, D. M., Graham, E. L., Haslett, S., Riipinen, I., Baltensperger, U., Bertrand, A., Giannoukos, S., Schoonbaert, J., El Haddad, I., Prevot, A. S. H., Huang, W., and Mohr, C.: Photolytically induced changes in composition and volatility of biogenic secondary organic aerosol from nitrate radical oxidation during night-to-day transition, Atmos. Chem. Phys., 21, 14907-14925, https://doi.org/10.5194/acp-21-14907-2021, 2021.

Wu, C., Wang, C., Wang, S., Wang, W., Yuan, B., Qi, J., Wang, B., Wang, H., Wang, C., Song, W., Wang, X., Hu, W., Lou, S., Ye, C., Peng, Y., Wang, Z., Huangfu, Y., Xie, Y., Zhu, M., Zheng, J., Wang, X., Jiang, B., Zhang, Z., and Shao, M.: Measurement report: Important contributions of oxygenated compounds to emissions and chemistry of volatile organic compounds in urban air, Atmos. Chem. Phys., 20, 14769-14785, https://doi.org/10.5194/acp-20-14769-2020, 2020.

Xiao, S. and Bertram, A. K.: Reactive uptake kinetics of NO3 on multicomponent and multiphase organic mixtures containing unsaturated and saturated organics, Phys. Chem. Chem. Phys., 13, 6628-6636, https://doi.org/10.1039/C0CP02682D, 2011.

Xu, L., Suresh, S., Guo, H., Weber, R. J., and Ng, N. L.: Aerosol characterization over the southeastern United States using high-resolution aerosol mass spectrometry: spatial and seasonal variation of aerosol composition and sources with a focus on organic nitrates, Atmos. Chem. Phys., 15, 7307-7336, https://doi.org/10.5194/acp-15-7307-2015, 2015.

Xu, L., Crounse, J. D., Vasquez, K. T., Allen, H., Wennberg, P. O., Bourgeois, I., Brown, S. S., Campuzano-Jost, P., Coggon, M. M., Crawford, J. H., DiGangi, J. P., Diskin, G. S., Fried, A., Gargulinski, E. M., Gilman, J. B., Gkatzelis, G. I., Guo,

H., Hair, J. W., Hall, S. R., Halliday, H. A., Hanisco, T. F., Hannun, R. A., Holmes, C. D., Huey, L. G., Jimenez, J. L., Lamplugh, A., Lee, Y. R., Liao, J., Lindaas, J., Neuman, J. A., Nowak, J. B., Peischl, J., Peterson, D. A., Piel, F., Richter, D., Rickly, P. S., Robinson, M. A., Rollins, A. W., Ryerson, T. B., Sekimoto, K., Selimovic, V., Shingler, T., Soja, A. J., St. Clair, J. M., Tanner, D. J., Ullmann, K., Veres, P. R., Walega, J., Warneke, C., Washenfelder, R. A., Weibring, P., Wisthaler, A., Wolfe, G. M., Womack, C. C., and Yokelson, R. J.: Ozone chemistry in western U.S. wildfire plumes, Sci. Adv., 7, eabl3648, https://doi.org/10.1126/sciadv.abl3648, 2021a.

Xu, W., Takeuchi, M., Chen, C., Qiu, Y., Xie, C., Xu, W., Ma, N., Worsnop, D. R., Ng, N. L., and Sun, Y.: Estimation of particulate organic nitrates from thermodenuder–aerosol mass spectrometer measurements in the North China Plain, Atmos. Meas. Tech., 14, 3693-3705, https://doi.org/10.5194/amt-14-3693-2021, 2021b.

Xu, W., Han, T., Du, W., Wang, Q., Chen, C., Zhao, J., Zhang, Y., Li, J., Fu, P., Wang, Z., Worsnop, D. R., and Sun, Y.: Effects of Aqueous-Phase and Photochemical Processing on Secondary Organic Aerosol Formation and Evolution in Beijing, China, Environ. Sci. Technol., 51, 762-770, 10.1021/acs.est.6b04498, 2017.

Ye, C., Yuan, B., Lin, Y., Wang, Z., Hu, W., Li, T., Chen, W., Wu, C., Wang, C., Huang, S., Qi, J., Wang, B., Wang, C., Song, W., Wang, X., Zheng, E., Krechmer, J. E., Ye, P., Zhang, Z., Wang, X., Worsnop, D. R., and Shao, M.: Chemical characterization of oxygenated organic compounds in the gas phase and particle phase using iodide CIMS with FIGAERO in urban air, Atmos. Chem. Phys., 21, 8455-8478, https://doi.org/10.5194/acp-21-8455-2021, 2021.

Yu, K., Zhu, Q., Du, K., and Huang, X.-F.: Characterization of nighttime formation of particulate organic nitrates based on high-resolution aerosol mass spectrometry in an urban atmosphere in China, Atmos. Chem. Phys., 19, 5235-5249, https://doi.org/10.5194/acp-19-5235-2019, 2019.

Yuan, B., Liu, Y., Shao, M., Lu, S., and Streets, D. G.: Biomass Burning Contributions to Ambient VOCs Species at a Receptor Site in the Pearl River Delta (PRD), China, Environ. Sci. Technol., 44, 4577-4582, https://doi.org/10.1021/es1003389, 2010.

Yuan, B., Koss, A. R., Warneke, C., Coggon, M., Sekimoto, K., and de Gouw, J. A.: Proton-Transfer-Reaction Mass Spectrometry: Applications in Atmospheric Sciences, Chem. Rev., 117, 13187-13229, https://doi.org/10.1021/acs.chemrev.7b00325, 2017.

Yuan, B., Hu, W. W., Shao, M., Wang, M., Chen, W. T., Lu, S. H., Zeng, L. M., and Hu, M.: VOC emissions, evolutions and contributions to SOA formation at a receptor site in eastern China, Atmos. Chem. Phys., 13, 8815-8832, https://doi.org/10.5194/acp-13-8815-2013, 2013.

Zhan, B., Zhong, H., Chen, H., Chen, Y., Li, X., Wang, L., Wang, X., Mu, Y., Huang, R.-J., George, C., and Chen, J.: The roles of aqueous-phase chemistry and photochemical oxidation in oxygenated organic aerosols formation, Atmos. Environ., 266, 118738, https://doi.org/10.1016/j.atmosenv.2021.118738, 2021.

Zhang, C., Lu, X., Zhai, J., Chen, H., Yang, X., Zhang, Q., Zhao, Q., Fu, Q., Sha, F., and Jin, J.: Insights into the formation of secondary organic carbon in the summertime in urban Shanghai, JEnvS, 72, 118-132, https://doi.org/10.1016/j.jes.2017.12.018, 2018.

Zhang, J. K., Cheng, M. T., Ji, D. S., Liu, Z. R., Hu, B., Sun, Y., and Wang, Y. S.: Characterization of submicron particles during biomass burning and coal combustion periods in Beijing, China, Sci. Total Environ., 562, 812-821, https://doi.org/10.1016/j.scitotenv.2016.04.015, 2016.

Zhao, Y., Thornton, J. A., and Pye, H. O. T.: Quantitative constraints on autoxidation and dimer formation from direct probing of monoterpene-derived peroxy radical chemistry, Proc. Natl. Acad. Sci. U. S. A., 115, 12142-12147, https://doi.org/10.1073/pnas.1812147115, 2018.

Zhao, Y., Nguyen, N. T., Presto, A. A., Hennigan, C. J., May, A. A., and Robinson, A. L.: Intermediate Volatility Organic Compound Emissions from On-Road Gasoline Vehicles and Small Off-Road Gasoline Engines, Environ. Sci. Technol., 50, 4554-4563, https://doi.org/10.1021/acs.est.5b06247, 2016.

Zhao, Z., Husainy, S., Stoudemayer, C. T., and Smith, G. D.: Reactive uptake of NO3 radicals by unsaturated fatty acid particles, Phys. Chem. Chem. Phys., 13, 17809-17817, https://doi.org/10.1039/c1cp21790a, 2011.

Zhu, Q., He, L. Y., Huang, X. F., Cao, L. M., Gong, Z. H., Wang, C., Zhuang, X., and Hu, M.: Atmospheric aerosol compositions and sources at two national background sites in northern and southern China, Atmos. Chem. Phys., 16, 10283-10297, https://doi.org/10.5194/acp-16-10283-2016, 2016.

Supporting information for "The Important Contribution of Secondary Formation and Biomass Burning to Oxidized Organic Nitrogen (OON) in a Polluted Urban Area: Insights from In Situ FIGAERO-CIMS Measurements"

Yiyu Cai[1,2,3,4,5*], Chenshuo Ye[6*], Wei Chen[1,2,3,4,5], Weiwei Hu[1,2,3,4], Wei Song[1,2,3,4], Yuwen Peng[7,8], Shan Huang[7,8], Jipeng Qi[7,8], Sihang Wang[7,8], Chaomin Wang[7,8], Caihong Wu[7,8], Zelong Wang[7,8], Baolin Wang[9], Xiaofeng Huang[10], Lingyan He[10], Sasho Gligorovski[1,2,3,4], Bin Yuan[7,8], Min Shao[7,8], Xinming Wang[1,2,3,4]

[1]State Key Laboratory of Organic Geochemistry, Guangzhou Institute of Geochemistry, Chinese Academy of Sciences, Guangzhou 510640. China
[2]CAS Center for Excellence in Deep Earth Science, Guangzhou, 510640, China
[3]Guangdong-Hong Kong-Macao, Joint Laboratory for Environmental Pollution and Control, Guangzhou Institute of Geochemistry, Chinese Academy of Science, Guangzhou 510640, China
[4]Guangdong Provincial Key Laboratory of Environmental Protection and Resources Utilization, Chinese Academy of Science, Guangzhou 510640, China
[5]University of Chinese Academy of Sciences, Beijing 100049, China
[6]Guangdong Provincial Academy of Environmental Science, Guangzhou, 510640, China
[7]Institute for Environmental and Climate Research, Jinan University, Guangzhou 511443, China
[8]Guangdong-Hongkong-Macau Joint Laboratory of Collaborative Innovation for Environmental Quality, Guangzhou 511443, China
[9]School of Environmental Science and Engineering, Qilu University of Technology, Jinan 250353, China
[10]Key Laboratory for Urban Habitat Environmental Science and Technology, School of Environment and Energy, Peking University Shenzhen Graduate School, Shenzhen, 518055, China

*Yiyu Cai and Chenshuo Ye contributed equally to this work.
Correspondence to: Weiwei Hu (weiweihu@gig.ac.cn); Bin Yuan (byuan@jnu.edu.cn).

Contents of this file

Text S1: Intercomparison of AMS-derived organic nitrates based on multiple methods

Nitrate signals (NO^+, NO_2^+, HNO_3^+) measured by a high-resolution time-of-flight aerosol mass spectrometer (HR-ToF-AMS) include both organic nitrates and inorganic nitrates. Many methods were established to separate the total measured nitrates from inorganic nitrates and particle-phase organic nitrates (i.e., the particle-phase nitrate functional group, $pOrgNO_{3,\ AMS}$), i.e., NO_2^+/NO^+ ratio method (Farmer et al., 2010), Positive Matrix Factorization (PMF) method (Hao et al., 2014; Sun et al., 2012; Xu et al., 2015) and Thermodenuder (TD) method (Xu et al., 2021). In this study, these three methods were applied to quantify $pOrgNO_{3,\ AMS}$. Note that in agreement with Dancey and Reidy (2007), we interpreted the absolute value of the Pearson correlation coefficient as (i) no correlation, if $|r| \leq 0.1$; (ii) weak correlation, if $0.1 < |r| \leq 0.3$; (iii) moderate correlation, if $|0.3 < r| \leq 0.7$; (iv) strong correlation, if $0.7 < |r| \leq 1$; and finally, (v) perfect correlation, if $|r| = 1$.

(1) **NO_2^+/NO^+ ratio method.** The organic nitrate and inorganic can be detected as NO^+ and NO_2^+ ions in the HR-ToF-AMS. Previous studies have reported much lower NO_2^+/NO^+ ratios of $pOrgNO_{3,\ AMS}$ (R_{ON}) than that of inorganic nitrates, i.e., NH_4NO_3 ($R_{NH_4NO_3}$) (Boyd et al., 2015; Farmer et al., 2010; Fry et al., 2013; Sato et al., 2010). Fry et al. (2013) quantified that the R_{ON} ratio is 2.25 times lower than the $R_{NH_4NO_3}$ based on multiple results using different AMSs in chamber studies. Recently, Day et al. (2022) and Fry et al. (2018) summarized more studies and redefined the ratio $R_{NH_4NO_3}/R_{ON}$ to be 2.75. The average $R_{NH_4NO_3}$ was estimated to be 0.37 from the standard calibration of NH_4NO_3, which is quite stable across this entire campaign. Then, the R_{ON} for this study was estimated to be 0.13 based on the $R_{NH_4NO_3}/R_{ON}$ ratio of 2.75.

Thus, the fraction of $pOrgNO_{3,\ AMS}$ in total nitrates (ON_{frac}) measured by the AMS can be calculated as (Farmer et al., 2010):

$$ON_{frac} = \frac{(R_{ambient} - R_{NH_4NO_3})(1+R_{ON})}{(R_{ON} - R_{NH_4NO_3})(1+R_{ambient})} \quad \text{(S1)}$$

where $R_{ambient}$ is the NO_2^+/NO^+ ratio of ambient nitrate. The final concentration of $pOrgNO_{3,\ AMS}$ can be calculated based on total nitrates and ON_{frac}. To calculate the uncertainty of ON_{frac} with the NO_2^+/NO^+ ratio method, ratios of 2.08 and 4.17 (R_{ON} = 0.18 and 0.09) obtained from isoprene- and monoterpene-derived $pOrgNO_{3,\ AMS}$, were used for calculating the upper (mean 0.85 μg m^{-3}) and lower (mean 0.53 μg m^{-3}) bounds of $pOrgNO_{3,\ AMS}$ (Xu et al., 2015; Xu et al., 2021), respectively. Thus, 27% was regarded as the average uncertainty of this method for the estimation $pOrgNO_{3,\ AMS}$ in this study. When the ambient nitrate signal is high in ambient air (e.g., >5 ug m^{-3}), the high nitrate signal was mainly contributed by the inorganic ammonium nitrate (Day et al., 2022). This leads to that the NO_2^+/NO^+ ratio of ambient nitrate is similar to that of pure inorganic ammonium nitrate, thus resulting in a large uncertainty in $pOrgNO_{3,\ AMS}$ estimation. This issue had been fully addressed in the method paper on how

to estimate $pOrgNO_{3,\ AMS}$ from AMS measurement (Day et al., 2022). The larger uncertainty of estimated $pOrgNO_{3,\ AMS}$ by AMS under high nitrate signal periods has also been found in other ambient studies (Yu et al., 2019; Zhu et al., 2016).

(2) **PMF method**. It is well known that the PMF analysis can be used for source appointment and estimation of various organic factors, e.g., primary organic aerosol and secondary organic aerosol (SOA). Combining the OA spectral matrix with NO^+ and NO_2^+ ions detected by AMS, different OA factors including organic NO^+ and NO_2^+ ions can provide insights regarding the relative contributions of $pOrgNO_{3,\ AMS}$ and inorganic nitrates (Sun et al., 2012; Xu et al., 2015). Therefore, the concentrations of $pOrgNO_{3,\ AMS}$ (NO^+_{org} and $NO^+_{2,org}$) are equal to the sum of NO^+ and NO_2^+ via Eqs. (S2) and (S3) (Xu et al., 2015):

$$NO^+_{2,org} = \sum \left([\text{OA factor}]_i \times f_{NO_2,i} \right) \quad \text{(S2)}$$

$$NO^+_{org} = \sum \left([\text{OA factor}]_i \times f_{NO,i} \right) \quad \text{(S3)}$$

where $[\text{OA factor}]_i$ is the mass concentration of OA factor i, $f_{NO_2,i}$ and $f_{NO,i}$ are the mass fractions of NO_2^+ and NO^+ in each factor, respectively.

(3) **TD method.** The method was developed for the estimation of $pOrgNO_{3,\ AMS}$ from the measurement of HR-ToF-AMS coupled with a thermodenuder based on the difference of volatility between $pOrgNO_{3,\ AMS}$ ($NO^+_{x,org}$) and inorganic nitrates ($NO^+_{x,inorg}$) in particles (Xu et al., 2021). It is assumed that (I) the remaining mass loading of nitrate fragments was dominated by $NO^+_{x,org}$, while $NO^+_{x,inorg}$ evaporated completely at T = 90℃ due to the higher volatility of $NO^+_{x,inorg}$ than $NO^+_{x,org}$ (Huffman et al., 2008; Ng et al., 2017); (II) The $C_xH_yN_z^+$ and $C_xH_yO_zN_p^+$ ions were supposed to have similar volatility as $NO^+_{x,org}$ which dominate the remaining fragments at T > 90℃ (Xu et al., 2021). Combined with the two assumptions, the mass concentration of $pOrgNO_{3,\ AMS}$ ($[NO_{3,org}]$) in the ambient atmosphere can be determined by Eq. (S4) (Xu et al., 2021):

$$[NO_{3,org}] = \frac{[NO_3]_{T=90℃}}{MFR_{CHN^+ + CHON^+ T=90℃}} \quad \text{(S4)}$$

The subscript "T = 90℃" denotes the mass concentration or the mass fraction remaining (MFR) of fragments at T = 90℃.

The intercomparison of $pOrgNO_{3,\ AMS}$ based on these three methods and the particle-phase oxidized organic nitrogen (pOON) measured by an iodide chemical ionization time-of-flight mass spectrometer installed with a Filter Inlet for Gases and AEROsols (FIGAERO-CIMS) in this campaign are presented in Fig. S2. The average concentrations of $pOrgNO_{3,\ AMS}$ and pOON are shown in Table S2. Generally, the $pOrgNO_{3,\ AMS}$ derived from PMF method increases with total nitrates and is largely overestimated

compared to other methods during the high nitrate periods. The $pOrgNO_{3,\ AMS}$ estimated from the TD method correlates well (R = 0.73) with that from NO_2^+/NO^+ ratio method. However, the former exhibits noisier especially under low nitrate periods probably due to the large uncertainty of the lower mass remaining fraction for $pOrgNO_{3,\ AMS}$ at higher temperature (>90℃). T = 90℃ was assumed to represent the temperature mentioned above at which inorganic nitrates have been evaporated completely. However, this might not be the case in some environments (Huffman et al., 2008). The drawback of NO_2^+/NO^+ ratio method is the slightly large uncertainty under high NO_x conditions such as during 25−26 October 2018 (Fig. S2a).

Finally, we chose NO_2^+/NO^+ ratio method for more analysis in the main text given its smooth profile and relative stable estimation of total $pOrgNO_{3,\ AMS}$ (Yu et al., 2019). The average mass fraction of $pOrgNO_{3,\ AMS}$ to total nitrates is 15% and that mass fraction increases with decreasing concentration of total nitrates (Fig. S2b), indicating the dominant role of pON chemistry under low nitrate atmospheric environment.

Text S2: The calculation of the production rate of gas-phase organic nitrates

In the presence of NO, the production rate of gas-phase oxidized organic nitrogen (gOON) from hydroxyl radical (OH) initiated oxidation with volatile organic compounds (VOCs) (P_{ON}^{OH}) can be calculated following Eq. (S5) (Liebmann et al., 2019):

$$P_{ON}^{OH} = [OH]\beta \sum \alpha_i^{RO_2} k_i^{OH} [C_i] \quad \text{(S5)}$$

where [OH] is the concentration of OH, which was obtained from a box model simulation based on master chemical mechanism v3.3.1 (MCM v3.3.1) (Wang et al., 2020; Wolfe et al., 2016). $[C_i]$ is the concentration of speciated VOC *i*. k_i^{OH} is the reaction rate coefficient between OH and VOC *i*, $\alpha_i^{RO_2}$ is the formation branching ratio of gOON for speciated VOC *i*, β represents the fraction of the peroxy radicals (RO_2) that react with NO which can be estimated by $\beta = \frac{k_{RO_2+NO}[NO]}{k_{RO_2+NO}[NO]+k_{RO_2+HO_2}[HO_2]}$ ($k_{RO_2+NO} = 9.0 \times 10^{-12}$ and $k_{RO_2+HO_2} = 2.3 \times 10^{-11}$ cm^3 $molecule^{-1}$ s^{-1} from MCM v3.3.1) (http://mcm.leeds.ac.uk/MCMv3.3.1/home.htt). The estimated values of β were 0.98−1.0 during the campaign, thus $\beta = 1$ was used in this calculation. The VOC species, reaction rate coefficients, yields, and branching ratios used for this calculation can be found in Table 1.

The nitrate radical (NO_3) concentration was calculated based on measured N_2O_5 by the CIMS assuming temperature equilibrium between these two species (Brown and Stutz, 2012). Then the gOON production rate from NO_3 initiated oxidation of VOC ($P_{ON}^{NO_3}$) can be calculated by Eq. (S6):

$$P_{ON}^{NO_3} = \sum \alpha_i k_{NO_3+C_i} [C_i][NO_3] \quad \text{(S6)}$$

where $[C_i]$ and $[NO_3]$ are the concentrations of speciated VOC i and NO_3, α_i is the gOON yield, $k_{NO_3+[C_i]}$ is the reaction rate coefficient as shown in Table 1. The reactions between alkanes and NO_3 are very slow accounting for negligible chemical changes in the ambient atmosphere so that alkanes were not included in this calculation. The VOC species of terpenes, aromatics, and alkenes (Table 1) measured during October 2018 were used to calculate the NO_3 loss rate. Only 2% of the NO_3 loss rate was attributed to alkenes. And the NO_3 loss rate attributed to cresol and phenol (30% on average, ranging from 13% to 60%) was three orders of magnitude higher than the other aromatics (~0.1%). Thus, we assumed that the alkanes, alkenes, and the other aromatics (excluding cresol and phenol) contributed little (<3%) to the total gOON production rate, which were not included in this calculation.

The gOON production rate of ozone (O_3) initiated oxidation of VOC ($P_{ON}^{O_3}$) can be calculated by Eq. (S7):

$$P_{ON}^{O_3} = [O_3]\beta \sum \alpha_i^{O_3} k_i^{O_3} [C_i] \alpha_i^{RO_2} \quad \text{(S7)}$$

where $[O_3]$ is the concentration of O_3, $k_i^{O_3}$ is the reaction rate coefficient between O_3 and VOC i, $\alpha_i^{O_3}$ is the yield of RO_2, and $\alpha_i^{RO_2}$ is the ON yield of the reaction RO_2+NO for speciated VOC (Table 1). β and $[C_i]$ are the same as in Eq. (S5). The short-chain alkenes including propene, butene and pentene yield negligible SOA as well as ON, thus we did not include them in the calculation.

Fig. ~~S3~~S4 shows the time series and average diurnal variations of OH, NO_3, and O_3 used in the calculation above. The average concentration of OH was $1.11 \pm 1.86\times10^6$ molecule m^{-3} which peaks at noon (mean $4.20 \pm 2.69\times10^6$ molecule m^{-3}). The averaged mixing ratio of NO_3 was 1.14 ± 2.82 ppt which peaks at 18:00 (2.25 ± 3.85 ppt) and night (2.35 ± 5.00 ppt), consistent with other studies in urban areas (Hamilton et al., 2021; Wang et al., 2017). No speciated monoterpene measurement was conducted in this campaign. Thus, we assume that the monoterpenes at this urban site were contributed by limonene and α-pinene with a ratio of 1:1 during this campaign. A recent study found that half of the ambient monoterpenes can be attributed to the VCP-dominated source based on measurements at altitude of 450 m in the Canton Tower in Guangzhou urban area (Li et al., 2022). The other half monoterpenes are mainly from visitor-related emissions since Canton tower is a tourism site. It is consistent with our finding that the ambient monoterpenes in this study is anthropogenic origins. Gkatzelis et al. (2021) found the limonene was the dominant isomer of monoterpenes in VCP emissions. And *Coggon et al.* (2021) found the α-pinene (19%) and limonene (53%) were the main isomers of monoterpene in the center of megacity New York. Thus, a 1:1 assumption of limonene and α-pinene applied here shall be reasonable. The concentration of sesquiterpenes could be calculated as a function of the monoterpene concentration, as described in Sommers et al. (2022). Since a large fraction of monoterpene in this study was assumed to be anthropogenic, thus, the calculated concentration of sesquiterpenes herein is a high limit. The calculated mass concentration of the sesquiterpenes is only 7% of the monoterpene concentration in this campaign. Omitting the sesquiterpenes in the gOON production rate calculation

should be within the estimated uncertainty of the gOON production rate. In addition, the yield parameters for gOON production rate from sesquiterpenes were missed. Thus, in this study, sesquiterpenes were not accounted for in the final gOON production rate calculation.

Text S3: Uncertainty estimation.

Uncertainty of gOON production rate estimation. Monte Carlo method was used to estimate the entire uncertainty of the gOON production rate with 10,000 calculations as shown in Fig. ~~S4~~S5. During the Monte Carlo method, the kinetic parameter sets were assigned according to Liebmann et al. (2019), which can involve the uncertainties of varies parameters, e.g., yields and branch ratios. Then the parameters were allowed randomly vary within the range and vast number of combinations of input parameters were used to be computed (Mckay et al., 2000). During the iteration, we estimated the uncertainty in the term NO_3 pathway of 58%, with 50% from [NO_3], 15% from $k_{NO_3+C_i}$, 50% from α_i, and 30% from [C_i]. If 30−50% uncertainties were added to the concentration ratio of α-pinene to limonene, the uncertainty of the term NO_3 pathway increased up to 62−70%. The uncertainty in the term OH pathway was 45%, with 50% from [OH], 15% from k_i^{OH}, 50% from $\alpha_i^{RO_2}$, 30% from β, and 35% from [C_i]. The uncertainty in the term O_3 pathway was 66%, with contribution of 10% from [O_3], 35% from [C_i], 15% from $k_i^{O_3}$, 50% from $\alpha_i^{RO_2}$, 30% from β, and 50% from $\alpha_i^{O_3}$. An overall uncertainty of 56% was estimated by this method.

Uncertainty for the ratio of $pOrgNO_3$ measured by CIMS and AMS ($pOrgNO_{3,CIMS}$ vs $pOrgNO_{3,AMS}$). This uncertainty estimation was based on the Eq. (S8) below combined with error propagation law.

$$\frac{pOrgNO_{3,CIMS}}{pOrgNO_{3,AMS}} = \frac{pOON_{CIMS} \times \frac{MW_{[NO_3]}}{MW_{[pOON]}}}{pOrgNO_{3,AMS}} \quad \text{(S8)}$$

The uncertainty of $pOON_{CIMS}$ was 47% according to the uncertainty of OON derived from the comparison of voltage scanning factors and calibration factors (Fig. S3), which was discussed in section 2.2.2 of the main text. The uncertainty of pOON molecular weight (MW, 234 ± 7.9 g mol^{-1}), which was obtained with CIMS measurement, was assigned to be 10%. The uncertainty of $pOrgNO_{3,AMS}$ was 30% that was regarded as a low limit due to the measurement uncertainty of AMS. For OON quantification, the uncertainty of the NO_2^+/NO^+ ratio method was estimated using the lower and higher NO_2^+/NO^+ ratio from ONs (0.18 and 0.09) based on Xu et al. (2015), which was calculated to be 27% as discussed in Text S1. Finally, the total uncertainty of the pOON ratio between CIMS and AMS was 63%. It suggests that the $pOrgNO_{3,CIMS}$ can explain 28 ± 18% of $pOrgNO_{3,AMS}$.

Uncertainty for the source apportionment of OON. Based on the Eq. (1−2), the uncertainty of the source apportionment of OON was estimated by Monte Carlo method with 10,000 calculations. The uncertainty of levoglucosan was 10% considering its standard calibration (Ye et al., 2021) and mass contribution (90 ± 2%) among isomers (referred to section 2.2.2). The uncertainty of the primary ratios of OON vs levoglucosan, $(([OON_{measured}]/[levo.])_{bb})$, was considered equal to their average standard deviation shown in Table S1, i.e., 20% and 42% for pOON and gOON, respectively. The concentration uncertainties for OON_{bb}

were calculated to be 19% and 37% for gas and particle phases, respectively. After accounting for the 47% uncertainty in OON, the uncertainties of the OON_{bb} fraction in total OON were around 9% and 11% for aerosol and gas phase, respectively. The standard deviations of averaged OON_{bb} fraction in total OON from the entire campaign were around 22% and 23% for aerosol and gas phase, respectively. By combining the uncertainty from Monte Carlo and standard deviation due to averaging, the final contributions with uncertainties of biomass burning to pOON and gOON are 49 ± 23% and 24 ±25%, respectively.

Text S4: The calculation of aromaticity index and seasonal decomposition

The aromaticity index (AI) is defined for the identification of aromatic and condensed aromatic structures, which was calculated by the Eq. (~~S8~~S9) (Koch and Dittmar, 2016, 2006):

$$AI = \frac{1+c-0.5o-0.5n-0.5h}{c-0.5o-n} \quad (~~S8~~S9)$$

where c, o, n, and h correspond to the number of C, O, N, and H atoms, respectively, in each molecule.

A time series usually comprises three components: a long-term trend, seasonal fluctuation, and a remainder component (containing anything else in the time series). A long-term trend is a tendency or state of affairs in which a phenomenon develops and changes continuously over a longer period of time. Seasonal fluctuation is the regular variation caused by seasonal change. The time series decomposition can distill the component of repeatability from complex data. This method is similar to the combination of two filters with large and small bandwidth. The bandwidth can be adjusted for different time resolution. If an additive decomposition was assumed, the Eq. is:

$$y_t = S_t + T_t + R_t \quad (~~S9~~S10)$$

where y_t is the data, S_t is the seasonal fluctuation, T_t is the long-term trend, and R_t is the remainder component, all at period t. Taking 24 hours as the "season" in the calculation, i.e., adjusting the "bandwidth", we can get a clearer diurnal variation preventing the trend blurred by the varies intensity between days. The detailed process of the calculation applied in this paper can refer to Hilas et al. (2006).

Table S1. The regression slopes between measured gOON (pOON) vs particle-phase levoglucosan in selected biomass burning emission episodes. The data used to derive these slopes are also shown in Figs. S12 and S13. The average values based on different biomass burning episodes are also shown.

Episode	Slope ($\mu g\ m^{-3}/\mu g\ m^{-3}$)	Episode	Slope ($\mu g\ m^{-3}/\mu g\ m^{-3}$)
Gas phase			
(06)	5.30 ± 2.10	(28)	3.57 ± 0.72
(20)	1.00 ± 0.18 [a]	(30)	3.99 ± 0.87
(22)	4.10 ± 1.54	Average	3.95 ± 1.67
(24)	5.75 ± 1.28		
Particle phase			
(06)	6.66 ± 2.28	(25)	5.14 ± 1.76
(07)	3.14 ± 1.05	(28)	5.61 ± 0.69
(13)	5.23 ± 0.26	(30)	4.37 ± 0.42
(20)	5.11 ± 0.40	Average	5.05 ± 1.01
(22)	5.15 ± 0.88		

Note. [a] The relatively low value from the episode at night on 20 October was also selected for the criteria used here, indicating the special low contribution from biomass burning to gOON during this episode.

Table S2. Summary of average mass concentrations of OON measured or calculated by the CIMS and the AMS, averaged values of gOON production rates, meteorological parameters, and other OON-related parameters during October 2018.

	Average ± SD		Average ± SD
$pOrgNO_{3,\ AMS}$ (μg m^{-3})	--	secondary gOON (μg m^{-3})	0.79 ± 0.67
NO_2^+/NO^+ ratio method	0.60 ± 0.46	**Total gOON production rate (ppb h^{-1})**	0.11 ± 0.11
TD method	1.10 ± 0.81	*OH initiated*	0.07 ± 0.10
PMF method	2.29 ± 2.38	*NO_3 initiated*	0.05 ± 0.07
$pOON_{CIMS}$ (μg m^{-3})	0.66 ± 0.53	*O_3 initiated*	0.01 ± 0.01
$gOON_{CIMS}$ (μg m^{-3})	1.00 ± 0.67	OA (μg m^{-3})	14.27 ± 8.20
$pC_{4-5}N$ (μg m^{-3})	0.10 ± 0.07	Nitrate (μg m^{-3})	4.44 ± 6.05
$pC_{6-9\_aro}N$ (μg m^{-3})	0.10 ± 0.09	$pOON_{CIMS}$/OA	0.05 ± 0.02
$pC_{8-10}N$ (μg m^{-3})	0.27 ± 0.21	NO (ppb)	9.24 ± 18.33
$pC_{11-20}N$ (μg m^{-3})	0.09 ± 0.08	NO_2 (ppb)	31.17 ± 18.38
$pC_{other}N$ (μg m^{-3})	0.12 ± 0.09	O_3 (ppb)	36.95 ± 31.21
levoglucosan (μg m^{-3})	0.06 ± 0.07	wind speed (m s^{-1})	4.50 ± 2.18
BB pOON (μg m^{-3})	0.32 ± 0.36	temperature (℃)	23.73 ± 2.92
secondary pOON (μg m^{-3})	0.34 ± 0.35	RH (%)	71.92 ± 17.43
BB gOON (μg m^{-3})	0.25 ± 0.29		

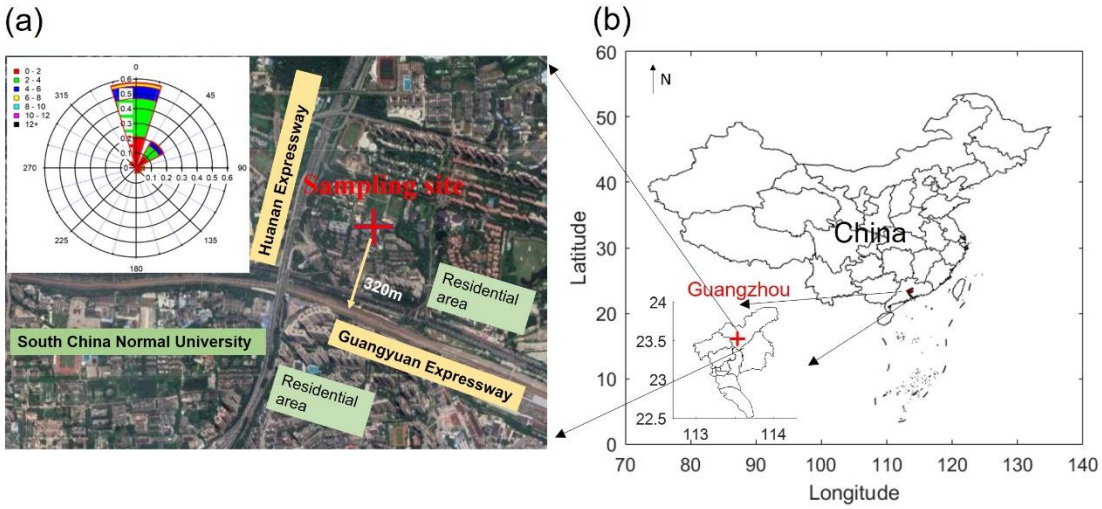

Figure S1. Site descriptions: (a) The satellite view of sampling site in Guangzhou, China. The sampling site is located in the campus of Guangzhou institute of Geochemistry (GIG), Chinese Academy of Sciences (CAS). The wind rose plot during the campaign is also shown as insert plot with color represents the wind speed. (b) The location of Guangzhou city in the map of China.

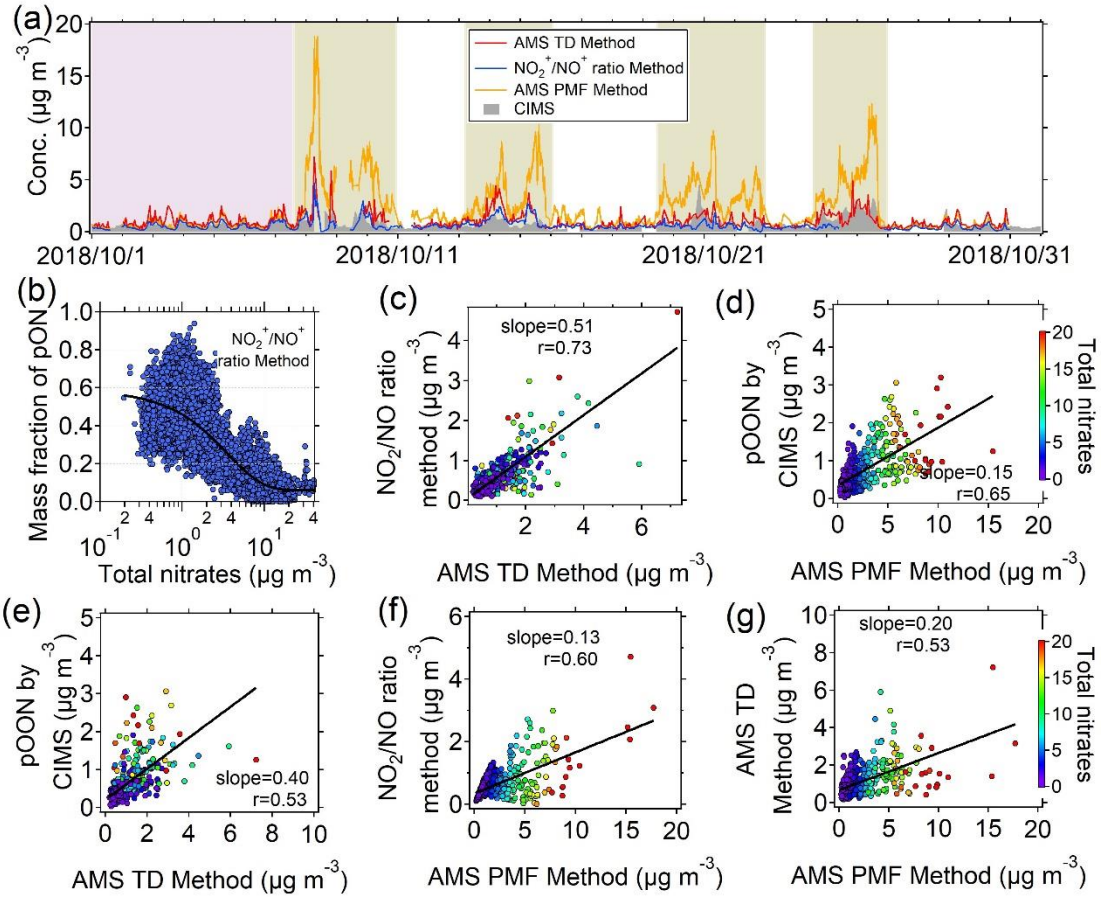

Figure S2. (a) Comparison of time series of pOON derived from the CIMS and $pOrgNO_{3,AMS}$ from the AMS based on three methods introduced in Text S1. The tinted backgrounds with light pink and light yellow indicate the period with low and high concentrations of nitrates, respectively. (b) Mass fraction of $pOrgNO_{3,AMS}$ (NO_2^+/NO^+ ratio method) to total nitrates as a function of total nitrate signal derived from the AMS. (c–g) Scatterplots of pOON measured by the CIMS and $pOrgNO_{3,AMS}$ calculated by three methods based on the AMS measurement. All the scatters are color-coded by the mass concentration of total nitrate signals measured by the AMS. All the linear fitting are based on the orthogonal distance regression (ODR) algorithm in this study.

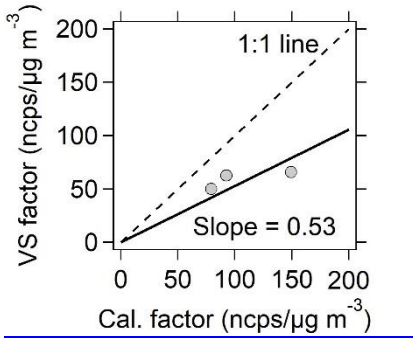

Figure S3. The scatterplot of calibration factors of three nitro-containing compounds (4-nitrophenol, 2,4-dinitrophenol, and 4-nitrocatechol) that derived from voltage scanning method and standard calibration. Based on the slope, 47% was regarded as the uncertainty of the voltage scanning method for OON calibration in this study. The detailed data can be found in the excel file of the supplement zip package of Ye et al. (2021).

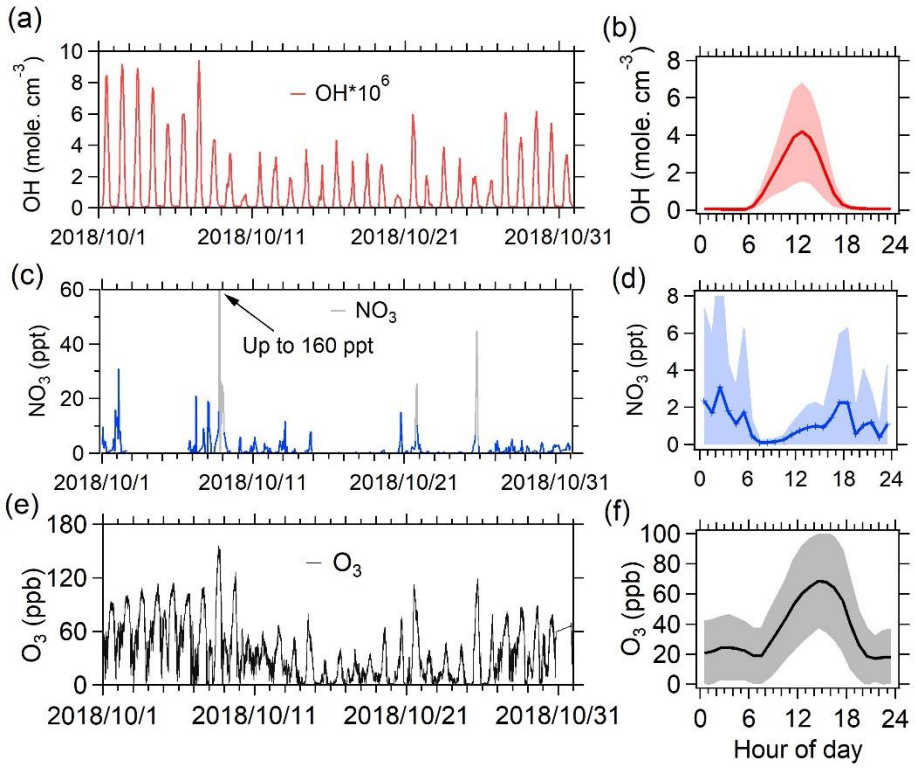

Figure S4. The time series and average diurnal variations of (a, b) OH, (c, d) NO_3 and (e, f) O_3 used in the calculation of the gOON production rate. The shaded areas mean the standard deviations. Based on the on-line measurement of N2O5 by the CIMS, extremely high concentration of NO3 was estimated, which cannot be explained by the box model. To avoid the interferences from extremely high concentration of NO3, the unexplained peaks color-coded using grey in (c) was not included in the final ON calculation. When such high episodes of measured NO3 were included in the calculation of gOON production rate, the contribution of gOON production rate from daytime NO3 oxidation is even larger.

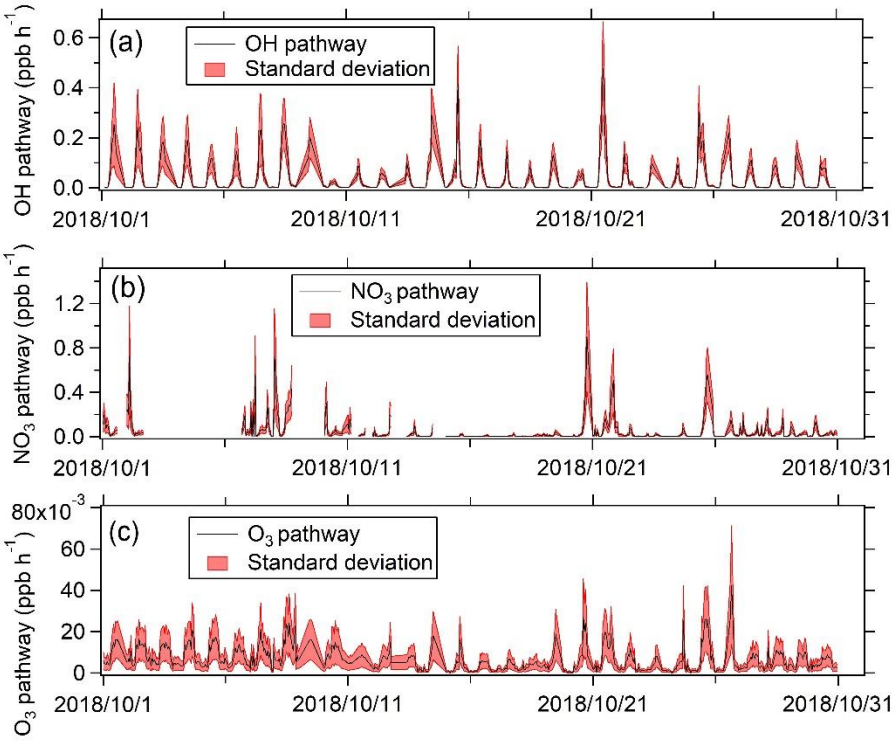

Figure ~~S4~~S5. The uncertainty of gOON production rate of (a) OH, (b) NO_3 and (c) O_3 pathway by Monte Carlo method with 10,000 calculations. The shaded areas mean the standard deviations.

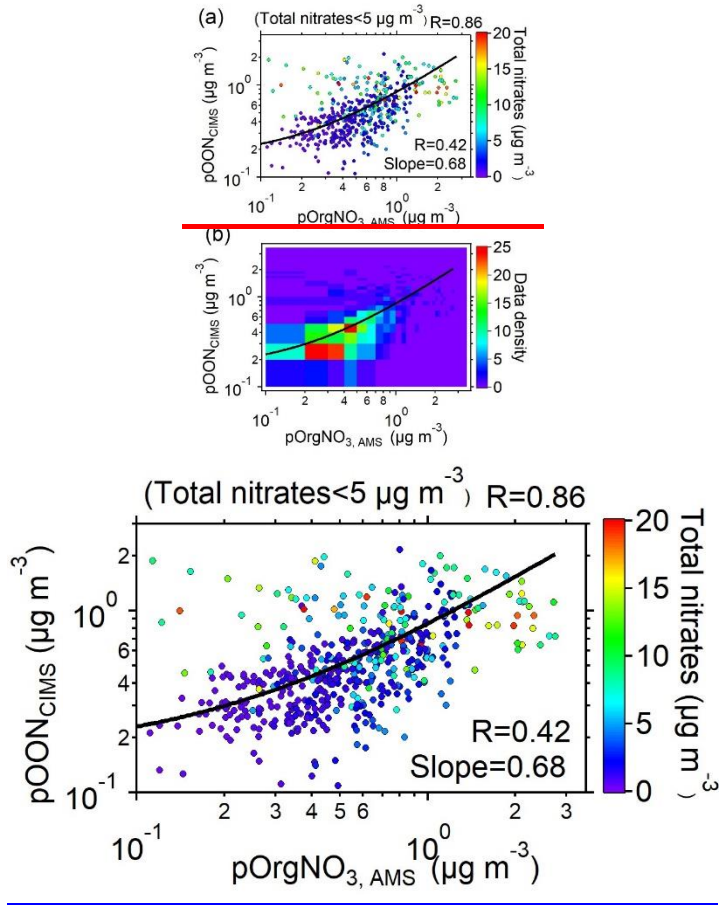

Figure ~~S5. (a)~~S6. Scatterplot of $pOON_{CIMS}$ versus $pOrgNO_{3,\ AMS}$ during the campaign. The points are color-coded using total nitrates (including inorganic nitrate and organic nitrate) measured by AMS. ~~(b) The corresponding joint histogram which the pixels have a resolution of 0.1 μg m^{-3} and color-coded using data density.~~

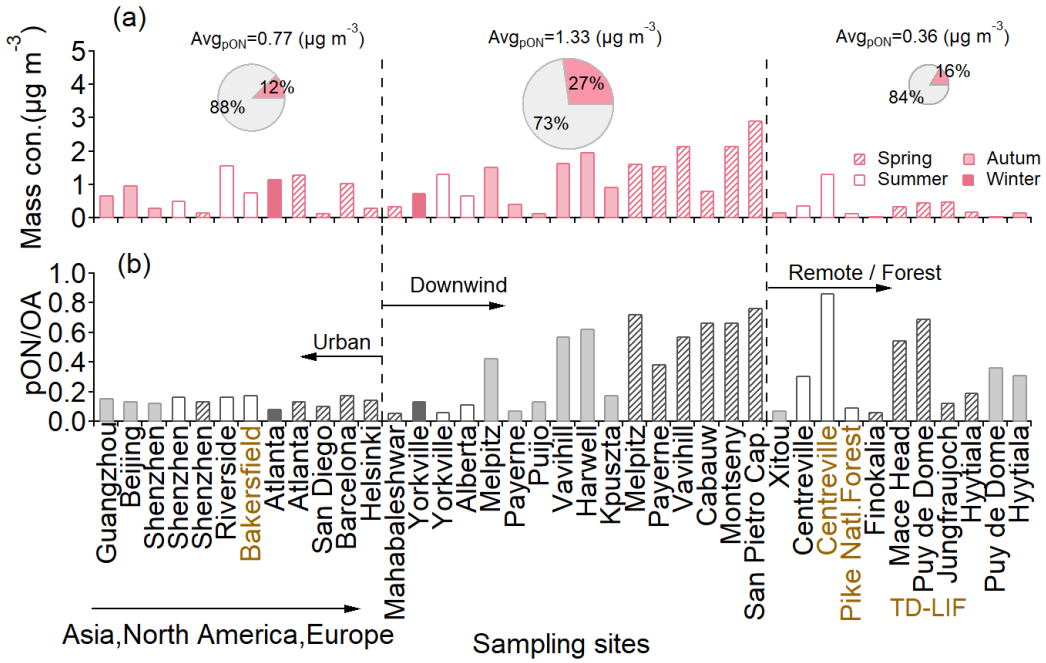

Figure ~~S6~~S7. (a) Mass concentration pON and (b) its fraction to OA at sites around the world (Ayres et al., 2015; Chen et al., 2020; Day et al., 2010; Farmer et al., 2010; Fisher et al., 2016; Fry et al., 2013; Kiendler-Scharr et al., 2016; Lanz et al., 2010; Lee et al., 2019; Rollins et al., 2012; Salvador et al., 2020; Singla et al., 2019; Xu et al., 2015; Yu et al., 2019) classified into urban sites, downwind sites (lied downwind of the cities where were influenced by the emissions from the cities), forest or remote sites with different seasons. The average molecular weight of ON used for all sites is assumed to be 200 g mol^{-1}. The inset pies indicate the average fraction of pON (pink) to OA at each type of site. The yellow indicates the data are measured by thermal dissociation laser-induced fluorescence instrument (TD-LIF). The method of the pON$_{AMS/TD-LIF}$/OA calculation was referred to Takeuchi and Ng (2019).

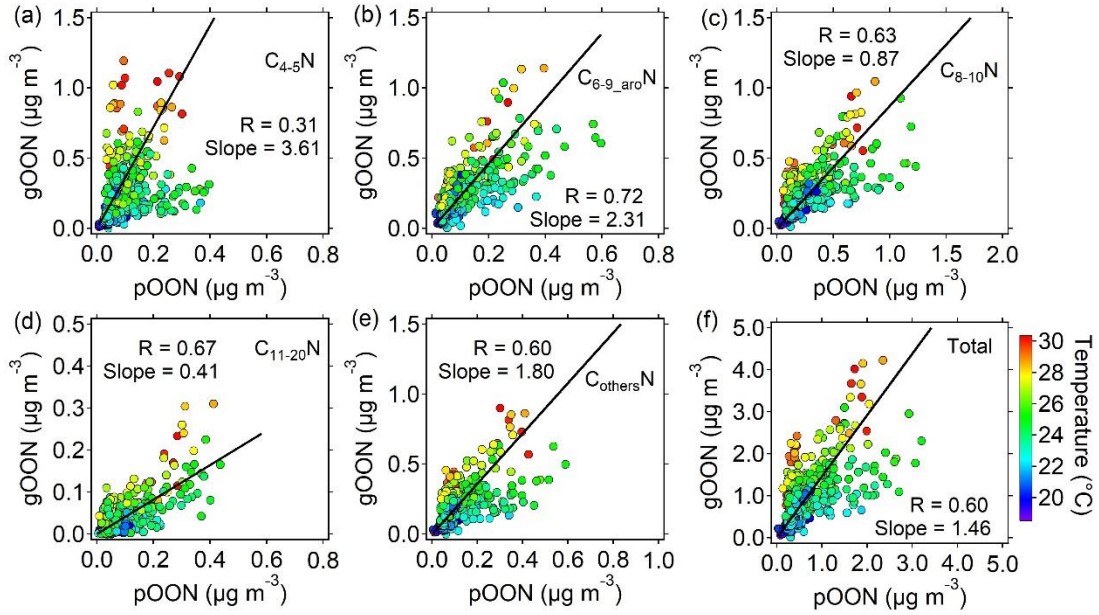

Figure ~~S7~~S8. Scatter plots between gOON and pOON in different categories, i.e., (a) $C_{4–5}N$, (b) $C_{6–9\_aro}N$, (c) $C_{8–10}N$, (d) $C_{11–20}N$, (e) $C_{other}N$ and (f) the total values. The plots are color-coded by ambient temperature.

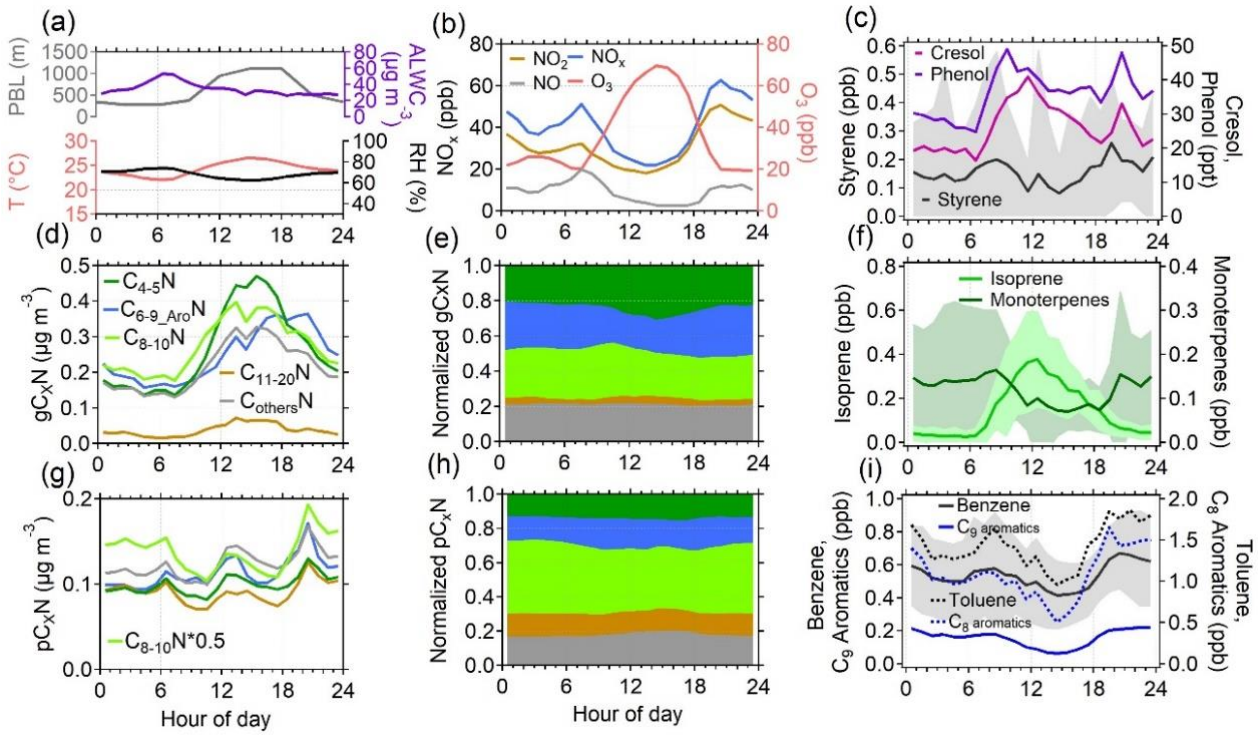

Figure ~~S8~~S9. The average diurnal variations of (a) planetary boundary layer height (PBL), aerosol liquid water contents (ALWC), temperature (T) and relative humidity (RH), (b) mixing ratios of nitrogen dioxide (NO_2), nitric oxide (NO), NO_x (NO_x = NO + NO_2), and ozone (O_3), (c) cresol, phenol, and styrene, (d) gas phase, and (g) particle phase C_xN groups measured by the CIMS, mass fraction of (e) gas- and (h) particle-phase C_xN groups, (f) isoprene and monoterpenes, (i) benzene, toluene, C_8 aromatics, C_9 aromatics during the campaign of October. The shaded areas mean the standard deviations.

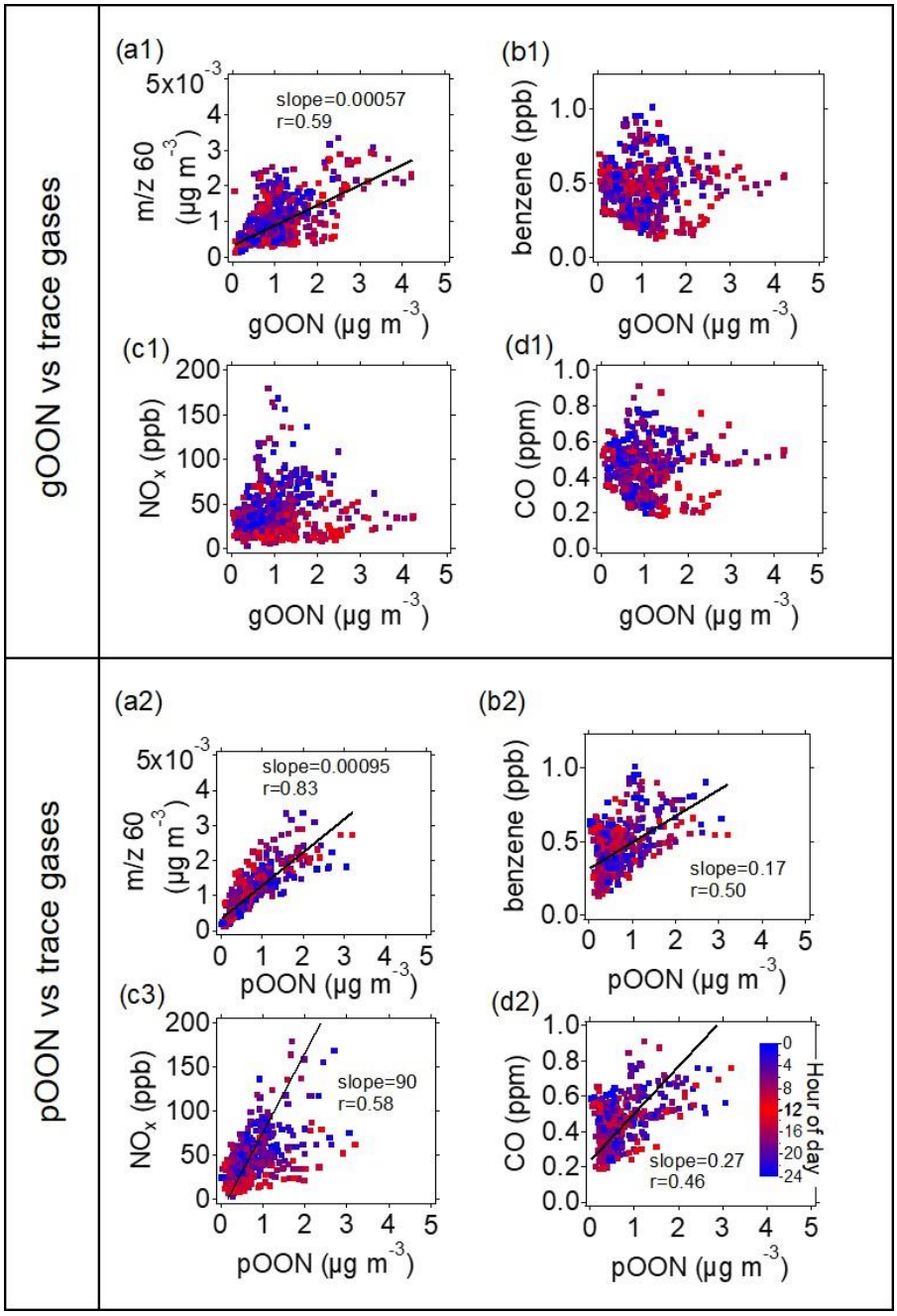

Figure ~~S9~~S10. Scatter plots between gOON (up panel) or pOON (down panel) measured by the CIMS and (a1, a2) *m/z* 60 fragment, (b1, b2) benzene, (c1, c2) NO_x, (d1, d2) carbon monoxide (CO). All scatter plots are color-coded using hour of the day. The HR peak, $C_2H_4O_2^+$, representing the levoglucosan, show similar variation as *m/z* 60.

260

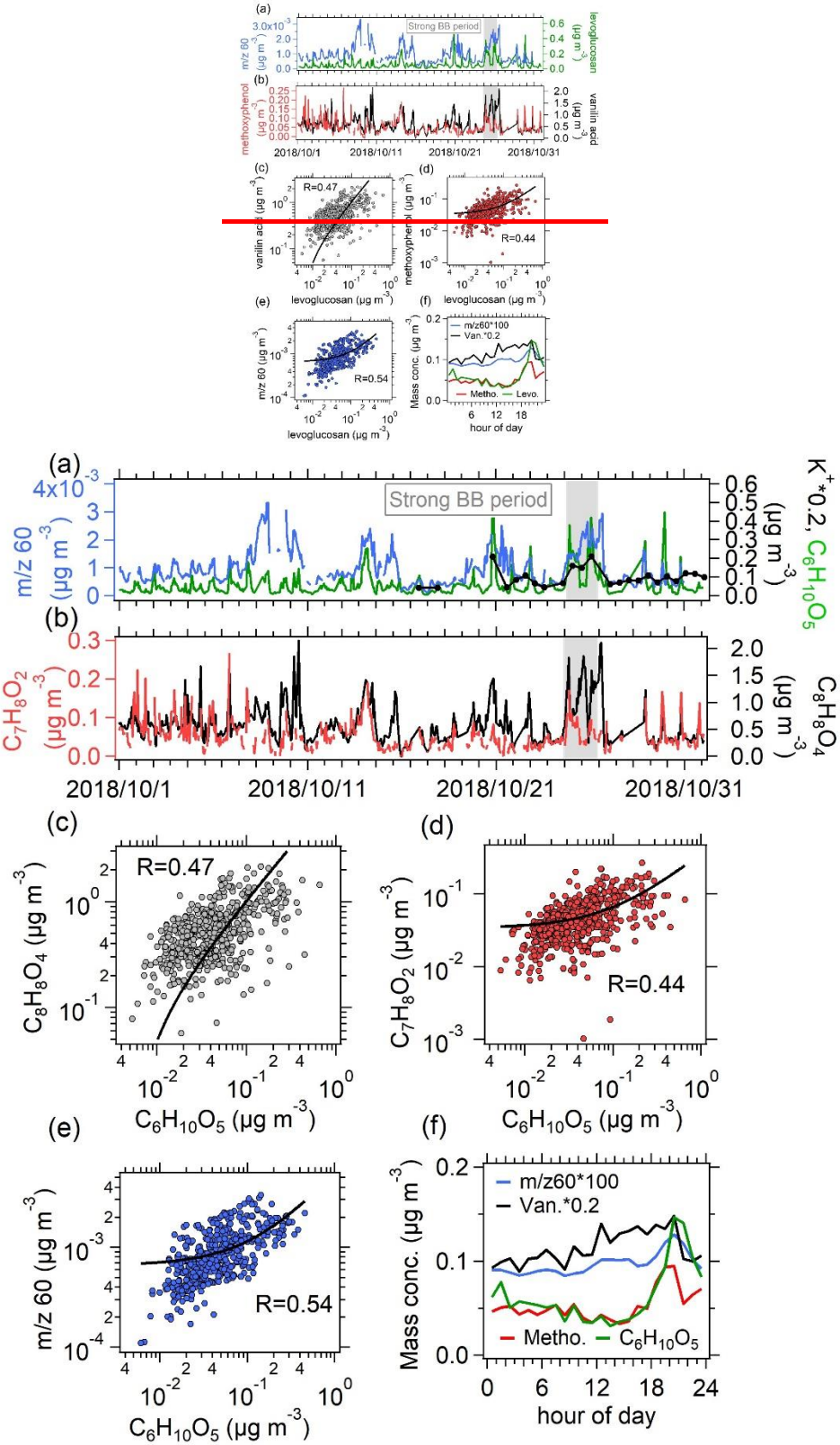

Figure ~~S10~~S11. (a) Time series of *m/z* 60 from the AMS, particulate $C_6H_{10}O_5$ (levoglucosan and its isomers), water-soluble potassium (K^+), (b) $C_7H_8O_2$ (methoxyphenol and ~~vanillin acid~~its isomers) and $C_7H_8O_2$ (methoxyphenol and its isomers) from CIMS. The *m/z* 60 was found to be a fragment from levoglucosan-like species and supposed to be a tracer of biomass burning (Cubison et al., 2011). Scatter plots of (c) $C_7H_8O_2$ (methoxyphenol and its isomers), (d) ~~vanillin~~$C_8H_8O_4$ (vanillic acid and its isomers), and (e) *m/z* 60 versus levoglucosan. Moderate agreement between them and ~~levoglucosan~~$C_6H_{10}O_5$ also demonstrates the existence of biomass burning emissions (Urban et al., 2012). (f) Diurnal variation of the four species.

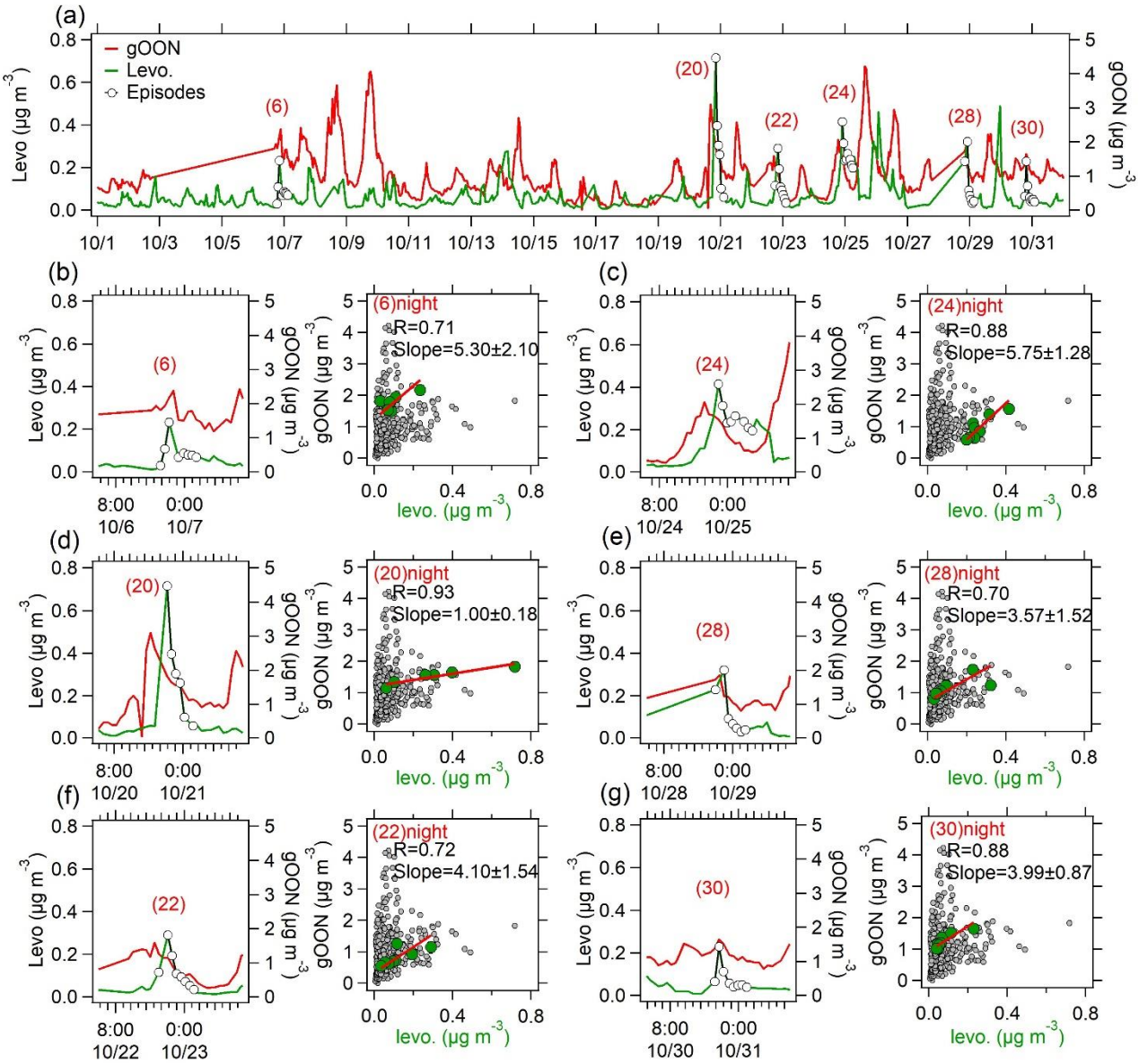

Figure ~~S11~~S12. (a) Time series of measured gOON and levoglucosan (levo., particle-phase $C_6H_{10}O_5$) measured by the CIMS. The biomass burning episodes are labeled based on selection criteria as well. (b−f) Six episodes were selected and used for calculating biomass burning ratios between gOON and levoglucosan. The time series and scatter plots during each episode are also shown here.

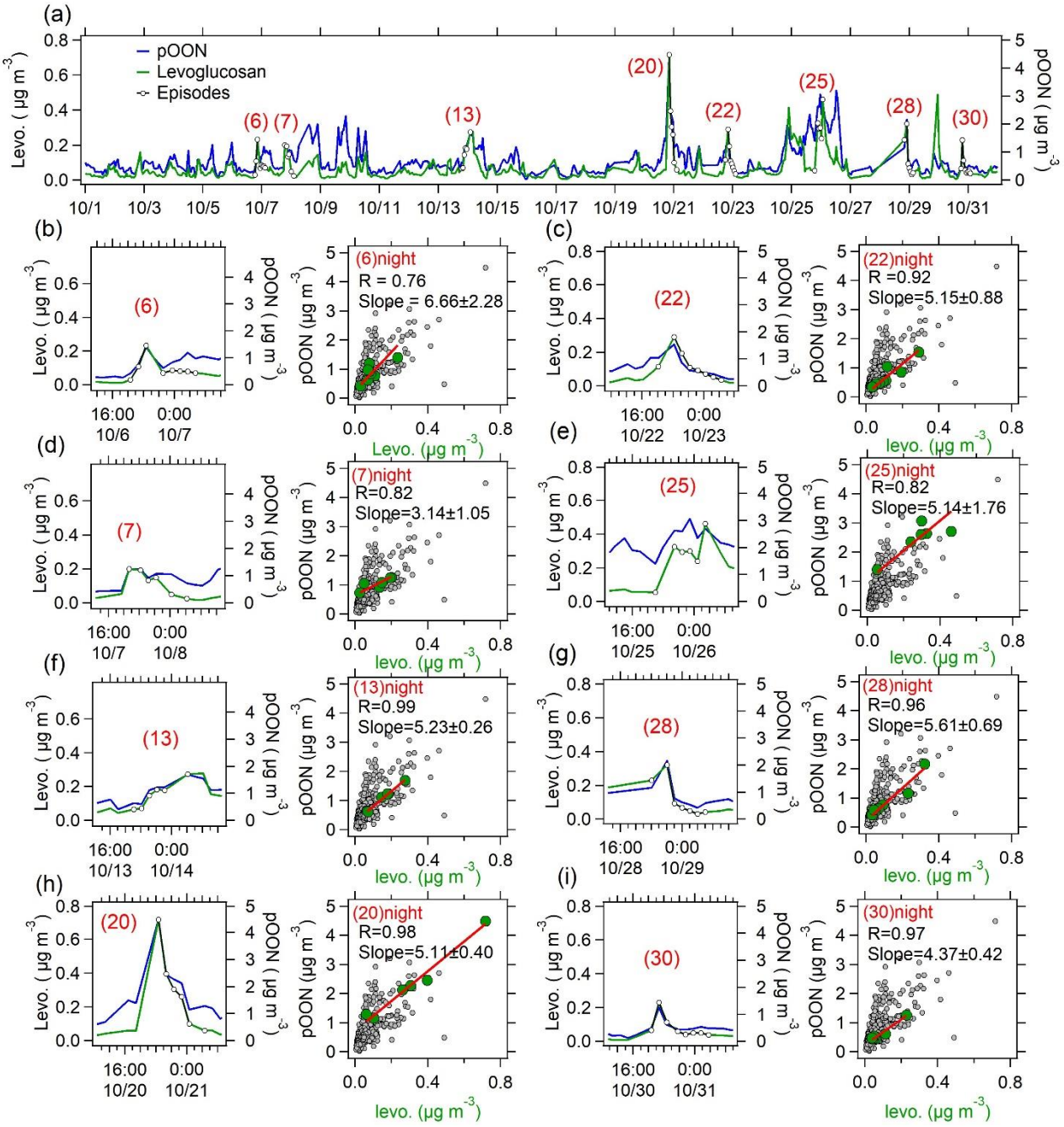

Figure ~~S12~~S13. (a) Time series of pOON and levoglucosan (levo.) measured by the CIMS. The biomass burning episodes are labeled based on the selection criteria as well. (b−i) Eight episodes were selected and used for calculating biomass burning ratios between pOON and levoglucosan. The time series and scatter plots during each episode are shown here.

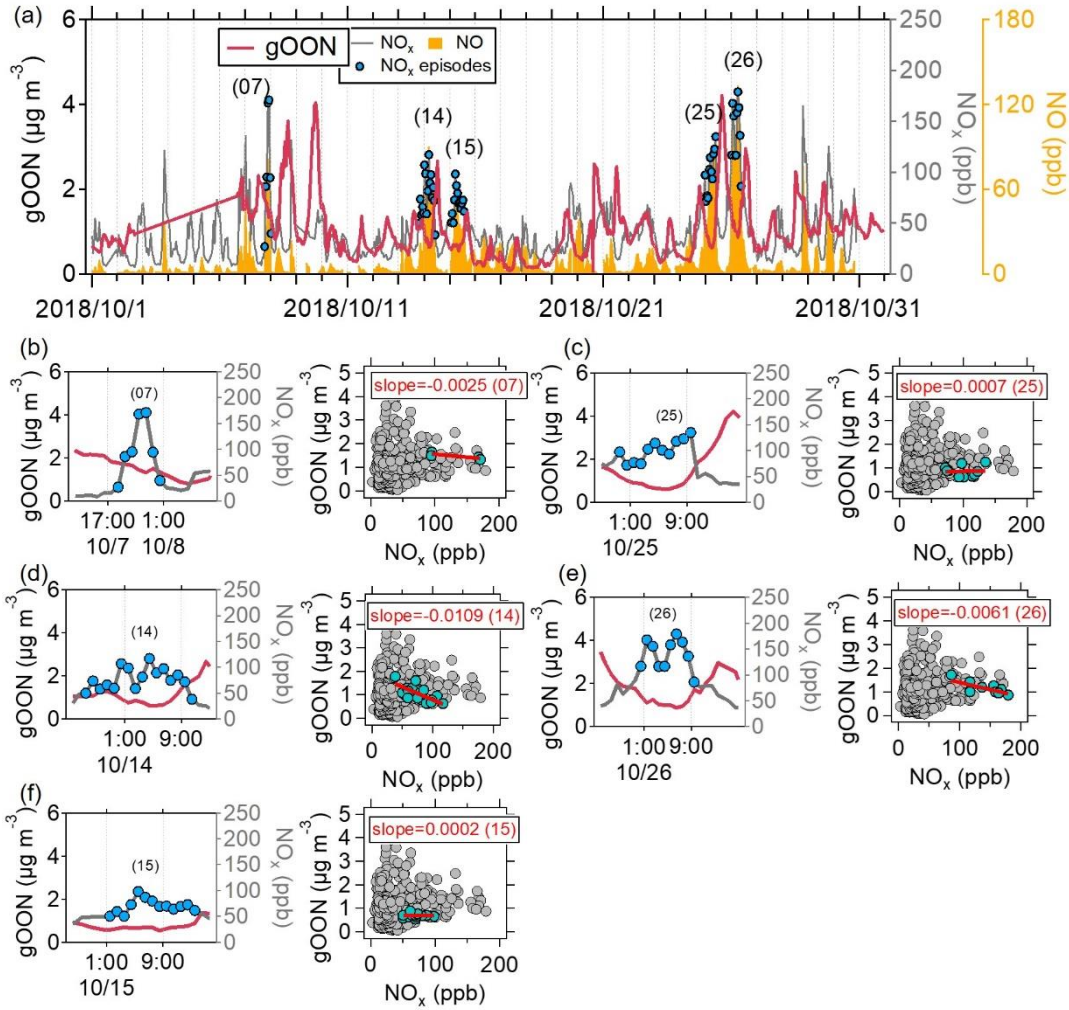

Figure ~~S13~~S14. (a) Time series of gOON measured by the CIMS, and NO/NO_x measured by a NO_x analyzer. The episodes are labeled based on the high concentration of NO_x. (b−f) Time series and scatter plots of gOON vs NO_x during five selected NO_x polluted episodes. NO_x was the tracer for vehicle emissions (Harrison et al., 2003; Krecl et al., 2017). The extremely high NO concentrations (100−200 ppb) indicate strong influences from fresh vehicle emissions. No consistent enhancement between gOON and NO_x was found during the high NO_x episodes, suggesting the vehicle emission is not an important source of gOON in the ambient air.

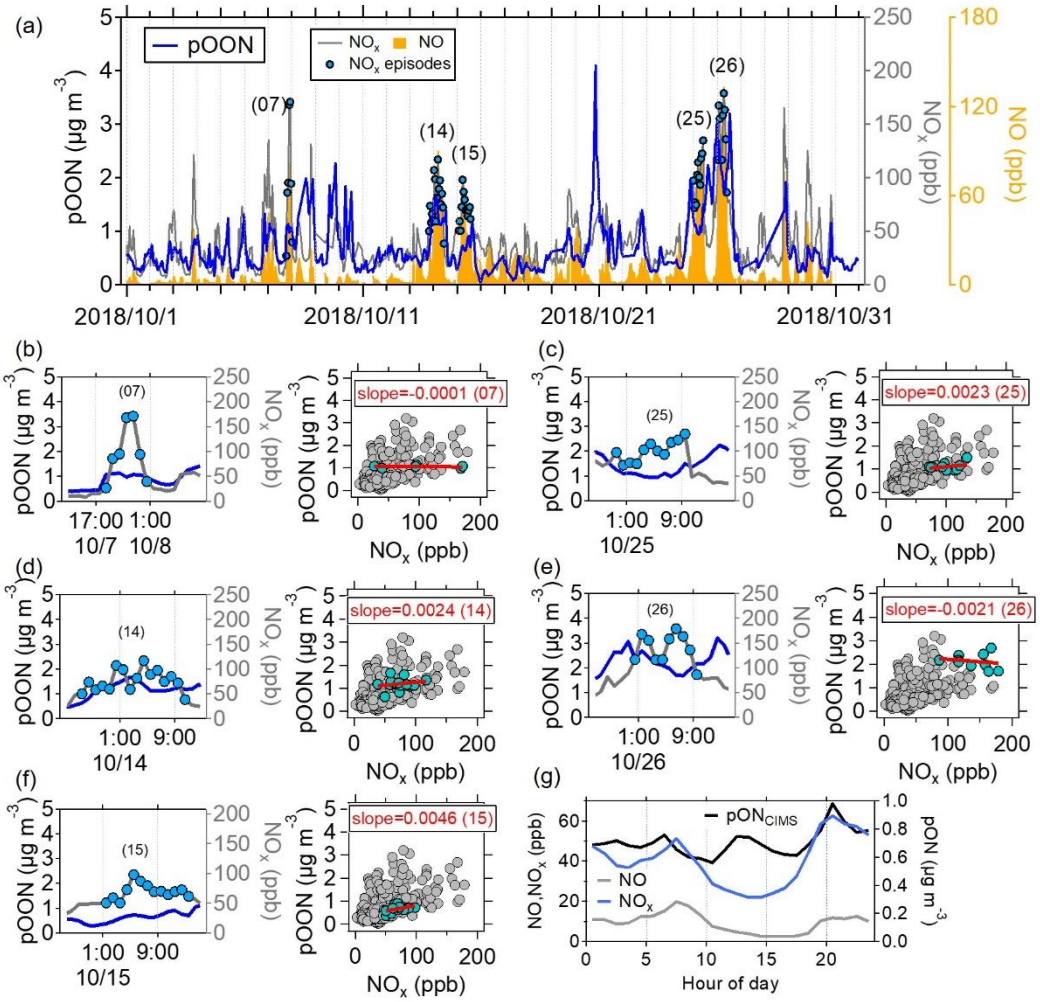

Figure ~~S14~~S15. (a) Time series of pOON measured by the CIMS, and NO/NO_x measured by the NO_x analyzer. The episodes are labeled based on the high concentration of NO_x. (b−f) Time series and scatter plots of pOON vs NO_x during five selected NO_x polluted episodes. (g) Diurnal variations of the measured pOON by the CIMS ($pOON_{CIMS}$), NO and NO_x. NO_x was the tracer for vehicle emissions (Harrison et al., 2003; Krecl et al., 2017). The extremely high NO concentrations (100−200 ppb) indicate strong influence from fresh vehicle emissions during that episode. However, no consistent enhancement between pOON and NO_x was found during these high NO_x episodes, suggesting the vehicle emission is not an important source of pOON in this study.

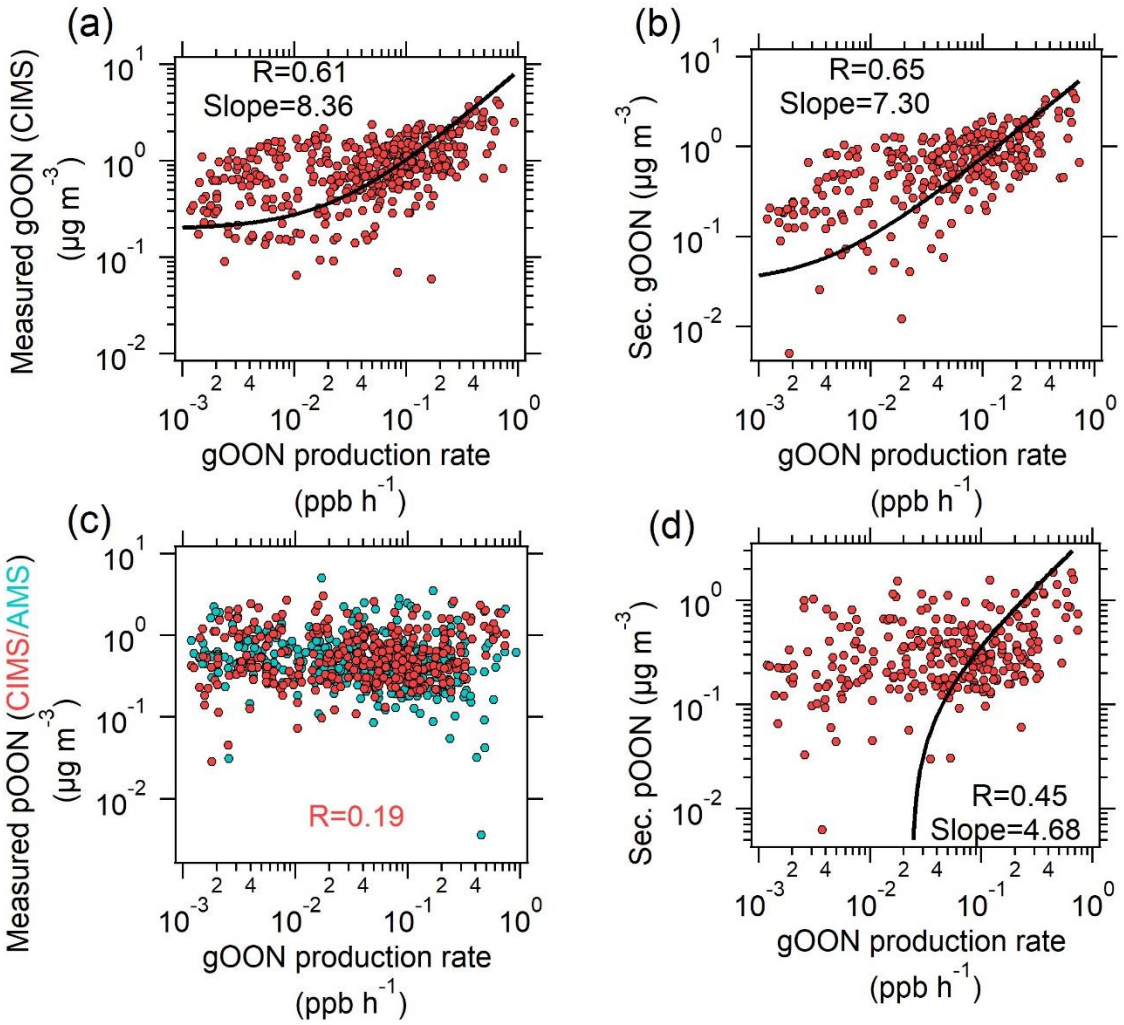

Figure ~~S15~~S16. Scatter plots between (a) measured gOON and (b) secondary gOON vs total secondary gOON production rate. Scatter plots of (c) measured pOON and (d) secondary pOON vs total secondary gOON production rate. The logarithm is applied for both axes.

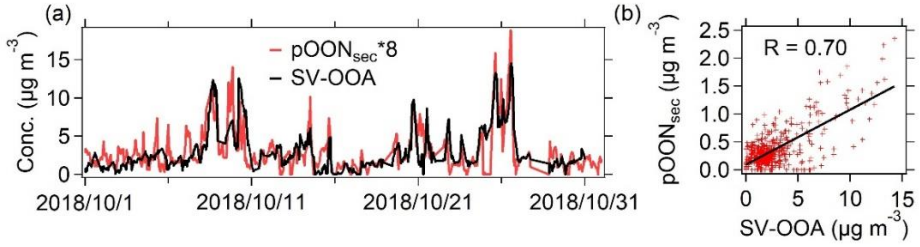

Figure S17. (a) The time series of $pOON_{sec}$ and semi-volatile oxygenated OA (SV-OOA) and (b) their scatterplot. The SV-OOA was treated as freshly formed secondary organic aerosol, which show good correlation with gas-phase oxidation product pentanones. The detailed information of SV-OOA can be found in Chen et al. (2021).

Figure S18. The field points of active fires or thermal anomalies from Modis Satellite around the sampling site, Guangzhou Institute of Geochemistry (GIG), in Guangzhou during the strong biomass burning period October 24–26th.

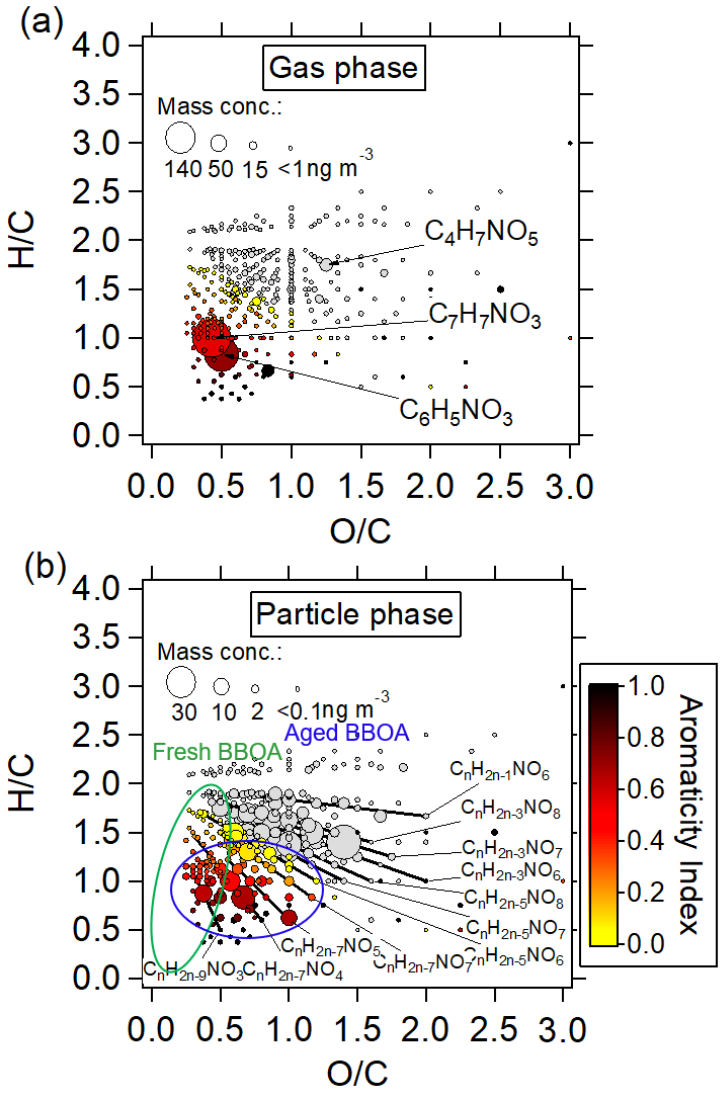

Figure S17S19. Van Krevelen (VK) diagram of all compounds from (a) gOON and (b) pOON. The size of symbols is proportional to the mean enhanced concentrations at 20:00 on October 22 of each compound. Ions are color-coded with Aromaticity Index between 0 and 1 (Wang et al., 2019). The green and blue ellipse represent OA from freshly emitted and aged biomass burning plumes, respectively, based on orbitrap (ESI^-) measurement in Wang et al. (2019). During the whole campaign, the most contributive species are $C_4H_7NO_5$ (7.9%), $C_6H_5NO_3$ (7.4%) and $C_7H_7NO_3$ (5.9%) in the gas phase and $C_8H_{11}NO_7$ (7.9%) in the particle phase. The enhancement concentration of $C_4H_7NO_5$ is much lower than its mean value, implying secondary formation is its dominant source.

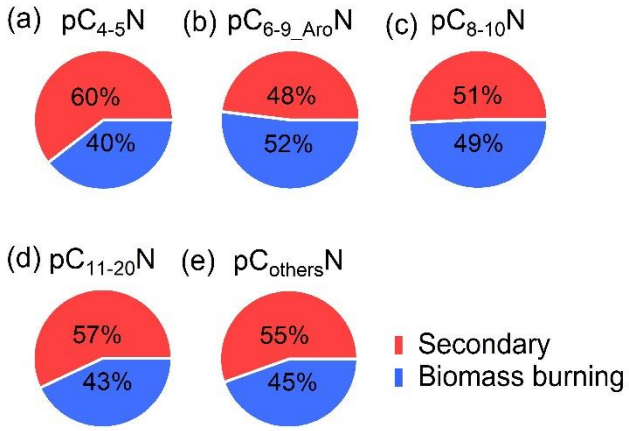

Figure S18S20. The contributions of biomass burning and secondary formation to each particle-phase C_xN (pC_xN) group following Eqs. (1) and (2) in section 3.2.

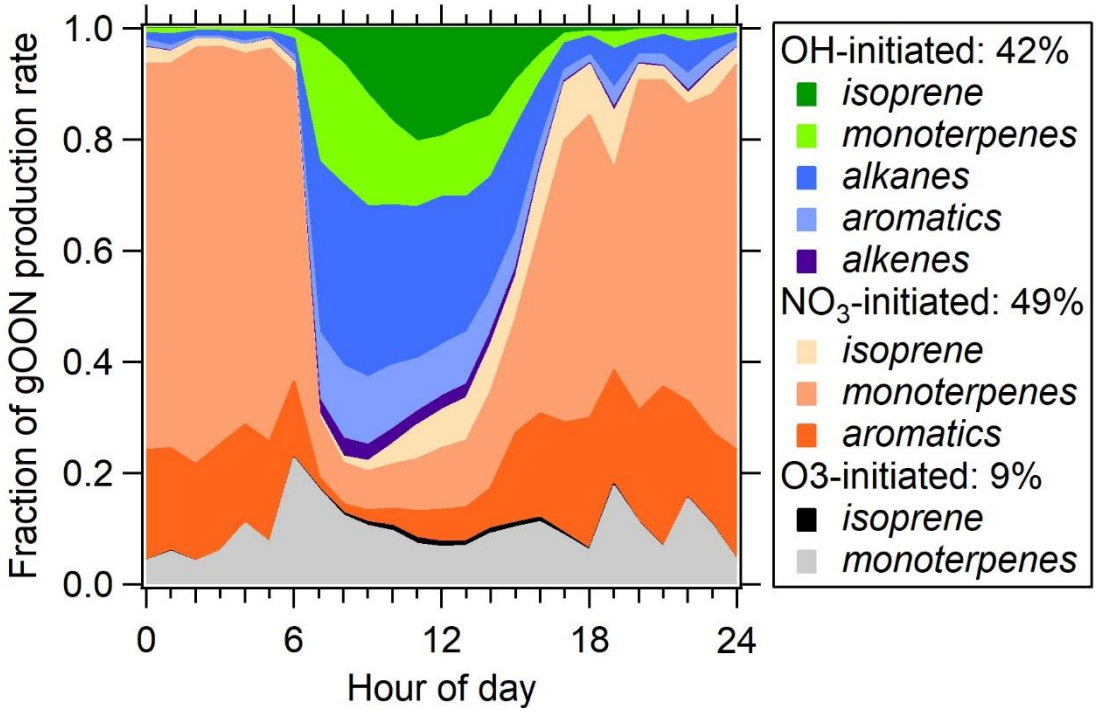

Figure S19S21. Average diurnal variations of the fractions of gOON production rate from OH initiated, NO_3 initiated and O_3 initiated oxidation pathways. For each pathway, contributions from classified VOCs are also shown.

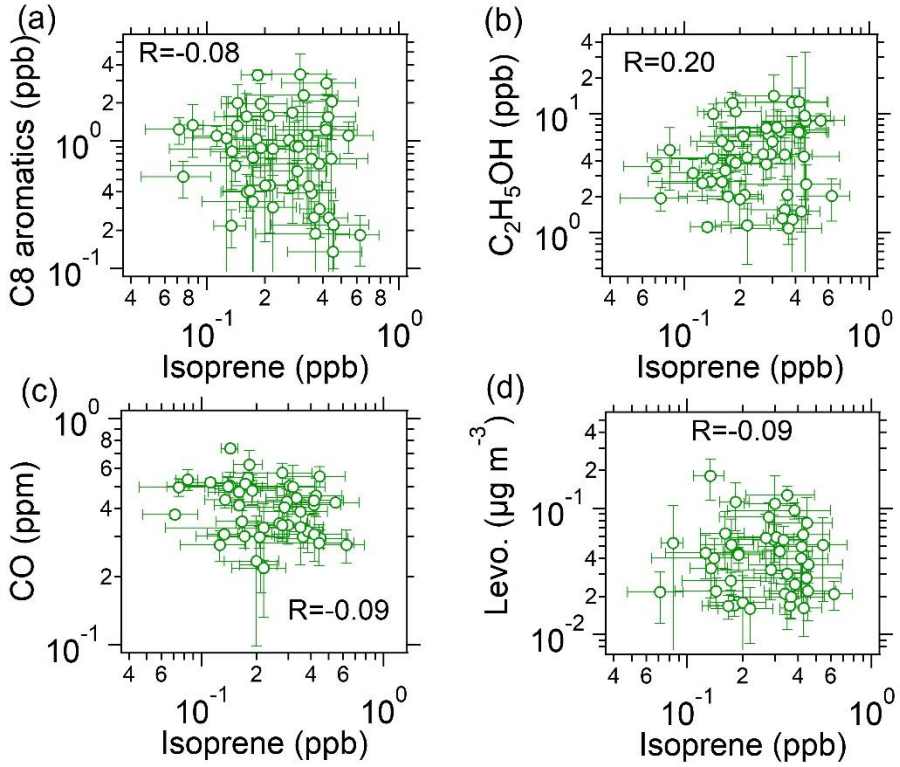

Figure ~~S20~~S22. Scatter plots between the averaged (a) C8 aromatics, (b) ethanol, (c) CO, and (d) levoglucosan vs isoprene during daytime (9:00−18:00) during the entire campaign. The error bars are standard deviations of average values during daytime. The logarithm is applied for both axes.

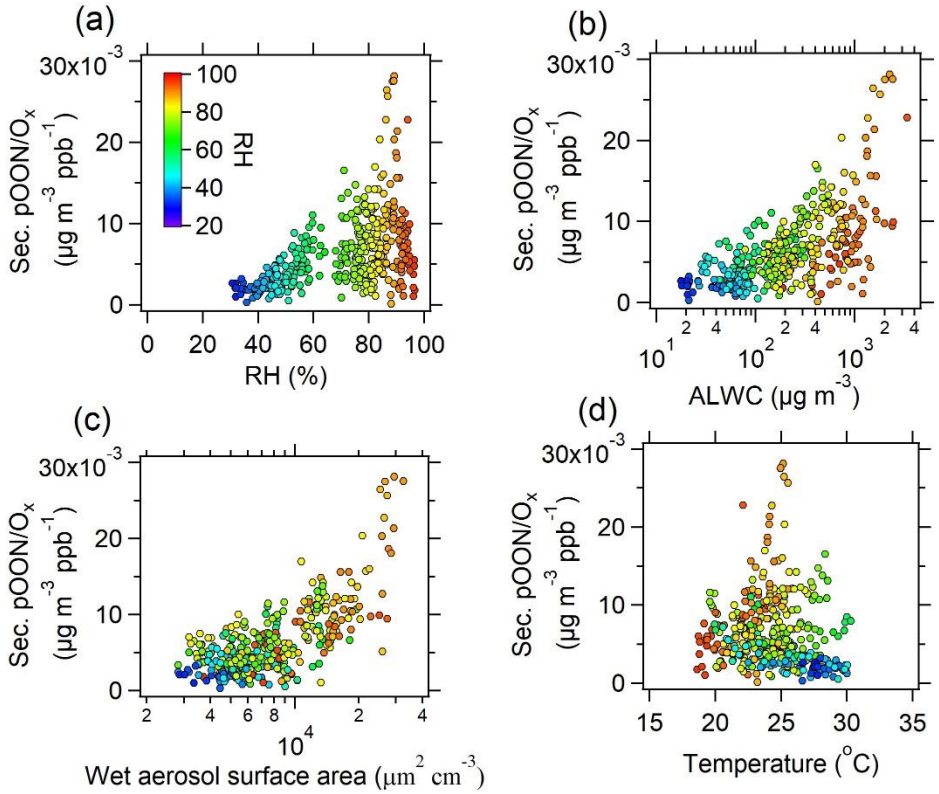

~~**Figure S21. The ratio of Secondary (Sec.) pOON to O_x versus the (a) RH, (b) aerosol liquid water content (ALWC), (c) wet aerosol surface area, and (d) ambient temperature color-coded using the RH during the campaign.**~~

Figure S23. The ratio of Secondary (Sec.) pOON to Ox versus the (a) RH, (b) aerosol liquid water content (ALWC), (c) wet aerosol surface area, and (d) ambient temperature color-coded using the RH during the campaign. Regression slopes between pOON and O_x in photochemically processed urban emissions provide a metric to investigate the relative efficiency of pOON versus O_3 formation during photochemical oxidation (Wood et al., 2010; Hayes et al., 2013). The different values of secondary pOON/O_x ratio can be attributed to photochemical oxidation from different VOC constituent (Nault et al., 2021), heterogenous/aqueous reaction (Zhang et al., 2018; Zhan et al., 2021; Xu et al., 2017; Dai et al., 2019; Hu et al., 2016), and mixing with air aloft that contains residual pOON and O_x during boundary layer growth (Wood et al., 2010). The secondary pOON/O_x ratios that positive correlated with ALWC and wet aerosol surface area suggested that partial pOON might be formed by heterogenous/aqueous reaction, which can efficiently produce secondary pOON but inefficiently on O_x.

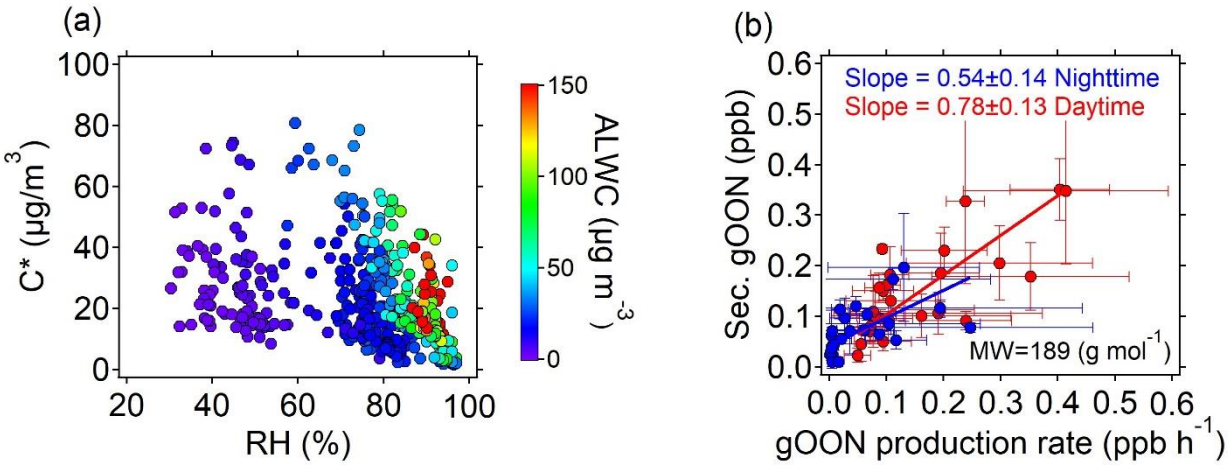

Figure ~~S22~~S24. (a) Scatterplot of saturation mass concentration of total OON (C^* = 1/(C_p/C_{OA}/C_g)) versus RH color-coded with ALWC. (b) Scatter plot between secondary gOON concentration and gOON production rate. The regression slope can be used to estimate the lifetime of gOON following Liebmann et al. (2019).

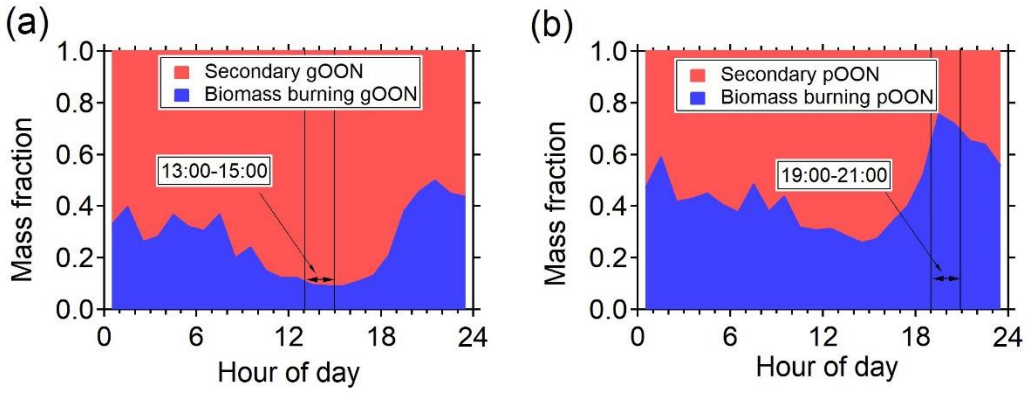

Figure ~~S23~~S25. The average diurnal mass fractions of the contributions from secondary formation and biomass burning to (a) gOON and (b) pOON, respectively. The time periods of 13:00−15:00 and 19:00−21:00 represented the secondary formation dominated period and biomass burning dominated period for the particle phase, respectively.

Reference

Ayres, B. R., Allen, H. M., Draper, D. C., Brown, S. S., Wild, R. J., Jimenez, J. L., Day, D. A., Campuzano-Jost, P., Hu, W., de Gouw, J., Koss, A., Cohen, R. C., Duffey, K. C., Romer, P., Baumann, K., Edgerton, E., Takahama, S., Thornton, J. A., Lee, B. H., Lopez-Hilfiker, F. D., Mohr, C., Wennberg, P. O., Nguyen, T. B., Teng, A., Goldstein, A. H., Olson, K., and Fry, J. L.: Organic nitrate aerosol formation via NO3+ biogenic volatile organic compounds in the southeastern United States, Atmos. Chem. Phys., 15, 13377-13392, https://doi.org/10.5194/acp-15-13377-2015, 2015.

Boyd, C. M., Sanchez, J., Xu, L., Eugene, A. J., Nah, T., Tuet, W. Y., Guzman, M. I., and Ng, N. L.: Secondary organic aerosol formation from the β-pinene+NO3 system: effect of humidity and peroxy radical fate, Atmos. Chem. Phys., 15, 7497-7522, https://doi.org/10.5194/acp-15-7497-2015, 2015.

Brown, S. S. and Stutz, J.: Nighttime radical observations and chemistry, Chem Soc Rev, 41, 6405-6447, https://doi.org/10.1039/c2cs35181a, 2012.

Chen, Y., Takeuchi, M., Nah, T., Xu, L., Canagaratna, M. R., Stark, H., Baumann, K., Canonaco, F., Prévôt, A. S. H., Huey, L. G., Weber, R. J., and Ng, N. L.: Chemical characterization of secondary organic aerosol at a rural site in the southeastern US: insights from simultaneous high-resolution time-of-flight aerosol mass spectrometer (HR-ToF-AMS) and FIGAERO chemical ionization mass spectrometer (CIMS) measurements, Atmos. Chem. Phys., 20, 8421-8440, https://doi.org/10.5194/acp-20-8421-2020, 2020.

Cubison, M. J., Ortega, A. M., Hayes, P. L., Farmer, D. K., Day, D., Lechner, M. J., Brune, W. H., Apel, E., Diskin, G. S., Fisher, J. A., Fuelberg, H. E., Hecobian, A., Knapp, D. J., Mikoviny, T., Riemer, D., Sachse, G. W., Sessions, W., Weber, R. J., Weinheimer, A. J., Wisthaler, A., and Jimenez, J. L.: Effects of aging on organic aerosol from open biomass burning smoke in aircraft and laboratory studies, Atmos. Chem. Phys., 11, 12049-12064, https://doi.org/10.5194/acp-11-12049-2011, 2011.

Dai, Q., Schulze, B. C., Bi, X., Bui, A. A. T., Guo, F., Wallace, H. W., Sanchez, N. P., Flynn, J. H., Lefer, B. L., Feng, Y., and Griffin, R. J.: Seasonal differences in formation processes of oxidized organic aerosol near Houston, TX, Atmos. Chem. Phys., 19, 9641-9661, 10.5194/acp-19-9641-2019, 2019.

Dancey, C. and Reidy, J.: Statistics without Maths for Psychology, London: Prentice Hall Paerson.2007.

Day, D. A., Liu, S., Russell, L. M., and Ziemann, P. J.: Organonitrate group concentrations in submicron particles with high nitrate and organic fractions in coastal southern California, Atmos. Environ., 44, 1970-1979, https://doi.org/10.1016/j.atmosenv.2010.02.045, 2010.

Day, D. A., Campuzano-Jost, P., Nault, B. A., Palm, B. B., Hu, W., Guo, H., Wooldridge, P. J., Cohen, R. C., Docherty, K. S., Huffman, J. A., de Sá, S. S., Martin, S. T., and Jimenez, J. L.: A systematic re-evaluation of methods for quantification of bulk particle-phase organic nitrates using real-time aerosol mass spectrometry, Atmos. Meas. Tech., 15, 459-483, https://doi.org/10.5194/amt-15-459-2022, 2022.

Farmer, D. K., Matsunaga, A., Docherty, K. S., Surratt, J. D., Seinfeld, J. H., Ziemann, P. J., and Jimenez, J. L.: Response of an aerosol mass spectrometer to organonitrates and organosulfates and implications for atmospheric chemistry, Proc. Natl. Acad. Sci. U. S. A., 107, 6670-6675, https://doi.org/10.1073/pnas.0912340107, 2010.

Fisher, J. A., Jacob, D. J., Travis, K. R., Kim, P. S., Marais, E. A., Miller, C. C., Yu, K., Zhu, L., Yantosca, R. M., Sulprizio, M. P., Mao, J., Wennberg, P. O., Crounse, J. D., Teng, A. P., Nguyen, T. B., St Clair, J. M., Cohen, R. C., Romer, P., Nault, B. A., Wooldridge, P. J., Jimenez, J. L., Campuzano-Jost, P., Day, D. A., Hu, W., Shepson, P. B., Xiong, F., Blake, D. R., Goldstein, A. H., Misztal, P. K., Hanisco, T. F., Wolfe, G. M., Ryerson, T. B., Wisthaler, A., and Mikoviny, T.: Organic nitrate chemistry and its implications for nitrogen budgets in an isoprene- and monoterpene-rich atmosphere: constraints from aircraft (SEAC(4)RS) and ground-based (SOAS) observations in the Southeast US, Atmos. Chem. Phys., 16, 5969-5991, https://doi.org/10.5194/acp-16-5969-2016, 2016.

Fry, J. L., Draper, D. C., Zarzana, K. J., Campuzano-Jost, P., Day, D. A., Jimenez, J. L., Brown, S. S., Cohen, R. C., Kaser, L., Hansel, A., Cappellin, L., Karl, T., Roux, A. H., Turnipseed, A., Cantrell, C., Lefer, B. L., and Grossberg, N.: Observations of gas- and aerosol-phase organic nitrates at BEACHON-RoMBAS 2011, Atmos. Chem. Phys., 13, 8585-8605, https://doi.org/10.5194/acp-13-8585-2013, 2013.

Fry, J. L., Brown, S. S., Middlebrook, A. M., Edwards, P. M., Campuzano-Jost, P., Day, D. A., Jimenez, J. L., Allen, H. M., Ryerson, T. B., Pollack, I., Graus, M., Warneke, C., de Gouw, J. A., Brock, C. A., Gilman, J., Lerner, B. M., Dubé, W. P., Liao, J., and Welti, A.: Secondary organic aerosol (SOA) yields from NO3 radical + isoprene based on nighttime aircraft power plant plume transects, Atmos. Chem. Phys., 18, 11663-11682, https://doi.org/10.5194/acp-18-11663-2018, 2018.

Gkatzelis, G. I., Coggon, M. M., McDonald, B. C., Peischl, J., Aikin, K. C., Gilman, J. B., Trainer, M., and Warneke, C.: Identifying Volatile Chemical Product Tracer Compounds in U.S. Cities, Environ. Sci. Technol., 55, 188-199, https://doi.org/10.1021/acs.est.0c05467, 2021.

Hamilton, J. F., Bryant, D. J., Edwards, P. M., Ouyang, B., Bannan, T. J., Mehra, A., Mayhew, A. W., Hopkins, J. R., Dunmore, R. E., Squires, F. A., Lee, J. D., Newland, M. J., Worrall, S. D., Bacak, A., Coe, H., Percival, C., Whalley, L. K., Heard, D. E., Slater, E. J., Jones, R. L., Cui, T., Surratt, J. D., Reeves, C. E., Mills, G. P., Grimmond, S., Sun, Y., Xu, W., Shi, Z., and Rickard, A. R.: Key Role of NO3 Radicals in the Production of Isoprene Nitrates and Nitrooxyorganosulfates in Beijing, Environ. Sci. Technol., 55, 842-853, https://doi.org/10.1021/acs.est.0c05689, 2021.

Hao, L. Q., Kortelainen, A., Romakkaniemi, S., Portin, H., Jaatinen, A., Leskinen, A., Komppula, M., Miettinen, P., Sueper, D., Pajunoja, A., Smith, J. N., Lehtinen, K. E. J., Worsnop, D. R., Laaksonen, A., and Virtanen, A.: Atmospheric submicron aerosol composition and particulate organic nitrate formation in a boreal forestland–urban mixed region, Atmos. Chem. Phys., 14, 13483-13495, https://doi.org/10.5194/acp-14-13483-2014, 2014.

Harrison, R. M., Tilling, R., Callén Romero, M. a. S., Harrad, S., and Jarvis, K.: A study of trace metals and polycyclic aromatic hydrocarbons in the roadside environment, Atmos. Environ., 37, 2391-2402, https://doi.org/10.1016/S1352-2310(03)00122-5, 2003.

Hayes, P. L., Ortega, A. M., Cubison, M. J., Froyd, K. D., Zhao, Y., Cliff, S. S., Hu, W. W., Toohey, D. W., Flynn, J. H., Lefer, B. L., Grossberg, N., Alvarez, S., Rappenglück, B., Taylor, J. W., Allan, J. D., Holloway, J. S., Gilman, J. B., Kuster, W. C., de Gouw, J. A., Massoli, P., Zhang, X., Liu, J., Weber, R. J., Corrigan, A. L., Russell, L. M., Isaacman, G., Worton, D. R., Kreisberg, N. M., Goldstein, A. H., Thalman, R., Waxman, E. M., Volkamer, R., Lin, Y. H., Surratt, J. D., Kleindienst, T. E., Offenberg, J. H., Dusanter, S., Griffith, S., Stevens, P. S., Brioude, J., Angevine, W. M., and Jimenez, J. L.: Organic aerosol composition and sources in Pasadena, California, during the 2010 CalNex campaign, J. Geophys. Res.: Atmos., 118, 9233-9257, 10.1002/jgrd.50530, 2013.

Hilas, C. S., Goudos, S. K., and Sahalos, J. N.: Seasonal decomposition and forecasting of telecommunication data: A comparative case study, Technological Forecasting and Social Change, 73, 495-509, https://doi.org/10.1016/j.techfore.2005.07.002, 2006.

Hu, W., Hu, M., Hu, W., Jimenez, J. L., Yuan, B., Chen, W., Wang, M., Wu, Y., Chen, C., Wang, Z., Peng, J., Zeng, L., and Shao, M.: Chemical composition, sources, and aging process of submicron aerosols in Beijing: Contrast between summer and winter, J. Geophys. Res.: Atmos., 121, 1955-1977, 10.1002/2015jd024020, 2016.

Huffman, J. A., Ziemann, P. J., Jayne, J. T., Worsnop, D. R., and Jimenez, J. L.: Development and Characterization of a Fast-Stepping/Scanning Thermodenuder for Chemically-Resolved Aerosol Volatility Measurements, Aerosol Sci. Technol., 42, 395-407, https://doi.org/10.1080/02786820802104981, 2008.

Kiendler-Scharr, A., Mensah, A. A., Friese, E., Topping, D., Nemitz, E., Prevot, A. S. H., Äijälä, M., Allan, J., Canonaco, F., Canagaratna, M., Carbone, S., Crippa, M., Dall Osto, M., Day, D. A., De Carlo, P., Di Marco, C. F., Elbern, H., Eriksson, A., Freney, E., Hao, L., Herrmann, H., Hildebrandt, L., Hillamo, R., Jimenez, J. L., Laaksonen, A., McFiggans, G., Mohr, C., O'Dowd, C., Otjes, R., Ovadnevaite, J., Pandis, S. N., Poulain, L., Schlag, P., Sellegri, K., Swietlicki, E., Tiitta, P., Vermeulen, A., Wahner, A., Worsnop, D., and Wu, H. C.: Ubiquity of organic nitrates from nighttime chemistry in the European submicron aerosol, Geophys. Res. Lett., 43, 7735-7744, https://doi.org/10.1002/2016gl069239, 2016.

Koch, B. P. and Dittmar, T.: From mass to structure: an aromaticity index for high-resolution mass data of natural organic matter, Rapid Commun. Mass Spectrom., 20, 926-932, https://doi.org/10.1002/rcm.2386, 2006.

Koch, B. P. and Dittmar, T.: From mass to structure: an aromaticity index for high-resolution mass data of natural organic matter, Rapid Commun. Mass Spectrom., 30, 250-250, https://doi.org/10.1002/rcm.7433, 2016.

Krecl, P., Johansson, C., Targino, A. C., Ström, J., and Burman, L.: Trends in black carbon and size-resolved particle number concentrations and vehicle emission factors under real-world conditions, Atmos. Environ., 165, 155-168, https://doi.org/10.1016/j.atmosenv.2017.06.036, 2017.

Lanz, V. A., Prévôt, A. S. H., Alfarra, M. R., Weimer, S., Mohr, C., DeCarlo, P. F., Gianini, M. F. D., Hueglin, C., Schneider, J., Favez, O., D'Anna, B., George, C., and Baltensperger, U.: Characterization of aerosol chemical composition with aerosol mass spectrometry in Central Europe: an overview, Atmos. Chem. Phys., 10, 10453-10471, https://doi.org/10.5194/acp-10-10453-2010, 2010.

Lee, A. K. Y., Adam, M. G., Liggio, J., Li, S.-M., Li, K., Willis, M. D., Abbatt, J. P. D., Tokarek, T. W., Odame-Ankrah, C. A., Osthoff, H. D., Strawbridge, K., and Brook, J. R.: A large contribution of anthropogenic organo-nitrates to secondary organic aerosol in the Alberta oil sands, Atmos. Chem. Phys., 19, 12209-12219, https://doi.org/10.5194/acp-19-12209-2019, 2019.

Li, X. B., Yuan, B., Wang, S., Wang, C., Lan, J., Liu, Z., Song, Y., He, X., Huangfu, Y., Pei, C., Cheng, P., Yang, S., Qi, J., Wu, C., Huang, S., You, Y., Chang, M., Zheng, H., Yang, W., Wang, X., and Shao, M.: Variations and sources of volatile organic compounds (VOCs) in urban region: insights from measurements on a tall tower, Atmos. Chem. Phys., 22, 10567-10587, https://doi.org/10.5194/acp-22-10567-2022, 2022.

Liebmann, J., Sobanski, N., Schuladen, J., Karu, E., Hellén, H., Hakola, H., Zha, Q., Ehn, M., Riva, M., Heikkinen, L., Williams, J., Fischer, H., Lelieveld, J., and Crowley, J. N.: Alkyl nitrates in the boreal forest: formation via the NO3-, OH- and O3 induced oxidation of biogenic volatile organic compounds and ambient lifetimes, Atmos. Chem. Phys., 19, 10391-10403, https://doi.org/10.5194/acp-19-10391-2019, 2019.

McKay, M. D., Beckman, R. J., and Conover, W. J.: A Comparison of Three Methods for Selecting Values of Input Variables in the Analysis of Output From a Computer Code, Technometrics, 42, 55-61, https://doi.org/10.1080/00401706.2000.10485979, 2000.

Nault, B. A., Jo, D. S., McDonald, B. C., Campuzano-Jost, P., Day, D. A., Hu, W., Schroder, J. C., Allan, J., Blake, D. R., Canagaratna, M. R., Coe, H., Coggon, M. M., DeCarlo, P. F., Diskin, G. S., Dunmore, R., Flocke, F., Fried, A., Gilman, J. B., Gkatzelis, G., Hamilton, J. F., Hanisco, T. F., Hayes, P. L., Henze, D. K., Hodzic, A., Hopkins, J., Hu, M., Huey, L. G., Jobson, B. T., Kuster, W. C., Lewis, A., Li, M., Liao, J., Nawaz, M. O., Pollack, I. B., Peischl, J., Rappenglück, B., Reeves, C. E., Richter, D., Roberts, J. M., Ryerson, T. B., Shao, M., Sommers, J. M., Walega, J., Warneke, C., Weibring, P., Wolfe, G. M., Young, D. E., Yuan, B., Zhang, Q., de Gouw, J. A., and Jimenez, J. L.: Secondary organic aerosols from anthropogenic volatile organic compounds contribute substantially to air pollution mortality, Atmos. Chem. Phys., 21, 11201-11224, 10.5194/acp-21-11201-2021, 2021.

Ng, N. L., Brown, S. S., Archibald, A. T., Atlas, E., Cohen, R. C., Crowley, J. N., Day, D. A., Donahue, N. M., Fry, J. L., Fuchs, H., Griffin, R. J., Guzman, M. I., Herrmann, H., Hodzic, A., Iinuma, Y., Jimenez, J. L., Kiendler-Scharr, A., Lee, B. H., Luecken, D. J., Mao, J., McLaren, R., Mutzel, A., Osthoff, H. D., Ouyang, B., Picquet-Varrault, B., Platt, U., Pye, H. O. T., Rudich, Y., Schwantes, R. H., Shiraiwa, M., Stutz, J., Thornton, J. A., Tilgner, A., Williams, B. J., and Zaveri, R. A.: Nitrate radicals and biogenic volatile organic compounds: oxidation, mechanisms, and organic aerosol, Atmos. Chem. Phys., 17, 2103-2162, https://doi.org/10.5194/acp-17-2103-2017, 2017.

Rollins, A. W., Browne, E. C., Min, K. E., Pusede, S. E., Wooldridge, P. J., Gentner, D. R., Goldstein, A. H., Liu, S., Day, D. A., Russell, L. M., and Cohen, R. C.: Evidence for NO(x) control over nighttime SOA formation, Science, 337, 1210-1212, https://doi.org/10.1126/science.1221520, 2012.

Salvador, C. M., Chou, C. C. K., Cheung, H. C., Ho, T. T., Tsai, C. Y., Tsao, T. M., Tsai, M. J., and Su, T. C.: Measurements of submicron organonitrate particles: Implications for the impacts of NOx pollution in a subtropical forest, Atmospheric Research, 245, https://doi.org/10.1016/j.atmosres.2020.105080, 2020.

Sato, K., Takami, A., Isozaki, T., Hikida, T., Shimono, A., and Imamura, T.: Mass spectrometric study of secondary organic aerosol formed from the photo-oxidation of aromatic hydrocarbons, Atmos. Environ., 44, 1080-1087, https://doi.org/10.1016/j.atmosenv.2009.12.013, 2010.

Singla, V., Mukherjee, S., Pandithurai, G., Dani, K. K., and Safai, P. D.: Evidence of Organonitrate Formation at a High Altitude Site, Mahabaleshwar, during the Pre-monsoon Season, Aerosol and Air Quality Research, 19, 1241-1251, https://doi.org/10.4209/aaqr.2018.03.0110, 2019.

Sommers, J. M., Stroud, C. A., Adam, M. G., O'Brien, J., Brook, J. R., Hayden, K., Lee, A. K. Y., Li, K., Liggio, J., Mihele, C., Mittermeier, R. L., Stevens, R. G., Wolde, M., Zuend, A., and Hayes, P. L.: Evaluating SOA formation from different sources of semi- and intermediate-volatility organic compounds from the Athabasca oil sands, Environmental Science: Atmospheres, 2, 469-490, https://doi.org/10.1039/D1EA00053E, 2022.

Sun, Y. L., Zhang, Q., Schwab, J. J., Yang, T., Ng, N. L., and Demerjian, K. L.: Factor analysis of combined organic and inorganic aerosol mass spectra from high resolution aerosol mass spectrometer measurements, Atmos. Chem. Phys., 12, 8537-8551, https://doi.org/10.5194/acp-12-8537-2012, 2012.

Takeuchi, M. and Ng, N. L.: Chemical composition and hydrolysis of organic nitrate aerosol formed from hydroxyl and nitrate radical oxidation of α-pinene and β-pinene, Atmos. Chem. Phys., 19, 12749-12766, https://doi.org/10.5194/acp-19-12749-2019, 2019.

Urban, R. C., Lima-Souza, M., Caetano-Silva, L., Queiroz, M. E. C., Nogueira, R. F. P., Allen, A. G., Cardoso, A. A., Held, G., and Campos, M. L. A. M.: Use of levoglucosan, potassium, and water-soluble organic carbon to characterize the origins of biomass-burning aerosols, Atmos. Environ., 61, 562-569, https://doi.org/10.1016/j.atmosenv.2012.07.082, 2012.

Wang, H., Lu, K., Chen, X., Zhu, Q., Chen, Q., Guo, S., Jiang, M., Li, X., Shang, D., Tan, Z., Wu, Y., Wu, Z., Zou, Q., Zheng, Y., Zeng, L., Zhu, T., Hu, M., and Zhang, Y.: High N2O5 Concentrations Observed in Urban Beijing: Implications of a Large Nitrate Formation Pathway, Environmental Science & Technology Letters, 4, 416-420, https://doi.org/10.1021/acs.estlett.7b00341, 2017.

Wang, S., Peng, Y., Peng, Q., Wu, C., Wang, C., Wang, B., Wang, Z., Kuang, Y., Song, W., Wang, X., Hu, W., Chen, W., Shen, J., Chen, D., Shao, M., and Yuan, B.: Different chemical removal pathways of volatile organic compounds (VOCs): Comparison of urban and regional sites, Acta Sci. Circumstantiae, 40, 2311-2322, https://doi.org/10.13671/j.hjkxxb.2020.0153, 2020.

Wang, Y., Hu, M., Lin, P., Tan, T., Li, M., Xu, N., Zheng, J., Du, Z., Qin, Y., Wu, Y., Lu, S., Song, Y., Wu, Z., Guo, S., Zeng, L., Huang, X., and He, L.: Enhancement in Particulate Organic Nitrogen and Light Absorption of Humic-Like Substances over Tibetan Plateau Due to Long-Range Transported Biomass Burning Emissions, Environ. Sci. Technol., 53, 14222-14232, https://doi.org/10.1021/acs.est.9b06152, 2019.

Wolfe, G. M., Marvin, M. R., Roberts, S. J., Travis, K. R., and Liao, J.: The Framework for 0-D Atmospheric Modeling (F0AM) v3.1, Geosci. Model Dev., 9, 3309-3319, https://doi.org/10.5194/gmd-9-3309-2016, 2016.

Wood, E. C., Canagaratna, M. R., Herndon, S. C., Onasch, T. B., Kolb, C. E., Worsnop, D. R., Kroll, J. H., Knighton, W. B., Seila, R., Zavala, M., Molina, L. T., DeCarlo, P. F., Jimenez, J. L., Weinheimer, A. J., Knapp, D. J., Jobson, B. T., Stutz, J., Kuster, W. C., and Williams, E. J.: Investigation of the correlation between odd oxygen and secondary organic aerosol in Mexico City and Houston, Atmos. Chem. Phys., 10, 8947-8968, 10.5194/acp-10-8947-2010, 2010.

Xu, L., Suresh, S., Guo, H., Weber, R. J., and Ng, N. L.: Aerosol characterization over the southeastern United States using high-resolution aerosol mass spectrometry: spatial and seasonal variation of aerosol composition and sources with a focus on organic nitrates, Atmos. Chem. Phys., 15, 7307-7336, https://doi.org/10.5194/acp-15-7307-2015, 2015.

Xu, W., Takeuchi, M., Chen, C., Qiu, Y., Xie, C., Xu, W., Ma, N., Worsnop, D. R., Ng, N. L., and Sun, Y.: Estimation of particulate organic nitrates from thermodenuder–aerosol mass spectrometer measurements in the North China Plain, Atmos. Meas. Tech., 14, 3693-3705, https://doi.org/10.5194/amt-14-3693-2021, 2021.

Xu, W., Han, T., Du, W., Wang, Q., Chen, C., Zhao, J., Zhang, Y., Li, J., Fu, P., Wang, Z., Worsnop, D. R., and Sun, Y.: Effects of Aqueous-Phase and Photochemical Processing on Secondary Organic Aerosol Formation and Evolution in Beijing, China, Environ. Sci. Technol., 51, 762-770, 10.1021/acs.est.6b04498, 2017.

Ye, C., Yuan, B., Lin, Y., Wang, Z., Hu, W., Li, T., Chen, W., Wu, C., Wang, C., Huang, S., Qi, J., Wang, B., Wang, C., Song, W., Wang, X., Zheng, E., Krechmer, J. E., Ye, P., Zhang, Z., Wang, X., Worsnop, D. R., and Shao, M.: Chemical characterization of oxygenated organic compounds in the gas phase and particle phase using iodide CIMS with FIGAERO in urban air, Atmos. Chem. Phys., 21, 8455-8478, https://doi.org/10.5194/acp-21-8455-2021, 2021.

Yu, K., Zhu, Q., Du, K., and Huang, X.-F.: Characterization of nighttime formation of particulate organic nitrates based on high-resolution aerosol mass spectrometry in an urban atmosphere in China, Atmos. Chem. Phys., 19, 5235-5249, https://doi.org/10.5194/acp-19-5235-2019, 2019.

Zhan, B., Zhong, H., Chen, H., Chen, Y., Li, X., Wang, L., Wang, X., Mu, Y., Huang, R.-J., George, C., and Chen, J.: The roles of aqueous-phase chemistry and photochemical oxidation in oxygenated organic aerosols formation, Atmos. Environ., 266, 118738, https://doi.org/10.1016/j.atmosenv.2021.118738, 2021.

Zhang, C., Lu, X., Zhai, J., Chen, H., Yang, X., Zhang, Q., Zhao, Q., Fu, Q., Sha, F., and Jin, J.: Insights into the formation of secondary organic carbon in the summertime in urban Shanghai, JEnvS, 72, 118-132, https://doi.org/10.1016/j.jes.2017.12.018, 2018.

Zhu, Q., He, L. Y., Huang, X. F., Cao, L. M., Gong, Z. H., Wang, C., Zhuang, X., and Hu, M.: Atmospheric aerosol compositions and sources at two national background sites in northern and southern China, Atmos. Chem. Phys., 16, 10283-10297, https://doi.org/10.5194/acp-16-10283-2016, 2016.